NATIONAL TECHNICAL UNIVERSITY OF ATHENS
School of Civil Engineering
Institute of Steel Structures

Aerodynamic calculation of loads and dynamic behavior of wind turbine towers

POSTGRADUATE THESIS

Stylianos M. Vernardos

Supervisor: Prof. Ch. Gantes

Athens, February 2013

EMK ME 2013/17

ΕΘΝΙΚΟ ΜΕΤΣΟΒΙΟ ΠΟΛΥΤΕΧΝΕΙΟ
Σχολή Πολιτικών Μηχανικών
Εργαστήριο Μεταλλικών Κατασκευών

Αεροδυναμικός υπολογισμός φορτίων και δυναμική συμπεριφορά πυλώνων ανεμογεννητριών

ΜΕΤΑΠΤΥΧΙΑΚΗ ΕΡΓΑΣΙΑ

Στυλιανός Μ. Βερνάρδος

Επιβλέπων: Χαρ. Γαντές, Καθηγητής ΕΜΠ

Αθήνα, Φεβρουάριος 2013

ΕΜΚ ΜΕ 2013/17

Βερνάρδος Σ. Μ. (2013).
Αεροδυναμικός υπολογισμός φορτίων και δυναμική συμπεριφορά πυλώνων ανεμογεννητριών
Μεταπτυχιακή Εργασία ΕΜΚ ΜΕ 2013/17
Εργαστήριο Μεταλλικών Κατασκευών, Εθνικό Μετσόβιο Πολυτεχνείο, Αθήνα.

Vernardos S. M. (2013).
Aerodynamic calculation of loads and dynamic behavior of wind turbine towers
Postgraduate Thesis EMK ME 2013/17
Institute of Steel Structures, National Technical University of Athens, Greece

Contents

ΕΘΝΙΚΟ ΜΕΤΣΟΒΙΟ ΠΟΛΥΤΕΧΝΕΙΟ
ΣΧΟΛΗ ΠΟΛΙΤΙΚΩΝ ΜΗΧΑΝΙΚΩΝ
ΕΡΓΑΣΤΗΡΙΟ ΜΕΤΑΛΛΙΚΩΝ ΚΑΤΑΣΚΕΥΩΝ

ΜΕΤΑΠΤΥΧΙΑΚΗ ΕΡΓΑΣΙΑ
ΕΜΚ ΜΕ 2013/17

Αεροδυναμικός υπολογισμός φορτίων και δυναμική συμπεριφορά πυλώνων ανεμογεννητριών

Στυλιανός Βερνάρδος

Επιβλέπων: Χάρης Γαντές, Καθηγητής ΕΜΠ

Περίληψη

Σε μία περίοδο ανεξέλεγκτης κατανάλωσης ενέργειας, οι ανεμογεννήτριες διαδραματίζουν το δικό τους σημαντικό ρόλο, ως αναπόσπαστο μέλος της ευρύτερης οικογένειας των εναλλακτικών πηγών. Η φαινομενικά απλή τους λειτουργία, ωστόσο, έρχεται σε πλήρη αντίθεση με την περίπλοκη φύση των φαινομένων τα οποία συντελούνται από την πρώτη επαφή της μάζας του αέρα με το μηχανισμό των περιστρεφόμενων πτερυγίων μίας τέτοιας κατασκευής. Ακριβώς αυτό το γεγονός δυσχεραίνει σε μεγάλο βαθμό την προσομοίωση των συνθηκών υπό τις οποίες μία ανεμογεννήτρια καλείται, τόσο να παράγει ωφέλιμο έργο, όσο και να αντεπεξέλθει με ασφάλεια σε κάθε είδους φορτίσεις. Το εγχείρημα της αναπαραγωγής αυτών των συνθηκών σε υπολογιστικό περιβάλλον αποτέλεσε το στόχο της παρούσας εργασίας, αφενός μέσω της δημιουργίας ενός πεδίου ανέμου από ένα σύνολο στοχαστικών διαδικασιών και αφετέρου μέσω της προσομοίωσης της αεροδυναμικής συμπεριφοράς των πτερυγίων αλλά και του πυλώνα. Οι σχετικοί υπολογισμοί πραγματοποιήθηκαν σε περιβάλλον Matlab, μέσω της παραγωγής ενός αλγορίθμου, ο οποίος, λαμβάνοντας υπόψη τις απαραίτητες, ποικίλες παραμέτρους που σχετίζονται με τα αεροδυναμικά φαινόμενα, καταλήγει στη δημιουργία χρονοϊστοριών φόρτισης λόγω ανέμου για τον πυλώνα της ανεμογεννήτριας. Τα αποτελέσματα ενσωματώθηκαν ως συνθήκες φόρτισης σε ένα μηχανικό προσομοίωμα πυλώνα, το οποίο δημιουργήθηκε με τη βοήθεια του προγράμματος SAP2000 και αναλύθηκε δυναμικά, μη γραμμικά, ώστε να εξεταστούν οι προκύπτουσες χρονοϊστορίες αποκρίσεων και τάσεων, καθώς και να ελεγχθεί η επάρκεια των διατομών που επιλέχθηκαν.

NATIONAL TECHNICAL UNIVERSITY OF ATHENS
SCHOOL OF CIVIL ENGINEERING
INSTITUTE OF STEEL STRUCTURES

POSTGRADUATE THESIS
EMK ME 2013/17

Aerodynamic calculation of wind loads and dynamic behavior of wind turbine towers

Stylianos Vernardos

Supervised by Prof. Charis Gantes

Abstract

In an era of massive energy consumption, wind turbines play their own important role as an integral part of the wider ensemble of alternative energy sources. Their seemingly simple function, however, contradicts the complex nature of the phenomena, occurring from the very first contact between the air mass and the rotating blades' mechanism of such a construction. It is exactly this fact that significantly hinders the simulation of the conditions, under which a wind turbine is expected to produce power and also safely withstand any kind of loads exerted on it. The venture of reproducing these conditions in a computational environment constituted the aim of the current thesis, through the generation of a wind field from a series of stochastic procedures, on the one hand, and the simulation of aerodynamic behavior of both the blades and the tower, on the other. The pertinent calculations were accomplished in Matlab environment, through the generation of an algorithm which, by taking into account various, necessary parameters related to the aerodynamic phenomena, produces wind load time histories for the wind turbine's tower. The results were incorporated as loading conditions into a computational model of the tower, which was created in SAP2000 software, and was subsequently analyzed dynamically, non-linearly, so that the resulting displacement and stress time histories could be examined and the selected sections could be checked for adequacy.

Acknowledgements

The completion of the current thesis gives me the opportunity to express my sincere gratitude to Professor Charis Gantes, for entrusting me with this interesting and challenging subject and for being available for me in every occasion his invaluable support was needed.

Additionally, I would like to acknowledge the significant contribution of PhD candidate Konstantina Koulatsou to this venture and thank her for providing her useful advices throughout the research. I am also gratefull to Francesco Petrini from Sapienza University of Rome for sharing his knowledge in wind engineering with us. Without his helping hand, this task would not be accomplished.

Finally, I am greatly thankful to my family for tirelessly standing by my side at all my career steps, as well as to my beloved friends for encouraging me at those moments I needed it most.

1 Introduction

1.1 General

In an era of massive energy consumption, alternative energy sources have already been established within our conscience as the last available link between this planet's sustainability and our own very existence. Among these sources, wind turbines are becoming all the more popular, since, with the progress of technology, such constructions promise to provide more efficient and simultaneously less expensive wind power utilization. Observing the evolution of wind power plants, from the windmills of the ancient times to today's modern wind turbines (see Fig. 1.1), one can easily notice the significant changes which have taken place to both the design characteristics and the overall performance of these plants. As time goes by, several aspects, regarding the aerodynamic elements of the rotor, the electrical mechanisms for power extraction, even the areas at which the wind power plants are installed, have been optimized, as to provide the highest possible power output. However huge the changes, though, power still depends on the very same factors on which it always did.

From the well-known expression:

$$P = \frac{1}{2} C_P \rho A V^3,$$

Figure 1.1: Evolution of wind power plants from the ancient Chinese vertical-axis windwheel for pumping water (left) to the modern horizontal-axis wind turbine for electrical power extraction (right).

it is obvious that the power output of a wind turbine is a function of the power coefficient, the air density, the rotor area and the wind velocity. The power coefficient varies with the tip speed ratio (see Chapter 3) and describes the fraction of the power in the wind that may be converted into mechanical work. Although several attempts have been made in order to increase its value, a maximum limit of 0.593 cannot be exceeded, as will be proven later on. As for the air density, its variations are essentially negligible. Thus, major changes in the power output can only be achieved by two means: either by increasing the swept area of the rotor, or by locating the wind turbines on sites with higher wind speeds. More specifically, a doubling of the rotor diameter leads to a four-time increase in power output. The influence of the wind speed is, of course, more pronounced with a doubling of wind speed leading to an eight-fold increase in power. This fact has led to today's enormous rotor diameters of 60m and tower heights of more than 100m, in order to take advantage of the increase of wind speed with height (see Chapter 2). Both these characteristics of modern wind turbines, despite the remarkable addition to the efficiency, encumber the tower with all the greater wind loads. The blades, the tower and finally the foundation of a wind turbine are exposed to even more significant forces and moments as the wind speed and rotor diameters increase. Furthermore, these loads are of a dynamic nature, that is, they vary with time and spatial distance, an aspect that renders their calculation a rather complex procedure. This complexity is based on two different factors: Firstly, the wind variations are impossible to predict and calculate using any kind of deterministic methods. The mean wind speed is subject to changes from one point to another, let alone the wind turbulence, which is a continuously varying parameter, which can only be approached by means of stochastic analysis. Secondly, the aerodynamic characteristics of the rotor follow their own, rather complicated physical laws. The less the simplistic assumptions made regarding these rules, the more one has to indulge into the subject in order to reach an adequate knowledge level.

1.2 Thesis's objective

The aim of this thesis is to offer a concise description of the phenomenon of airflow passing through the rotor of a modern horizontal-axis wind turbine, as well as an algorithm with the utilization of which the dimensioning of the tower can be achieved. In chapters 2, 3 the above-mentioned complex concepts are analyzed with the simpler language possible. Additionally, chapter 2 describes the way a stochastic wind field can be digitally simulated, while chapter 3 provides the means by which the aerodynamic theory of the rotating rotor exposed to airflow can be computationally approached. In chapter 4 the reader shall find some information regarding the algorithm produced in this thesis, in the MATLAB environment, for both the simulation of the wind velocity field and the calculation of the loads exerted on the rotor and, consequently on the top of the tower. In the 5^{th} chapter of this thesis the results of the program's execution are demonstrated. These results are obtained

for several wind turbines and different values of the most decisive parameters affecting the wind field variations and the aerodynamics of the rotor. Finally, different wind velocity time-histories are produced, followed by the correspondent wind load time-histories on the top of the tower. In chapter 6 the previously calculated loads are exerted on a wind-turbine tower simulation, created using the software SAP2000. On this tower model, the displacements and stresses are calculated, both along the tower itself, as well as at the foundation of it. Moreover, the dimensioning of the tower is also presented in this chapter using different loading results. In the last chapter some useful conclusions are extracted and a few suggestions for further studying are made for anyone interested in taking this subject a little further.

2 The wind resource

2.1 Wind variations

The very same element, that constitutes a significantly important source of energy, is also the one causing insurmountable difficulties through its extremely high level of complexity. Indeed, either observing the phenomenon of wind blowing from a macroscopic point of view, or watching its variations through the most microscopic scale, one word can only describe its behavior: unpredictability.

Since the source of the wind is mainly the temperature differentiation between different regions, it is quite clear why unpredictability is the main attribute of wind's nature. Insolation varies with latitude, but also physical geography or even human activity, humidity and vegetation affect the absorption levels of solar radiation. In other words, the variability of wind speed depends on such a large number of factors, that forecasting is impossible if it refers to more than a few days ahead and to any other but temporal variations of a large or medium scale, namely, seasonal or diurnal variations. This means that as far as a more microscopic scale is concerned, high-frequency fluctuations, the so-called "turbulence", are not predictable whatsoever.

Concerning the large scale variations, met on a yearly or seasonal basis, the most appropriate model to be used to describe them is the Weibull distribution, representing the variation in hourly mean wind speed over a year. The form of this variation is given in Eq.2.1:

$$F(U) = exp\left(-\left(\frac{U}{c}\right)^{k}\right) \tag{2.1}$$

where *c* and *k* are scale and shape parameters respectively. The *k* factor describes the variability about the mean and *c* refers to the annual mean wind speed, $\overline{U}$, by the relationship of Eq.2.2:

$$\overline{U} = c\Gamma(1 + 1/k) \tag{2.2}$$

where Γ is the complete gamma function. The lower the value of *k* for a location, the greater the variability of hourly mean wind speed about the annual mean and vice versa. The following figure (Fig.2.1) depicts the Weibull distribution, as a description of annual wind speed variations, for several different values of *k*:

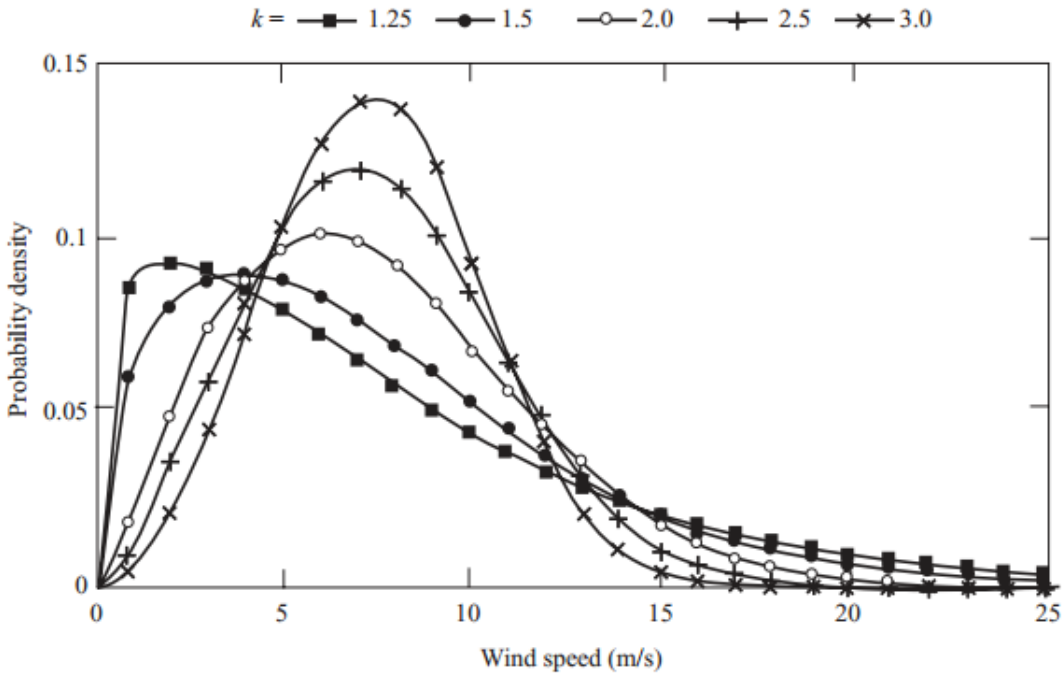

Figure 2.1: Example Weibull distributions

On the other hand, such deterministic equations cannot apply to the turbulence case. Apparently, even this complex process is the result of certain phenomena, namely the friction of the wind flow with the earth's surface or thermal effects as a result of temperature variations, or a combination of both. Moreover, turbulence obeys to certain physical laws such as those related to the conservation of mass, momentum and energy. In other words, turbulence can be described by a set of differential equations taking into account these concepts and using specific initial and boundary conditions, thus rendering the process predictable, up to an extent, as soon as those equations are integrated forward in time. However, due to the fact that even the slightest differences in initial or boundary conditions may result in large differences in the predictions, practically, the determination of the turbulence fluctuations with a deterministic formula is highly unlikely. It is, therefore, wiser to attempt the approach of turbulence in terms of its statistical properties.

2.2 Turbulence intensity

One of the most useful descriptors of turbulence is its intensity, which is a measure of overall level of turbulence and is defined as in Eq.2.3:

$$I = \frac{\sigma}{\overline{U}} \tag{2.3}$$

where σ represents the standard deviation of wind speed variations about the mean wind speed $\overline{U}$, usually defined over 10 min or 1 h. While turbulent wind speed variations can be considered to be normally distributed (roughly Gaussian), the tails

of the distribution are far from this model, rendering such an approximation inappropriate.

The factors that seriously affect the turbulence intensity are the roughness of the ground surface, the topographical features and the thermal behavior of the atmosphere. Concerning the ground surface, the influence of its characteristics is limited to a certain height, above which the air flow can be considered unobstructed and is only affected by the large scale pressure differences and the earth's rotation. This state of the air flow is named "geostrophic wind". Apparently, however, this is not the case for the type of wind loading the various structures, due to their proximity to the ground. A wind turbine, for example, is exposed to a significantly disturbed air flow, at the atmosphere's lowest layer, the so-called "boundary layer" (see Fig. 2.2)

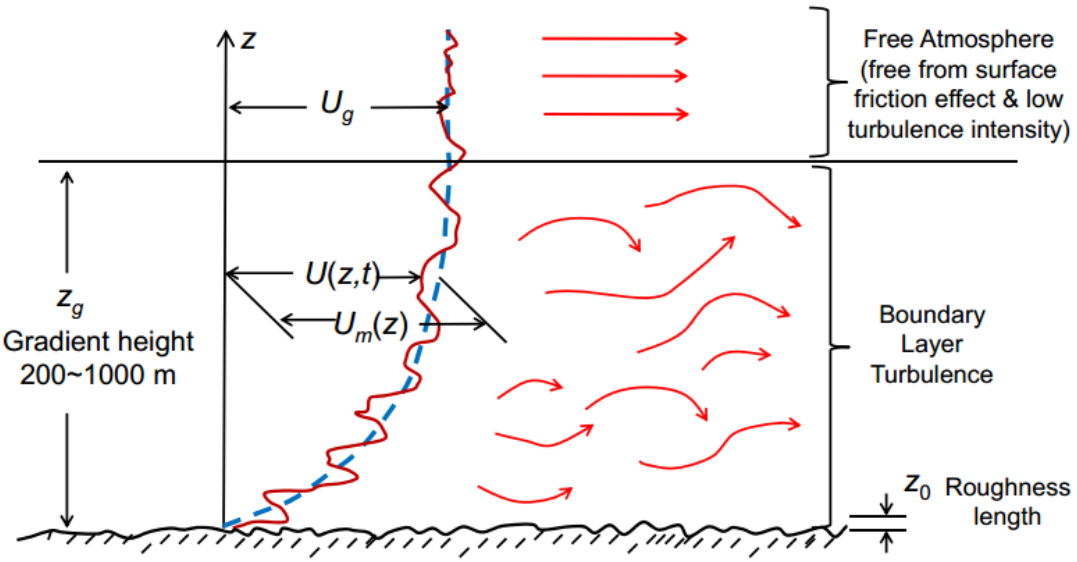

U_g: gradient wind speed (maintained above z_g)

$U(z,t)$: wind speed at height z above the ground

$U_m(z)$ = mean wind speed at height z

z_g = gradient height (depends on surface roughness)

z_0 = roughness length (depends on surface features, vegetation, buildings, etc.)

- - - - - mean wind profile

Figure 2.2: Boundary Layer: A common occurrence with fluid flow over a solid surface

Since several equations are proposed for the determination of turbulence intensity's values by different standards, a summary chart (Fig. 2.3) would be useful:

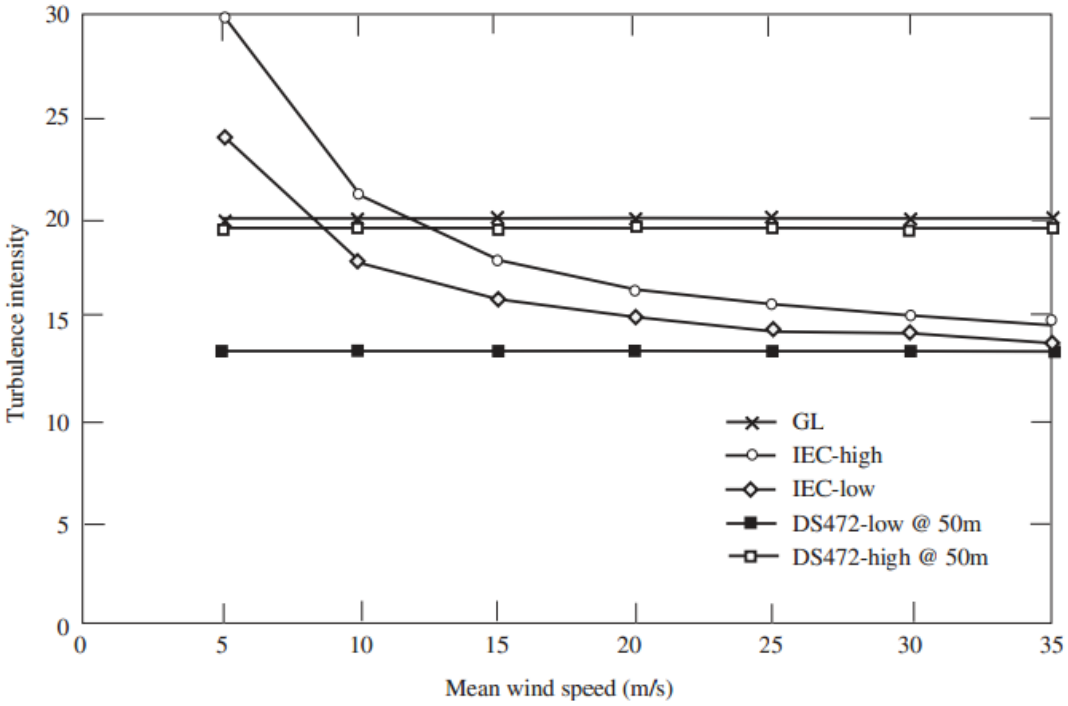

Figure 2.3: Turbulence intensities according to various standards

2.3 The boundary layer properties

The boundary layer and its properties are directly dependant on the strength of the geostrophic wind, the surface roughness, Coriolis effects due to earth's rotation and thermal effects. The latter, can be divided into three categories: stable, unstable and neutral stratification, depending on whether a thermal equilibrium is achieved or not between the warm air rising because of surface heating and the surrounding air at greater heights. Regarding wind energy applications, such as the calculation of turbulent wind loads on a turbine, the most important condition is the one related to neutral stability, since it is accompanied by the strongest winds. However both the unstable and stable stratifications should also be considered as they can cause sudden gusts or asymmetric loadings, respectively.

The surface roughness is taken into account through the roughness length z_0. Typical values of z_0 are presented in Table 2.1:

Type of terrain	Roughness length z_o(m)
Cities, forests	0.7
Suburbs, wooded countryside	0.3
Villages, countryside with trees and hedges	0.1
Open farmland, few trees and buildings	0.03
Flat grassy plains	0.01
Flat desert, rough sea	0.001

Table 2.1: Typical surface roughness lengths

Concerning the Coriolis effect, the Coriolis parameter has to be taken into consideration, defined as in Eq. 2.4:

$$f = 2\Omega \sin|\lambda| \tag{2.4}$$

where Ω is the angular velocity of the earth's rotation and λ is the latitude. Obviously, the latitude at the equator is zero, so the Coriolis parameter is zero at this region, as well.

Regarding the regions of temperate latitude, such as the country of Greece, the height of the boundary layer can be calculated by Eq. 2.5

$$h = u^*/(6f) \tag{2.5}$$

where u^* is the friction velocity, given by Eq.2.6:

$$u^*/\overline{U}(z) = \kappa/[\ln(z/z_0) + \Psi] \tag{2.6}$$

where κ is the von Karman constant (approximately 0.4), z is the height above ground, z_0 is the surface roughness length and Ψ is a function which depends on stability (negative for unstable conditions, positive for stable conditions and equal to $34.5fz/u^*$ for neutral conditions). In most cases regarding temperate latitudes, Ψ is negligible compared to $\ln(z/z_0)$. Thus, if it is ignored, the wind shear is given by the logarithmic wind profile of Eq. 2.7:

$$\overline{U}(z) \propto \ln(z/z_0) \tag{2.7}$$

Alternatively, the wind shear can be given by the power law approximation of Eq. 2.8:

$$\overline{U}(z) \propto z^a \tag{2.8}$$

where α varies with the type of terrain.

2.4 The wind velocity as a stochastic process

It is clear that, since the wind incorporates turbulence in its nature, the total wind velocity cannot be approached by deterministic means alone. It may be stated that the total wind velocity is consisted of two separate parts; the mean wind speed referring to the seasonal, synoptic and diurnal variations on a time-scale of one to several hours and the turbulent fluctuations, with a zero mean when averaged over about 10 min, superimposed.

Modeled as a normal stochastic process, the wind velocity at a given point location in space is mainly described by its power spectral density (PSD) function. However, when referring to structures exposed to airflow, one point characterization is not enough. Several point locations have then to be examined, rendering the wind velocity a stochastic time-dependent field, constituted of the coordinates of each point and the time variable, as well: $V = V(x_1, x_2, x_3, t)$. For a finite number of points, say n, the discretized, stochastic, velocity field may become a *n*-variate, one-dimensional *(n-V - 1D)* stochastic vector process, if the velocities in the different points $V_1(t)$, $V_2(t)$, …, $V_n(t)$ are collected into a vector.

Therefore, the velocity *V(x, y, z; t)* at a given point location can be described either as a one-variate four-dimensional random field *(1V-4D)* or a time-dependent *1V-3D* stochastic field process. According to the previous characterization of the wind velocity as the sum of two separate parts, if $\bar{V}(z)$ is the mean value of V(x, y, z; t), and *v(x, y, z; t)* is its fluctuating component with a zero mean, then Eq. 2.9 holds:

$$V(x, y, z; t) = \bar{V}(z) + v(x, y, z; t) \tag{2.9}$$

As already stated, the mean value can be described by Eq. 2.10 (ignoring the Ψ factor):

$$\bar{V}(z) = \frac{1}{\kappa} u^* \ln(z/z_0) \tag{2.10}$$

where κ=0.4 is the Von Karman constant, u^* is the shear velocity and z_0 is the roughness length.

Regarding the zero-mean normal stochastic field, from a probabilistic point of view, the correlation function has to be determined. In order to simplify the problem, the fluctuating part will be examined as a *1V-2D*, time-dependent stochastic field, that is the *x* coordinate is considered equal to zero. Thus, for two points *P, P'* located in the plane *y-z*, the correlation function is given in Eq. 2.11:

$$R_V(y, z, y', z'; t, t') = E[V(y, z; t)\, V(y', z'; t')] \tag{2.11}$$

where *E [ ]* is the stochastic average. If Eq. 2.12 holds

$$R_V(y, z, y', z'; t, t') = R_V(\eta, \zeta; \tau) \tag{2.12}$$

where (Eq. 2.13)

$$\eta = y - y', \qquad \zeta = z - z', \qquad \tau = t - t', \tag{2.13}$$

then the (stationary) field is called "homogeneous". In this case, the correlation function $R_V(\eta, \zeta; \tau)$ is symmetric with respect to the separation distances η, ζ; τ, which means that (Eq. 2.14):

$$R_V(\eta, \zeta; \tau) = R_V(-\eta, -\zeta; -\tau) \tag{2.14}$$

Furthermore, if the homogeneous field depends only on *ν*, the absolute value of the distance between the two points' locations, then the field is also called "isotropic" and the following relation (Eq. 2.15) holds:

$$R_V(\eta, \zeta; \tau) = R_V(\nu; \tau) \tag{2.15}$$

For a homogeneous field, the threefold Fourier transformation of $R_V(\eta, \zeta; \tau)$ yields the so-called PSD function of *V(y, z; t)* (Eq. 2.16):

$$S_V(k_1, k_2; \omega) = \frac{1}{(2\pi)^3} \iiint_{-\infty}^{\infty} R_V(\eta, \zeta; \tau)\, exp[-i(k_1\eta + k_2\zeta + \omega\tau)] d\eta\, d\zeta\, d\tau \tag{2.16}$$

where k_1, k_2 are wave numbers and ω is the radian circular frequency. The inverse relationship of Eq. 2.16 is the Eq. 2.17:

$$R_V(\eta, \zeta; \tau) = \iiint_{-\infty}^{\infty} S_V(k_1, k_2; \omega)\ exp[i(k_1\eta + k_2\zeta + \omega\tau)] dk_1\, dk_2\, d\omega \tag{2.17}$$

This pair of equations constitutes the n-dimensional version of the Wiener-Khintchine transform pair.

Since the correlation function of the random wind field velocity depends on *z* and *z'* taken separately, the field is not homogeneous. In this case, in order to fully characterize the velocities of two points, $V_1 = V(y_1, z_1;\ t_1)$ and $V_2 = V(y_2, z_2;\ t_2)$, as two stochastic processes, the complex cross-PSD function (Eq. 2.18) is required:

$$S_{V_1V_2}(\omega) = \sqrt{S_{V_1V_1}(\omega) S_{V_2V_2}(\omega)} \exp[-f_{12}(\omega)] \tag{2.18}$$

where the imaginary part has been neglected and $\exp[-f_{12}(\omega)]$ is the so-called "coherency function", in which (Eq. 2.19):

$$f_{12}(\omega) = \frac{|\omega| \sqrt{C_y^2\eta^2 + C_z^2\zeta^2}}{2\pi[\bar{V}(z_1) + \bar{V}(z_2)]} \tag{2.19}$$

where C_y and C_z are appropriate decay coefficients.

The corresponding correlation function is derived by the Fourier transformation of Eq. (2.18), that is (Eq. 2.20):

$$R_{V_1V_2}(\tau) = \int_{-\infty}^{\infty} S_{V_1V_2}(\omega) e^{i\omega\tau} d\omega \tag{2.20}$$

From Eqs. (2.18) to (2.20) it is obvious that the correlation function of the wind fluctuations depends on τ (stationary in time), η, ζ, the mean values $\bar{V}(z_1)$, $\bar{V}(z_2)$ and also on $S_{V_1V_1}(\omega), S_{V_2V_2}(\omega)$ which are directly related to the height from the ground.

On the other hand, in the case of an imaginary string-like exposed structure, existing only in the plane *y-z*, the wind velocity field would be not only homogeneous but isotropic, as well. Indeed, between two points P_1, P_2 of this string-like structure, the cross-PSD function would be (Eq. 2.21):

$$S_{V_1V_2}(\omega) = S_{VV}(\omega) exp\left(-\frac{C_y d}{4\pi\bar{V}(h)}|\omega|\right) \tag{2.21}$$

where *h* is the height from the ground and *d* is the distance between the two points. Then, the Fourier transform of Eq. (2.21) yields the corresponding correlation function (Eq. 2.22):

$$R_{V_1V_2}(\eta, \zeta; \tau) = R_{V_1V_2}(d; \tau) \tag{2.22}$$

which shows that the random field is isotropic, since the correlation function depends only on the absolute value of the distance between the two point locations (isotropic in the space) and on the time difference τ (stationary in time). It should be noted, however, that the cross-PSD, given in Eq. (2.21), is not the complete Fourier transform of the random field already defined in Eq. (2.17), because the physical variables are defined over a mixed spatial-temporal grid of points. The complete Fourier transformation of Eq. (2.22), with the incorporation of the wave number *k*, would be Eq. 2.23:

$$S_V(k, \omega) = 4S_{VV}(\omega) \frac{\omega C_y}{C_y^2\omega^2 + k^2[4\pi\bar{V}(h)]^2} \tag{2.23}$$

Regarding $S_{VV}(\omega)$, several spectra have been proposed in the literature, i.e. (Eqs. 2.24, 2.25)

Kaimal spectrum: $$\frac{nS_{VV}(\omega)}{\sigma_V^2} = \frac{4nL_u/\bar{V}}{(1 + 6nL_u/\bar{V})^{5/3}} \tag{2.24}$$

von Karman spectrum: $$\frac{nS_{VV}(\omega)}{\sigma_V^2} = \frac{4nL_u/\bar{V}}{(1 + 70.8(nL_u/\bar{V})^2)^{5/6}} \tag{2.25}$$

where *n* denotes the frequency in Hz, L_u the integral length scale of turbulence and σ_V^2 the variance of the longitudinal component of the velocity fluctuations.

In the wind field simulation of the present thesis, the more recent Solari model has been used (Eq. 2.26):

$$S_{VV}(\omega) = \frac{6.868\sigma_V^2 f L_u/h}{(\omega/2\pi)(1+10.302 f L_u/h)^{5/3}} \tag{2.26}$$

Here, f represents the Monin coordinate (Eq. 2.27):

$$f = \frac{\omega h}{2\pi \bar{V}(h)} \tag{2.27}$$

With these tools in hand, the zero-mean normal stochastic vector process, *V(t)*, can now be completely characterized by means of the PSD matrix $S_V(\omega)$. This matrix is symmetric, positive and, with its imaginary part neglected, it can be defined as follows (Eq. 2.28):

$$S_V(\omega) = \begin{bmatrix} S_{V_1V_1}(\omega) & S_{V_1V_2}(\omega) & \cdots & S_{V_1V_n}(\omega) \\ S_{V_1V_2}(\omega) & S_{V_2V_2}(\omega) & \cdots & S_{V_2V_n}(\omega) \\ \vdots & \vdots & \cdots & \vdots \\ S_{V_1V_n}(\omega) & S_{V_2V_n}(\omega) & \cdots & S_{V_nV_n}(\omega) \end{bmatrix} \tag{2.28}$$

where $S_{V_jV_k}(\omega)$ is given in Eq. (2.18), while $S_{V_jV_j}(\omega)$ is defined in Eq. (2.26), after properly selecting the height from the ground and the distance between the location points P_j and P_k.

2.5 Wind simulation

Concerning the problem of digital simulation of the wind field, the simplest way to approach it is by means of the discretized version of the stochastic field, since, as already stated, the field is not homogeneous.

For a zero-mean normal 1V-1D stochastic process *V(t)* the digital simulation can be achieved by three different methods:

1. the transformational method, based on filtering Gaussian white noise signals;

2. the correlation method, in which the velocity of a small body of air at the end of a time step is calculated as the sum of a velocity correlated with the velocity at the start of the time step and a random, uncorrelated increment;

3. the harmonic series method, involving the summation of a series of cosine waves at different frequencies with amplitudes weighted in accordance with the power spectrum.

Since the last method is now the one in widest use, the digital simulation of the wind field in this thesis will be performed by superposition of harmonic waves. In this case, the stochastic process is given in two different forms. The first one is described by Eq. 2.29:

$$V(t) = \sum_{j=1}^{N} \sqrt{2S_{VV}(\omega)\Delta\omega}\cos(\omega_j t + \varphi_j) \tag{2.29}$$

where $\omega_j = j\Delta\omega$ $(j = 1, 2, \dots, N)$, $N\Delta\omega = \omega_u$ is the upper cut-off frequency above which $S_{VV}(\omega)$ may be assumed to be zero and φ_j are independent phase angles uniformly distributed over the range (0 - 2π).

Alternatively, the following representation (Eq. 2.30) of stationary random process can be used:

$$V(t) = \int_{-\infty}^{\infty} \sqrt{S_{VV}(\omega)}\, e^{i\omega t} dB(\omega) \tag{2.30}$$

where *B(ω)* is a zero-mean normal complex process having orthogonal increments, that is (Eq. 2.31):

$$\begin{aligned} E[dB(\omega)] = 0, \qquad & dB(\omega) = dB^*(-\omega), \\ & E[dB(\omega_r)\, dB^*(\omega_s)] = \delta_{\omega_r\omega_s}\, d\omega_r \end{aligned} \tag{2.31}$$

where the star means complex conjugate and δ is the Kronecker delta ($\delta_{\omega_r\omega_s} = 1$ if $\omega_r \equiv \omega_s$, $\delta_{\omega_r\omega_s} = 0$ if $\omega_r \neq \omega_s$). The stochastic process *V(t)* is a real process whose PSD function is $S_{VV}(\omega)$ and the corresponding correlation function is (Eq. 2.32):

$$\begin{aligned} & R_{VV}(\tau) = E[V(t+\tau)\, V^*(t)] \\ & = \int_{-\infty}^{\infty}\int_{-\infty}^{\infty} \sqrt{S_{VV}(\omega_1)S_{VV}(\omega_2)}\, e^{i\omega_1(t+\tau)} e^{-i\omega_2 t} dB(\omega_1)\, dB^*(\omega_2) \\ & \overset{(2.31)}{\Longrightarrow} R_{VV}(\tau) = \int_{-\infty}^{\infty} S_{VV}(\omega) e^{i\omega t} d\omega = \int_{-\infty}^{\infty} S_{VV}(\omega)\cos\omega\tau\, d\omega \end{aligned} \tag{2.32}$$

The discretized version of Eq. (2.30) is given by Eq. 2.33:

$$V(t) = \sum_{j=-N}^{N} \sqrt{S_{VV}(\omega_j)\Delta\omega}\ \exp(i\omega_j t)\, P_j \tag{2.33}$$

where P_j are independent zero mean, complex random numbers normally distributed with unit variance and, hence, Eq. 2.34 holds:

$$E[P_j] = 0, \qquad E[P_j\ , P_k^*] = \delta_{jk}\,, \qquad P_{-k} = P_k^* \tag{2.34}$$

The real form of Eq. (2.33) is the following (Eq. 2.35):

$$V(t) = 2\sum_{j=-N}^{N} \sqrt{S_{VV}(\omega_j)\Delta\omega}\ (R_j cos\ \omega_j t + I_j sin\omega_j t) \tag{2.35}$$

where, for the real (R_j) and imaginary (I_j) part of P_j,it is (Eq. 2.36):

$$P_j = R_j - iI_j \tag{2.36}$$

As stated in section 4, the collection of the 1V-1D stochastic processes $V_j(x_j,\ y_j,\ z_j;\ t)$ into an *n*-vector *V(t)* transforms the time-dependent field into a *n*V-1D stochastic process, that is, into a multivariate one-dimensional field. For this type of field, once the PSD matrix is determined, the next step for the digital simulation is the decomposition of the PSD matrix. This can be achieved with the help of two different approaches, which are:

1. the Choleski method
2. the Proper Orthogonal Decomposition (P.O.D.)

In the first case, the PSD matrix is equated to the product of a triangular transformation matrix, *H*, and its transpose, H^T (Eq. 2.37):

$$S_V(\omega) = H(\omega)H^*(\omega)^T \tag{2.37}$$

where $H(\omega)$ is given by Eq. 2.38:

$$H(\omega) = \begin{bmatrix} H_{11}(\omega) & & & \\ H_{21}(\omega) & H_{22}(\omega) & & \\ \vdots & \vdots & & \\ H_{n1}(\omega) & H_{n2}(\omega) & \cdots & H_{nn}(\omega) \end{bmatrix} \tag{2.38}$$

If the quadrature spectrum is neglected, then the matrix *H* is a real one. The $H_{ij}(\omega)$ elements can be determined using the standard Choleski method. Then, the generation of the multivariate stochastic process can be performed as in Eq. 2.39:

$$V_r(t) = \int_{-\infty}^{\infty} H_{r1}(\omega)\, e^{i\omega t} dB_1(\omega) + \int_{-\infty}^{\infty} H_{r2}(\omega)\, e^{i\omega t} dB_2(\omega) + \cdots + \int_{-\infty}^{\infty} H_{rr}(\omega)\, e^{i\omega t} dB_r(\omega), \qquad r = 1, 2, \ldots, n \tag{2.39}$$

where δ is the Kronecker delta and $dB_j(\omega)$ are independent orthogonally incremental stochastic processes, such that Eq. 2.40 holds:

$$E\left[dB_j(\omega_r)\, dB_k(\omega_s)\right] = \delta_{\omega_r \omega_s}\, \delta_{jk}\, d\omega_r \tag{2.40}$$

The discretized version of Eq. (2.40) which can be used for digital simulation purposes is given by Eq. 2.41:

$$V_r(t) = 2\sum_{j=1}^{N}\left[H_{r1}(\omega_j) g_j^{(1)}(t) + H_{r2}(\omega_j) g_j^{(2)}(t) + \cdots + H_{rr}(\omega_j) g_j^{(r)}(t)\right]\sqrt{\Delta\omega} \tag{2.41}$$

where $g_j^{(k)}(t)$ is described by Eq. 2.42:

$$g_j^{(k)}(t) = R_j^{(k)} \cos\omega_j t + I_j^{(k)} \sin\omega_j(t) \tag{2.42}$$

with $R_j^{(k)}$, $I_j^{(k)}$ being zero-mean normal random numbers obeying the orthogonality relationships of Eq. 2.43:

$$E\left[R_j^{(r)}\, R_k^{(s)}\right] = \frac{1}{2}\delta_{jk}\, \delta_{rs}\,, \qquad E\left[I_j^{(r)}\, I_k^{(s)}\right] = \frac{1}{2}\delta_{jk}\, \delta_{rs}\,, \qquad E\left[R_j^{(r)}\, I_k^{(s)}\right] = 0 \tag{2.43}$$

A useful alternative states that the vector process *V(t)* can be written as a summation of independent fully coherent stochastic processes as follows (Eq. 2.44):

$$V(t) = \sum_{k=1}^{n} Y_k(t) \tag{2.44}$$

where $Y_k(t)$ is given by Eq. 2.45:

$$Y_k(t) = \int_{-\infty}^{\infty} q_k(\omega) e^{i\omega t} dB_k(\omega) \tag{2.45}$$

Here, $dB_k(\omega)$ again obey the Eq. (2.40) and $q_k(\omega)$ are *n*-vectors which, if collected in a square matrix *Q(ω)*, satisfy the following relationship (Eq. 2.46):

$$Q(\omega)\, Q^*(\omega)^T = S_V(\omega) \tag{2.46}$$

Concerning the wind velocity, the matrix *Q(ω)* is a real one. The decomposition of the matrix $S_V(\omega)$ can now be achieved by an infinite number of ways. One of them is to set the *Q(ω)* matrix as the previously mentioned matrix *H(ω).* In this case, Eq. (2.44), in conjunction with Eq. (2.45), yields the same result with Eq. (2.39). Therefore, Eq. (2.45) can be written in a discretized form as in Eq. 2.47:

$$Y_k(t) = 2\sum_{j=1}^{N}\left[q_k(\omega) g_j^{(k)}(t)\right]\sqrt{\Delta\omega} \tag{2.47}$$

which exactly coincides with Eq. (2.41).

On the other hand, the P.O.D. method is based on the decomposition of the PSD matrix in its frequency-dependent eigenvectors.

If $\psi_k(\omega)$ is the *k*th eigenvector, normalized with respect to the identity matrix, then, for the square matrix $\Psi(\omega)$, named the "spectral matrix" and being the collection of these vectors, the orthogonality relationships of Eq. 2.48 hold:

$$\Psi^T(\omega)\,\Psi(\omega) = I, \qquad \Psi^T(\omega)\, S_V(\omega)\Psi(\omega) = \Lambda(\omega) \tag{2.48}$$

Here, the matrix $\Lambda(\omega)$ is diagonal and consists of the eigenvalues of the matrix $S_V(\omega)$. The eigenvectors are orthogonal and, since the quadrature spectrum is neglected, they are real as well. Thus, the generation of the wind field can be performed as in Eq. 2.49:

$$Y_k(t) = \int_{-\infty}^{\infty} \psi_k(\omega)\, \sqrt{\Lambda_k(\omega)}\, e^{i\omega t}\, dB_k(\omega) \tag{2.49}$$

The discretized version of Eq. (2.49), which can be used for digital simulation purposes, is described by Eq. 2.50:

$$Y_k(t) = 2\sum_{j=1}^{N} \psi_k(\omega_j)\sqrt{\Lambda_k(\omega_j)\Delta\omega}\, g_j^{(k)}(t) \tag{2.50}$$

In the present thesis, the P.O.D. method was used for the digital simulation of the stochastic part of the wind field, due to the conclusions of M. Di Paola. However it has to be noted that in most cases, the Choleski method is suggested, since the spectral decomposition using the eigenvectors is computationally significantly more

demanding. This can be derived from the fact that, by examining the previous equations, the computational effort for the Choleski decomposition increases with the $n(n+1)/2$ law while for the P.O.D. method the same increase follows the n^2 law.

3 Aerodynamics of a wind turbine

3.1 Actuator disk concept

The apprehension of the theory behind the function of a wind turbine is founded on the principal concept of the actuator disk. Without having any specific design in mind, this fundamental idea can be described as follows.

To begin with, we make the initial, simplistic assumption that the blades of the wind turbine are expanded to form a uniform disk, called "the actuator disk". This hypothesis, although seemingly over-simplifying, is capable of providing a rough but useful description of an, otherwise, rather complicated phenomenon. The man behind this conception is Albert Betz, who, between 1922 and 1925 published writings to show that, by applying elementary physical laws, it is possible to obtain a common physical basis for the understanding of the operation of wind energy converters, irrespective to their designs.

Betz's "momentum theory", as the whole of the idea is named, assumes a lossless energy converter, operating in a steady, frictionless airflow. Moreover, the air flow is considered inviscid, incompressible and only axial. The mass of air passing through the actuator disc and, thus, being affected by it, is, in a theoretical manner, separated from the total mass flow. A boundary surface is, therefore, created in the three-dimensional space, which forms a stream-tube from the upstream to the downstream of the rotor. No mass can be transferred through this surface.

While the air is approaching the actuator disc, it is gradually slowed down, losing its initial kinetic energy:

$$E = \frac{1}{2}mu^2 \quad (N*m) \tag{3.1}$$

The mass flow of density ρ, passing through a cross-sectional area A with velocity u, is:

$$\dot{m} = \rho u A \qquad (Kg/s) \tag{3.2}$$

and the corresponding volume:

$$\dot{V} = uA \qquad (m^3/s) \tag{3.3}$$

These equations show that, while the air has its velocity reduced, the above-mentioned stream-tube has to expand, so that the mass flow rate remains the same. The closer the air particles get to the actuator disc, the slower they become, while the cross-sectional area of the stream tube is gradually widened. These simultaneous phenomena reach a peak at a short distance after the contact with the disc. Thereafter,

air velocity and stream-tube volume slowly gain their initial values as the air mass returns to its free-flow state. Figure 3.1 depicts the above process up to its peak:

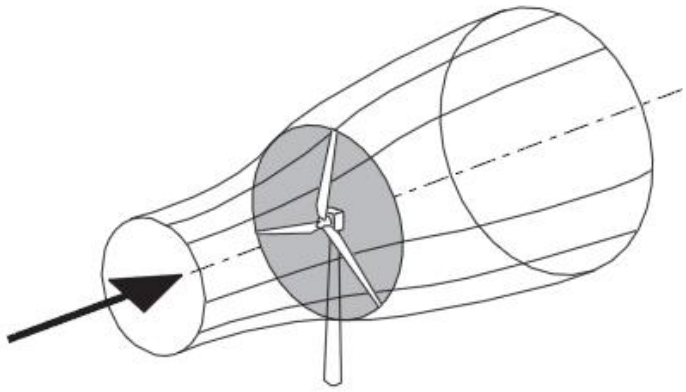

Figure 3.1: The energy extracting stream-tube of a wind turbine

Meanwhile, as the initial velocity of the stream is reduced while approaching the actuator disk, the dynamic pressure is also reduced and therefore, since the total pressure has to be constant along the streamline, the static pressure is forced to an increase. On the other hand, right behind the rotor, the reverse procedure takes place until the free-flow values are reached again.

To observe the phenomenon in greater detail we can use Figure 3.2, below:

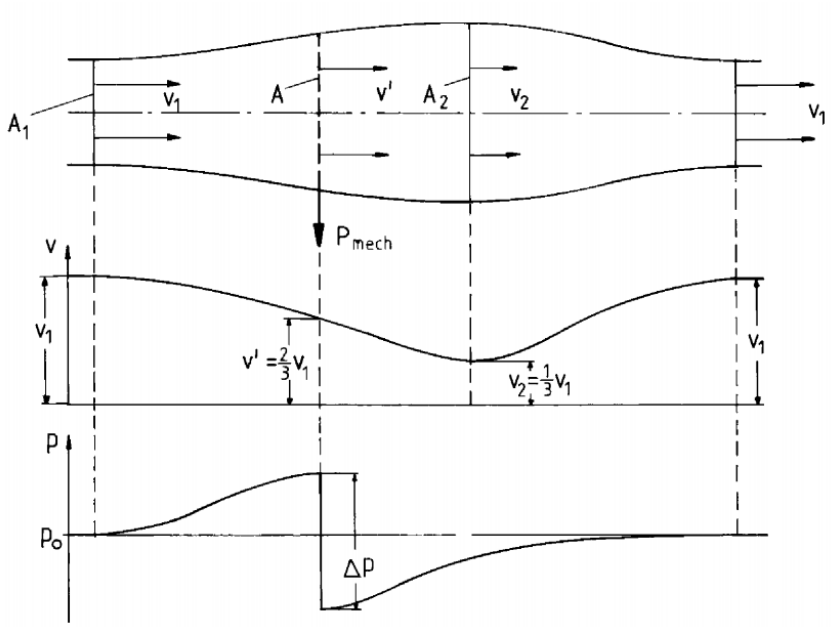

Figure 3.2: Flow conditions of the stream through an ideal disk-shaped energy converter with the maximum possible extraction of mechanical power

Here, v_1 is the free-stream air velocity before the disk, whereas v' represents the flow velocity through the converter and v_2 is the air velocity behind the disk. From now on, though, these symbols will be substituted for V_∞ , V_d and V_w respectively. As mentioned before, v_1 is restored again, beyond the influence of the rotor. The

indicator “w” is referred to the term “wake” as the area behind the actuator disk is called.

The diagram in the middle of the figure depicts the variation of the velocity of the air stream, while the latter is gradually affected by the rotor. The third diagram shows the static pressure variation accordingly. Since the flow is stationary, incompressible, frictionless and no external forces act on the fluid, the static pressure remains constant in the far upstream and downstream boundaries and Bernoulli equation is valid from far upstream to just in front of the rotor and from just behind the rotor to far downstream:

$$\begin{cases} p_\infty + \frac{1}{2}\rho V_\infty^2 = p_d + \frac{1}{2}\rho V_d^2 \\ p_d - \Delta p + \frac{1}{2}\rho V_d^2 = p_\infty + \frac{1}{2}\rho V_w^2 \end{cases} \qquad (N/m^2) \tag{3.4}$$

Thus, the pressure drop Δp over the rotor is obtained:

$$\Delta p = \frac{1}{2}\rho(V_\infty^2 - V_w^2) \qquad (N/m^2) \tag{3.5}$$

In order to produce a relation between the velocities V_∞ , V_d , V_w , we have to reconsider the goal of a rotor, which obviously is to convert the kinetic energy of the free-flow wind to mechanical work. The equations expressing the kinetic energy of the moving air and the mass flow yield the amount of energy passing through cross-section A per unit time. The mechanical energy, which the disk-shaped converter extracts from the airflow, corresponds to the power difference of the air stream before and after the converter:

$$\begin{aligned} P &= \frac{1}{2}\rho A_\infty V_\infty^3 - \frac{1}{2}\rho A_w V_w^3 \\ &= \frac{1}{2}\rho(A_\infty V_\infty^3 - A_w V_w^3) \qquad (W) \end{aligned} \tag{3.6}$$

Since the mass flow has to be maintained, then

$$\rho V_\infty A_\infty = \rho V_w A_w \qquad (kg/s) \tag{3.7}$$

and thus,

$$P = \frac{1}{2}\rho V_\infty A_\infty (V_\infty^2 - V_w^2) \qquad (W) \tag{3.8}$$

or

$$P = \frac{1}{2}\dot{m}(V_\infty^2 - V_w^2) \qquad (W) \tag{3.9}$$

One could assume that, in order to maximize the power, the value of V_w would have to be zero. In other words the air should lose all its velocity just behind the converter and thus become still. This would also mean, however, that the inflow velocity right before the converter should have a zero value as well, thus making the air flow impossible. A physically more rational case would occur at a certain ratio of V_w/V_∞, at which the power would reach its greatest possible value.

Having this in mind, we continue seeking a relation between the velocities using another utility - the momentum conservation law. The force which the air exerts on the converter, defined as "thrust"[1], can be expressed as:

$$F = \dot{m}(V_\infty - V_w) \qquad (N) \tag{3.10}$$

and has to be equally exerted to the air by the converter as a reaction, thus producing power equal to:

$$P = FV_d = \dot{m}(V_\infty - V_w)V_d \qquad (W) \tag{3.11}$$

This power is equal to that derived from the conservation of mass, thus yielding the following equation:

$$\frac{1}{2}\dot{m}(V_\infty^2 - V_w^2) = \dot{m}(V_\infty - V_w)V_d \qquad (W) \tag{3.12}$$

or

$$V_d = \frac{1}{2}(V_\infty + V_w) \qquad (m/s) \tag{3.13}$$

which corresponds to the arithmetic mean of V_∞ and V_w.

Using the equation above, the mass flow can now be rewritten as:

$$\dot{m} = \rho A V_d = \frac{1}{2}\rho A(V_\infty + V_w) \qquad (Kg/s) \tag{3.14}$$

and the power output of the converter as:

$$P = \frac{1}{4}\rho A(V_\infty^2 - V_w^2)(V_\infty + V_w) \qquad (W) \tag{3.15}$$

[1] Beyond this point, the symbol referring to the thrust of the rotor will be the word's initial letter: "T".

The output of a converter, though, would mean nothing without being compared to the potential of the free flow, or in other words, the power of the unobstructed air stream:

$$P_0 = \frac{1}{2}\rho A V_\infty^3 \qquad (W) \tag{3.16}$$

Thus, the efficiency of the converter can be represented by the following ratio, named "power coefficient", or "c_P":

$$c_P = \frac{P}{P_0} = \frac{\frac{1}{4}\,\rho A(V_\infty^2 - V_w^2)(V_\infty + V_w)}{\frac{1}{2}\rho A V_\infty^3} = \frac{1}{2}\left[1 - \left(\frac{V_w}{V_\infty}\right)^2\right]\left(1 + \frac{V_w}{V_\infty}\right) \tag{3.17}$$

The graphical representation of the power coefficient versus the ratio of the flow velocity, before and after the actuator disk, can provide us with a maximum value as the following chart shows:

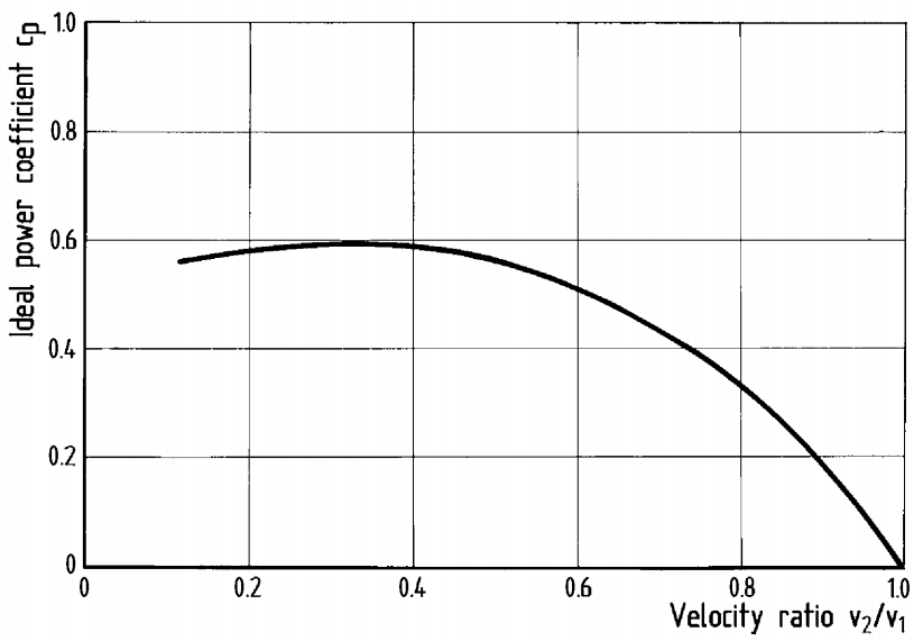

Figure 3.3: Power coefficient versus the flow velocity ratio of the flow before and after the energy converter

Both graphically and analytically, as will later be shown, the maximum value of the c_p can be obtained for $V_w/V_\infty = 1/3$ and becomes:

$$c_P = \frac{16}{27} = 0.593 \tag{3.18}$$

Therefore, ideally, the flow velocity at the actuator disk shall be:

$$V_d = \frac{2}{3} V_\infty \tag{3.19}$$

and the velocity at the far wake:

$$V_w = \frac{1}{3} V_\infty \tag{3.20}$$

Thus, the values in figure 2 can now be realized.

Already mentioned Mr. Betz is again responsible for the derivation of this upper limit of the power coefficient and, consequently, this value of c_P is named after him as “Betz limit” or “Betz factor”.

Considering the reduction in velocity, we can make the assumption that, while the air stream approaches the disk, a variation is superimposed on its free -flow velocity. The stream-wise component of this induced flow at the disk is given by $-aV_\infty$, where a is called “axial flow induction factor”. The so called factor can, then, be defined as:

$$a = \frac{V_\infty - V_d}{V_\infty} \tag{3.21}$$

A new relation can now be derived between the free-flow velocity and that at the rotor plane, using a:

$$V_d = (1 - a)V_\infty \tag{3.22}$$

as well as a new one between the free-stream velocity and that of the far wake:

$$V_w = (1 - 2a)V_\infty \tag{3.23}$$

It is now obvious that the wind loses half its initial speed upstream of the actuator disk and half of it downstream.

Using the relations above, it is possible to rewrite the power *P* and the thrust *T* as:

$$P = 2\rho A V_\infty^3 a(1 - a)^2 \tag{3.24}$$

$$T = 2\rho A V_\infty^2 a(1 - a) \tag{3.25}$$

and therefore, the power coefficient becomes

$$c_P = 4a(1 - a)^2 \tag{3.26}$$

By differentiating c_P with respect to a, we can obtain the analytical solution of the -previously graphically solved problem- of the maximization of the power, yielded by the ideal wind turbine:

$$\frac{dc_P}{da} = 4(1-a)(1-3a) \tag{3.27}$$

which proves that the Betz limit of $c_{P_{max}} = \frac{16}{27} = 0.593$ for $a = {}^{1}/_{3}$ is correct.

Another coefficient can now be introduced, related to the available thrust as a fraction of the force that the free-stream wind would exert on the actuator disk. That would be the so called "thrust coefficient", or c_T :

$$c_T = \frac{T}{T_0} = \frac{\rho A V_d (V_\infty - V_w)}{\frac{1}{2}\rho A V_\infty^2} \tag{3.28}$$

which can be redefined as a function of α :

$$c_T = 4a(1-a) \tag{3.29}$$

The following chart (Figure 3.4) depicts the relation between the axial induction factor and both the power and thrust coefficients. It is clearly shown that the maximum power limit is reached for a lower induction factor value than the maximum thrust limit.

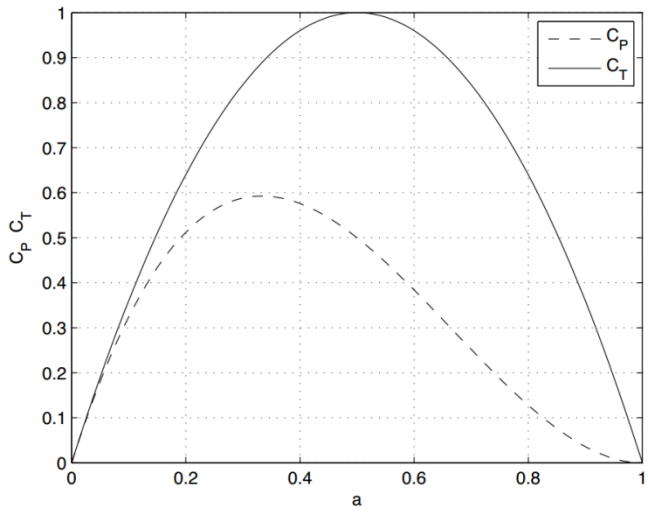

Figure 3.4: Power and drag coefficients C_P and C_T as a function of the axial induction factor a

3.2 Rotor disk theory

Approaching the real case a little more, we have to realize that an energy converter is not a static disk but one that rotates with an angular velocity Ω, about an

axis normal to the rotor plane and parallel to the direction of the wind movement. As the air is passing through the rotating disk, in order to resist the consequent change to its initial condition, it exerts an angular force to the rotor, in a direction opposite to that of the rotation of the disk. This reaction counteracts the torque exerted by the rotor to the air, keeping the rotational speed constant. The work done by the aerodynamic torque on the generator is converted into electrical energy. On the other hand, the above-mentioned reaction causes, as an aftereffect, the air particles to gain angular momentum and thus to have both a tangential as well as an axial velocity component. This results to an increase of the kinetic energy, compensated by an abrupt drop of the static pressure, right behind the actuator disk, additional to that described in the previous section. The change of the tangential velocity from zero to its highest value, takes place entirely in inside the thickness of the disk. In order to determine the amount of such a speed increase, another factor has to be introduced; the "tangential induction factor", symbolized by a*'*. With this parameter's help, we can follow the gradual increase of the tangential velocity: at the middle of the disk thickness and at a radial distance *r* from the axis of rotation, the induced tangential velocity is *Ωr*a*'*, while, immediately downstream, it changes to *2Ωr*a*'*.

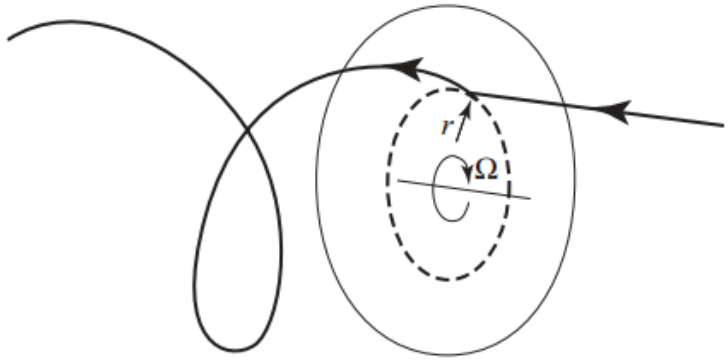

Figure 3.5: The trajectory of an air particle passing through the rotor disk

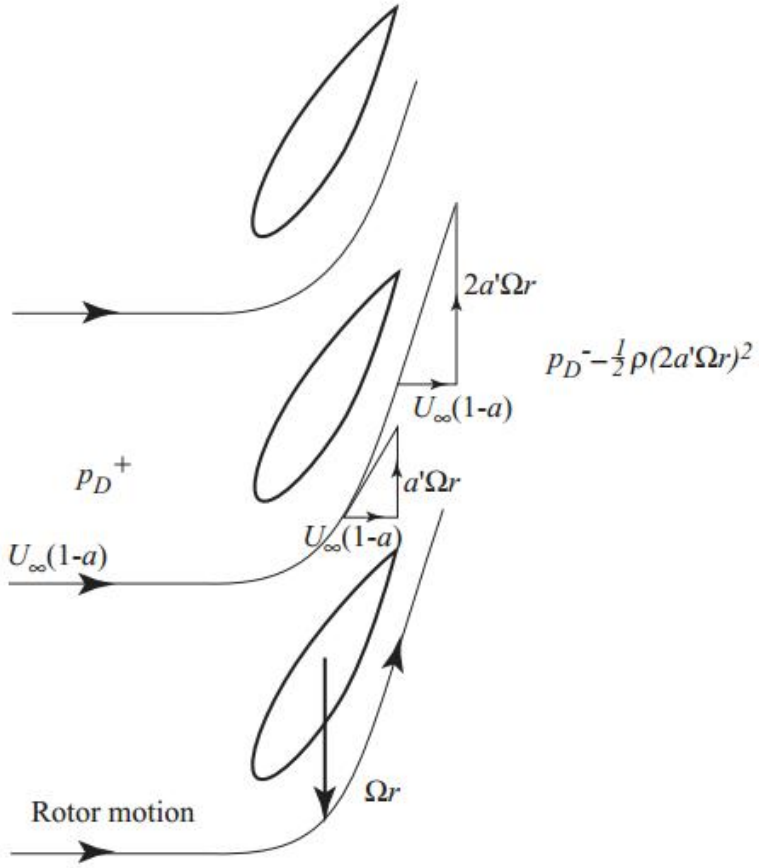

Figure 3.6: Tangential velocity grows across the disk thickness

It is obvious that these values are radius-depended and this applies to the axial induced velocity, as well. To further examine the behavior of both the air particles and the rotor, we can assume that the whole disk comprises a multiplicity of annular rings of radius *dr*, with each ring acting independently.

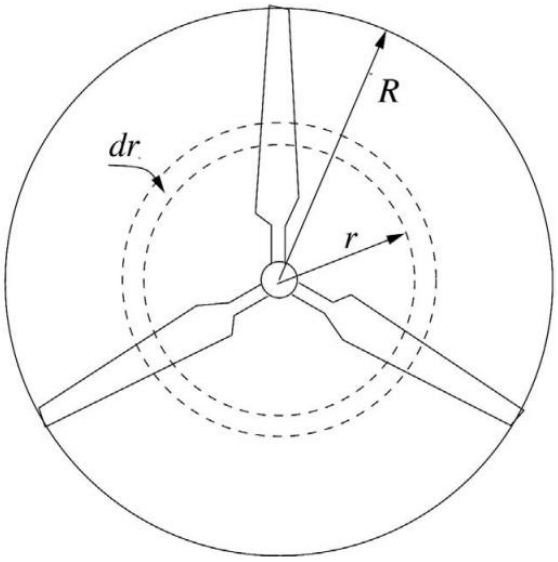

Figure 3.7: Rotor of a three-bladed wind turbine with rotor radius *R*

Having one of these fictional rings in mind, we can calculate the torque exerted to the air passing through an area of $\delta A_d = 2\pi r \delta r$,that the ring covers:

$$\delta Q = \rho \delta A_d V_\infty (1-a) 2\Omega \mathrm{a}' r^2 \tag{3.30}$$

This torque, however, is also the one which produces power by driving the rotor shaft. Thus, the power output can be determined:

$$\delta P = \delta Q \Omega = \rho \delta A_d V_\infty (1-a) 2\Omega^2 \mathrm{a}' r^2 \tag{3.31}$$

Equating this result with the one yielded in the previous section, we take:

$$\rho \delta A_d V_\infty (1-a) 2\Omega^2 \mathrm{a}' r^2 = 2\rho \delta A_d V_\infty^3 a (1-a)^2 \tag{3.32}$$

or

$$V_\infty^2 a(1-a) = \Omega^2 r^2 a' \tag{3.33}$$

We call the ratio $\Omega r / V_\infty$ "local speed ratio", or "λ_r", and it represents a comparison between the tangential velocity of the spinning annual ring and the free-stream air velocity. At the edge of the disk $r = R$ and so, $\lambda = \Omega R / V_\infty$ is called "tip speed ratio". Therefore:

$$a(1-a) = \lambda_r^2 a' \tag{3.34}$$

Inducing the local speed ratio into the previous equation corresponding to the power output of the shaft, we get:

$$\delta P = dQ\Omega = \left(\frac{1}{2}\rho V_\infty^3 2\pi r \delta r\right) 4a'(1-a)\lambda_r^2 \tag{3.35}$$

Substituting the term outside the brackets with "η_r", we have:

$$\delta P = \left(\frac{1}{2}\rho V_\infty^3 2\pi r \delta r\right) \eta_r \tag{3.36}$$

Apparently, the term inside the brackets depicts the power potential of the free-flow wind through the annular ring, while "η_r" represents the efficiency of the blade element in "seizing" the power available.

In order to determine the optimum values of *a* and *a'* we have to differentiate η_r by either factor and put the result equal to zero:

$$\frac{\partial \eta_r}{\partial a} = 0 \rightarrow \frac{\partial [4a^{'}(1-a)\lambda_r^2]}{\partial a} = 0 \rightarrow 4\lambda_r^2 \left[(1-a)\frac{da'}{da} - a'\right] = 0 \rightarrow \frac{da'}{da} = \frac{a'}{(1-a)} \tag{3.37}$$

Differentiating the previously yielded equation:

$$a(1-a) = \lambda_r^2 a' \tag{3.38}$$

by *a*, we also take:

$$\frac{d[a(1-a)]}{da} = \lambda_r^2 \frac{da'}{da} \rightarrow \frac{da'}{da} = \frac{(1-2a)}{\lambda_r^2} \tag{3.39}$$

By combining the last three equations, the optimum values for *a* and *a'* are yielded:

$$a = \frac{1}{3} \quad , \quad a^{'} = \frac{a(1-a)}{\lambda^2 \mu^2} \tag{3.40}$$

where μ represents the ratio r/R and shows that, while the optimum value of *a* remains uniformly constant, the ideal value of *a'* varies with radius.

Now, the maximum power can be determined in the non-dimensional form of the power coefficient:

$$\frac{dc_P}{dr} = \frac{4\pi\rho V_\infty^3 (1-a)a^{'\lambda_r^2} r}{\frac{1}{2}\rho V_\infty^3 \pi R^2} = \frac{8(1-a)a^{'\lambda_r^2} r}{R^2} \tag{3.41}$$

or

$$\frac{dc_P}{d\mu} = 8(1-\mathrm{a})\mathrm{a}'\lambda^2\mu^3 \tag{3.42}$$

and after integration:

$$\int_0^1 8(1-\mathrm{a})\mathrm{a}^{'\lambda^2\mu^3} d\mu = \int_0^1 8(1-\mathrm{a})\left[\frac{a(1-a)}{\lambda^2\mu^2}\right]\lambda^2\mu^3 d\mu = 4\mathrm{a}(1-\mathrm{a})^2 = \frac{16}{27} = 0.593 \tag{3.43}$$

In other words, even after the application of the rotating disk theory to the static disk concept, the Betz limit will always restrain the wind power usage.

3.3 An abstract definition of loads' fundamentals

As we gradually leave the simple mechanism of the actuator disk behind, it is easy for one to realize that the shape of the rotor and, hence, the shape of its blades are of a significant importance. A wind turbine blade can be - quite precisely - simulated by an airfoil and this will be the examined model from now on, regarding the induced loads.

In order to understand the nature of the loads that appear on an airfoil, one has to keep in mind the principal idea of the drag and lift forces coexistence. These forces are experienced by any body exposed to airflow. Drag force has a direction parallel to the wind's velocity, while lift force is always perpendicular to the wind direction. Depending on the object's shape, the ratio $lift/drag$ varies significantly. In the case of wind energy converters, older models used mainly the wind's drag force over lift and vice versa concerning the newer ones. Avoiding further analysis of the drag force and its source, since they are beyond the purpose of this document, it has to be stated that a drag-using machine can only utilize one third of the Betz limit, in terms of power coefficient. Contrary, lift devices can be highly efficient and this fact has led to the development of airfoil shapes which allow a lift to drag ratio of even up to 200. Thus, it is obvious why modern wind turbines are to be considered as lift-force dependant.

Lift-utilizing devices are of a similar shape, which is, as the figure below shows, the propeller type with a horizontal rotational axis.

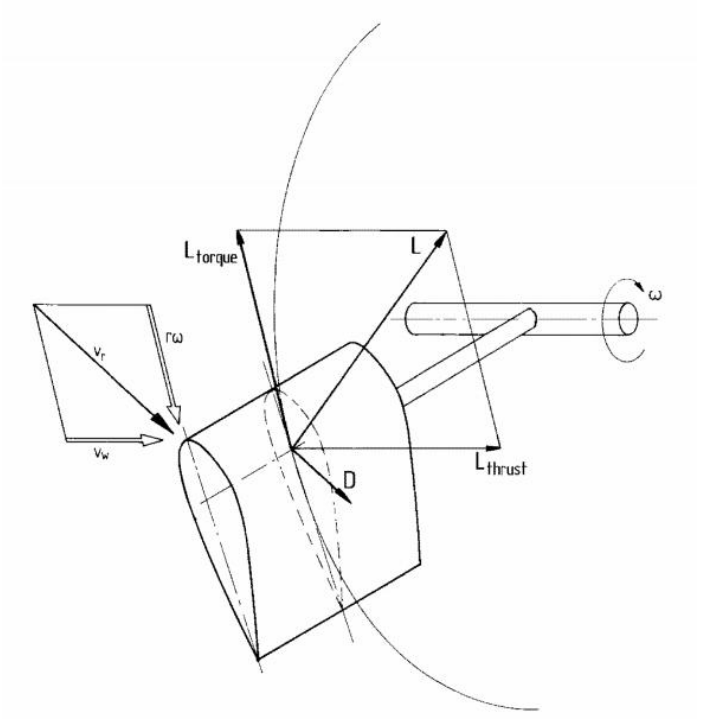

Figure 3.8: Flow velocities and aerodynamic forces acting on a propeller-like rotor

In this case, the wind does not impinge on the blade from its initial direction. On the contrary, it is vectorially combined with the peripheral velocity $r\omega$ of the rotor blade cross section on which it impinges, at a certain distance from the axis of rotation. The result of this combination is a certain angle of attack between the airfoil's chord and the wind's resultant free-stream velocity. The aerodynamic force exerted on the blade is resolved into the pre-mentioned drag and lift components, due to air circulation along the span of the airfoil and pressure differentiation among its upper and lower surfaces.

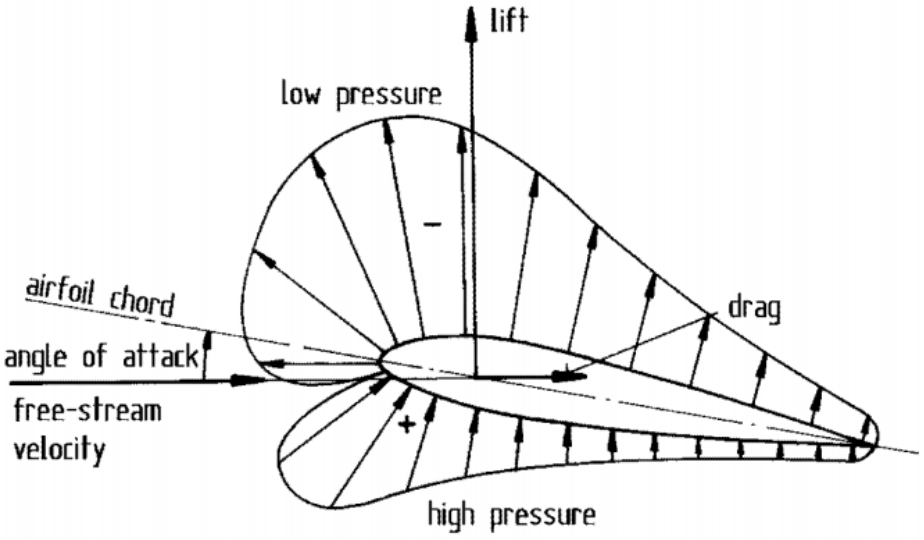

Figure 3.9: Aerodynamic forces acting on an airfoil exposed to an air stream

In turn, the lift component can further be resolved into a component tangential to the plane of rotation and another, perpendicular to it. The former is the one producing the torque necessary for the energy production, while the latter, called "thrust", is the cause of the undesired loads exerted on the blades and, therefore, on the wind turbine as a whole.

Two factors can be introduced at this point, related to the two different types of force exerted on airfoils. The first one, called "drag coefficient", denotes the ratio of drag force induced to the force potential of the wind, when it reaches the rotor plane:

$$C_d = \frac{Drag/unit\ span}{\frac{1}{2}\rho V_d^2 c} \tag{3.44}$$

, where c is the chord of the airfoil.

The drag term is strongly dependent on the air's Reynolds's number, which is, in turn, related to viscosity and velocity of the air. When referring to real fluids like the atmospheric air, viscosity is low while velocities are high and, therefore, Reynolds's number is high. This means that, since drag coefficient is inversely proportional to Reynolds's number, it, nevertheless, remains quite low.

The other factor is the "lift coefficient", which, as its name denotes, represents the proportion of lift force per unit span to the wind's force:

$$C_l = \frac{Lift/unit\ span}{\frac{1}{2}\rho V_d^2 c} = \frac{\rho(\Gamma \times V_d)}{\frac{1}{2}\rho V_d^2 c} \tag{3.45}$$

, where $\Gamma = \pi V_d c \sin a$ the circulation . Here, α is the angle of attack described earlier. Hence:

$$C_l = \frac{\rho\pi V_d c \sin a V_d}{\frac{1}{2}\rho V_d^2 c} = 2\pi \sin a \tag{3.46}$$

In practice, though, the correct equation is: $C_l = a_0 \sin a$, where $a_0 = 5.73\ (0.1/degree)$ rather than 2π .

It was mentioned that the velocity of the free-flow wind (V_∞) is combined with the net tangential flow velocity experienced by the blade element, which is the sum of the tangential velocity of the blade (*Ωr)* plus that of the wake (a'*Ωr),* or, finally, $(1 + a')\Omega r$. However, the blade is also obverted by its span axis in order to maximize the overall efficiency of the wind turbine and this, so called "pitch angle", has to be added to the attack angle as to produce the total angle at which the wind finally impinges on the plane of rotation.

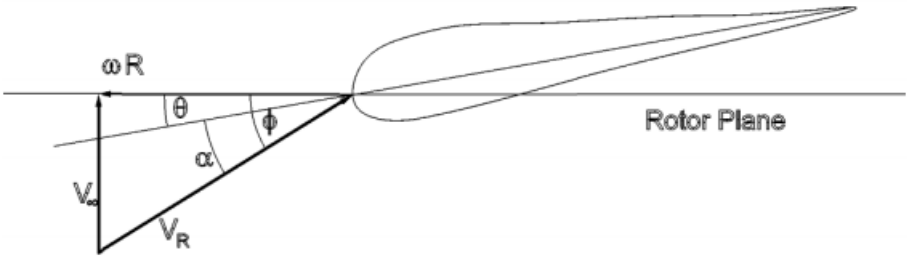

Figure 3.10: Velocities and angles at the rotor plane

In the figure above, the pitch angle is denoted by θ while the total angle is represented by φ. Moreover, V_R is the relative velocity as a result of the vectorially combined tangential and axial velocities:

$$V_R = \sqrt{V_\infty^2(1 - a)^2 + \Omega^2 r^2(1 + a')^2} \tag{3.47}$$

Thus:

$$\sin\varphi = \frac{V_\infty(1-a)}{V_R}\ ,\quad \cos\varphi = \frac{\Omega r(1+a')}{V_R} \tag{3.48}$$

Concerning the fore-mentioned forces, drag force is parallel to the relative velocity's direction, while the lift force is normal to it. These two forces combined, yield the total aerodynamic force (R) generated by the airfoil, which can be projected along the rotor plane and its orthogonal direction. In this case, the already noted driving force (T) and axial force (A) are derived and can be easily calculated as functions of the relative velocity angle (φ):

$$T = L\sin\varphi - D\cos\varphi \quad [2] \tag{3.49}$$

$$A = L\cos\varphi + D\sin\varphi \tag{3.50}$$

The first equation highlights the negative contribution of the drag force to the driving torque.

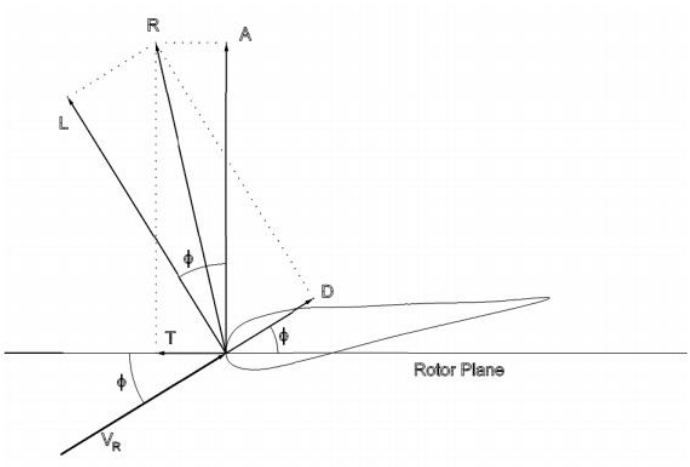

Figure 3.11: Force *R* decomposition on the velocity direction in lift *L* and drag *D* or in the rotor plane in driving *T* and axial *A* forces

3.4 The blade element – momentum (BEM) theory

Having already calculated the lift and drag coefficients, it is convenient to break the actuator disk into small pieces – annular rings that consist of a radius width of δr and are completely undependable on each other. This means that, practically, there is no interaction between the air particles passing through two successive rings, in terms of momentum interchange. This scenario would be close to reality if the axial induction factor was uniform along the whole rotor surface. Apparently, this is not really the case, since the axial induction factor usually varies from the root of a blade to the outer edge of it. However, experiments made by C. Lock in 1924 verified the negligibility of the errors, occurring due this assumption.

[2] In this equation only , T does not represent the thrust but the driving torque, in order to comply with the figure's symbols.

According to this hypothesis, then, we can abstract an annular ring of length δr and obtain the lift force, normal to the V_R direction and the drag force, parallel to it:

$$\delta L = \frac{1}{2}\rho V_R^2 c C_l \delta r \tag{3.51}$$

$$\delta D = \frac{1}{2}\rho V_R^2 c C_d r \delta r \tag{3.52}$$

Thus, for N blade elements, resolving in the axial direction, we obtain:

$$Axial\ Force = L\cos\varphi + D\sin\varphi = \frac{1}{2}\rho V_R^2 Nc(C_l\cos\varphi + C_d\sin\varphi)\delta r \tag{3.53}$$

On the other hand, the rotor torque is:

$$\begin{aligned} Torque &= r(\delta L\sin\varphi - \delta D\cos\varphi) \\ &= \frac{1}{2}\rho V_R^2 Nc(C_l\sin\varphi - C_d\cos\varphi)r\delta r \end{aligned} \tag{3.54}$$

The rate of change of axial momentum can be calculated:

$$\begin{aligned} (V_\infty - V_w)\rho A V_d &= [V_\infty - (1-2\mathrm{a})V_\infty]\rho 2\pi r\delta r(1-\mathrm{a})V_\infty \\ &= 4\pi\rho {V_\infty}^2 \mathrm{a}(1-\mathrm{a})r\delta r \end{aligned} \tag{3.55}$$

Taking into account the pressure drop in the wake due to rotation, which is: $\frac{1}{2}\rho(2\mathrm{a}'\Omega r)^2$ and the responding additional axial force: $\frac{1}{2}\rho(2\mathrm{a}'\Omega r)^2 2\pi r\delta r$, we can equate the result with the previously yielded axial force. Thus:

$$\frac{1}{2}\rho V_R^2 Nc(C_l\cos\varphi + C_d\sin\varphi)\delta r = 4\pi\rho\left[{V_\infty}^2\mathrm{a}(1-\mathrm{a}) + (\mathrm{a}'\Omega r)^2\right]r\delta r \tag{3.56}$$

and after some rearrangement:

$$\frac{V_R^2}{{V_\infty}^2}N\frac{c}{R}(C_l\cos\varphi + C_d\sin\varphi) = 8\pi[\mathrm{a}(1-\mathrm{a}) + (\mathrm{a}'\lambda\mu)^2]\mu \tag{3.57}$$

At the same time, the rate of change of angular momentum would be:

$$\rho V_\infty(1-\mathrm{a})\Omega r 2\mathrm{a}' r 2\pi r\delta r = 4\pi\rho V_\infty \Omega r\mathrm{a}'(1-\mathrm{a})r^2\delta r \tag{3.58}$$

This should be equated with the above-derived result for torque and therefore:

$$\frac{1}{2}\rho V_R^2 Nc(C_l\sin\varphi - C_d\cos\varphi)r\delta r = 4\pi\rho V_\infty\Omega r\mathrm{a}'(1-\mathrm{a})r^2\delta r \tag{3.59}$$

which, in turn, gives:

$$\frac{V_R^2}{{V_\infty}^2} N \frac{c}{R} (C_l \sin\varphi - C_d \cos\varphi) = 8\pi\lambda\mu^2 \mathrm{a}'(1-\mathrm{a}) \tag{3.60}$$

If, in the axial force and torque equations, the terms in parenthesis are substituted as below,

$$C_x = C_l \cos\varphi + C_d \sin\varphi \tag{3.61}$$

$$C_y = C_l \sin\varphi - C_d \cos\varphi \tag{3.62}$$

then, with simple calculations, two equations can be yielded:

$$\left\{ \begin{array}{c} \dfrac{\mathrm{a}}{1-\mathrm{a}} = \dfrac{\sigma_r}{4\sin\varphi^2}\left(C_x - \dfrac{\sigma_r}{4\sin\varphi^2} {C_y}^2\right) \\ \dfrac{\mathrm{a}'}{1+\mathrm{a}'} = \dfrac{\sigma_r C_y}{4\sin\varphi\cos\varphi} \end{array} \right\} \tag{3.63}$$

, where

$$\sigma_r = \frac{Nc}{2\pi r} = \frac{N}{2\pi\mu}\frac{c}{R} \tag{3.64}$$

is called “chord solidity”.

In these two, non-linear equations a and a’ can be determined through an iterative process, beginning with zero values for both factors and changing them until a final convergence is achieved. In each step, the total inflow angle has to be calculated as a function of the axial and tangential induction factors, the tip speed ratio and the radial position:

$$\varphi = \tan^{-1}\left[\frac{1-\mathrm{a}}{\lambda\mu(1+\mathrm{a}')}\right] \tag{3.65}$$

, so that the local angle of attack can be determined as: $a = \varphi - \beta$

Afterwards, the lift and drag coefficients can be read off from a manufacturer’s table and then, C_x and C_y can be easily extracted by them. This procedure will result in a new value for a and a’ and so on. As will later be discussed, this iterative process is the foundation on which the determination of the aerodynamic loads will be based.

3.5 Five significant points concerning B.E.M.

It is argued that the drag coefficient should not appear in the previous equations. Generally, the ratio of pressure drag (which mainly affects the drag coefficient) to total drag at zero angle of attack is approximately the same as the thickness to chord ratio and increases with the angle of attack.

B.E.M. is only applicable as long as circulation and, consequently, induction factor a is span-wisely uniform. If that is not the case, an exchange of momentum takes place through adjacent elemental annular rings and, therefore, it cannot be stated that the only axial force acting on the flow through a given annular ring is due to the pressure drop across the disc. Although this assumption has already been ,made, the error occurring is relatively small, at tip-speed ratios greater than 3.

There exists a special case when the induction factor is very high (say a=1), where momentum theory cannot be applied and an empirical determination of the thrust coefficient has to be made.

Up to this point, it has been assumed that the rotor is constituted by a solid disk, or in other words, it is made up by such a great number of blades, that every single air particle passing through the rotor plane interacts with a blade, thus undergoing the very same loss of momentum with any other. This is obviously not the case, as, at any instant, most of the air particles will pass between the -only few- blades of the wind turbine. Therefore, as a result of the discreteness of the blades, the flow induction factor will vary within the vicinity of the rotor disk, affecting the power extracted, as well as the loads exerted on the wind turbine.

In order to surpass this problem, L. Prandtl suggested that the following correction factor, named “Prandtl’s tip-loss factor”, be added to the previous equations, due to the great influence of the above-mentioned simplification on the tip of the blades and the outer parts of them in general. The pertinent equation is:

$$f(\mu) = \frac{2}{\pi}\cos\left[e^{((N/2)(1-\mu)/\mu)\sqrt{1+(\lambda\mu)^2/(1-\mathrm{a})^2}}\right] \tag{3.66}$$

With this addition, the equations for the determination of the axial and tangential factors become:

$$\left\{\begin{array}{c} \dfrac{\mathrm{a}f}{1-\mathrm{a}} = \dfrac{\sigma_r}{4\sin\varphi^2}\left(C_x - \dfrac{\sigma_r}{4\sin\varphi^2}{C_y}^2\right)\dfrac{1-\mathrm{a}}{1-\mathrm{a}f} \\ \dfrac{\mathrm{a}'f}{1+\mathrm{a}'} = \dfrac{\sigma_r C_y}{4\sin\varphi\cos\varphi}\dfrac{1-\mathrm{a}}{1-\mathrm{a}f} \end{array}\right\} \tag{3.67}$$

The momentum theory presents a breakdown when the axial induction factor becomes high enough for the rotating blades to have a similar behavior to a solid disk plate. This could be the case when a high tip-speed ratio is reached and, consequently, the rotor presents a decreasingly permeable disk to the flow. The air

particles that cannot pass through the disk are forced to move radially outwards and are separated from the flow when they reach the outer edge, causing a low static pressure to develop behind the disk. Meanwhile, the particles that managed to pass to the other side experience the low pressure condition and, in order to reach the higher, ambient static pressure for equilibrium to be achieved, they are forced to compensate for the lack of energy by mixing with the separated particles and thus gaining energy from the turbulent wake that has been developed.

The difference between the upstream high static pressure state and the low static pressure one downstream causes a higher drag coefficient to occur than that predicted by the momentum theory. Therefore, another correction has to be made to the equations when the axial induction factor exceeds a certain value, a_c, which is usually 0.4. In this case, the equations become:

$$\left\{\begin{array}{c}(1-\mathrm{a})^2\frac{\sigma_r}{\sin\varphi^2}C_x+4\left(\sqrt{C_{T_1}}-1\right)(1-\mathrm{a})-C_{T_1}=0\\ \frac{\mathrm{a}'}{1+\mathrm{a}'}=\frac{\sigma_r C_y}{4\sin\varphi\cos\varphi}\end{array}\right\} \tag{3.68}$$

where, C_{T_1} is usually taken equal to 1.6, according to Wilson and Lissaman (1974).

3.6 An alternative method

According to the author M. Hansen, a simpler B.E.M. approach is also accurate. He suggests the derivation of a and a' from the equations:

$$\left\{\begin{array}{c}\mathrm{a}=\frac{1}{\frac{4f\sin^2\varphi}{\sigma_r \mathrm{C_x}}+1}\\ \mathrm{a}'=\frac{1}{\frac{4f\sin\varphi\cos\varphi}{\sigma_r \mathrm{C}_y}-1}\end{array}\right\} \tag{3.69}$$

Here, Prandtl's tip loss factor is also a necessity and this is taken into account with the addition of the f term in the equations.

As for Glauert's correction, in the case that a exceeds a_c, the equations are substituted for:

$$\begin{cases} a = \frac{1}{2}\left[2 + \frac{4f\sin^2\varphi}{\sigma_r C_x}(1-2a_c) - \sqrt{\left(\frac{4f\sin^2\varphi}{\sigma_r C_x}(1-2a_c)\right)^2 + 4\left(\frac{4f\sin^2\varphi}{\sigma_r C_x}a_c^2 - 1\right)}\right] \\ a' = \frac{1}{\frac{4f\sin\varphi\cos\varphi}{\sigma_r C_y} - 1} \end{cases} \quad (3.70)$$

The differences between the two methods, although insignificant, are presented in the next chapter, through the correspondent graph.

3.7 Tower shadow

The tower of the wind turbine becomes a significant obstacle for the wind's free flow, especially in the case of tubular towers. Thus, in order to produce a realistic model which reflects the behavior of free wind stream approaching a wind turbine, the velocity deficits upwind of a tubular tower have to be taken into consideration. In the case of upwind turbines, the flow around a cylindrical tower is derived by superposing a doublet, i.e., a source and sink at very close spacing, on a uniform flow,V_∞, giving the stream function:

$$\psi = V_\infty y\left(1 - \frac{(D/2)^2}{x^2 + y^2}\right) \quad (3.71)$$

where D is the tower diameter and x, y are the longitudinal and lateral coordinates with respect to the tower centre (see Figure 3.12). Differentiation of ψ with respect to y yields the following expression for the flow velocity in the x direction:

$$V = V_\infty\left(1 - \frac{(D/2)^2(x^2 - y^2)}{(x^2 + y^2)^2}\right) \quad (3.72)$$

Here, the second term within the brackets represents the velocity deficit as a proportion of the undisturbed wind speed. The velocity deficit on the flow axis of symmetry is equal to $V_\infty(D/2x)^2$ and the total width of the deficit region is twice the upwind distance. As a result, the velocity gradient encountered by a rotating blade decreases rapidly as the upwind distance, x, increases. The effect of tower shadow on blade loading can be estimated by setting the local velocity component at right angles to the plane of rotation equal to $V(1-a)$ in place of $V_\infty(1-a)$, and applying blade element theory as usual.

Figure 3.13 illustrates the tower shadow effect on the wind speed field in front of the rotor on an up-wind type rotor and a cylindrical tower.

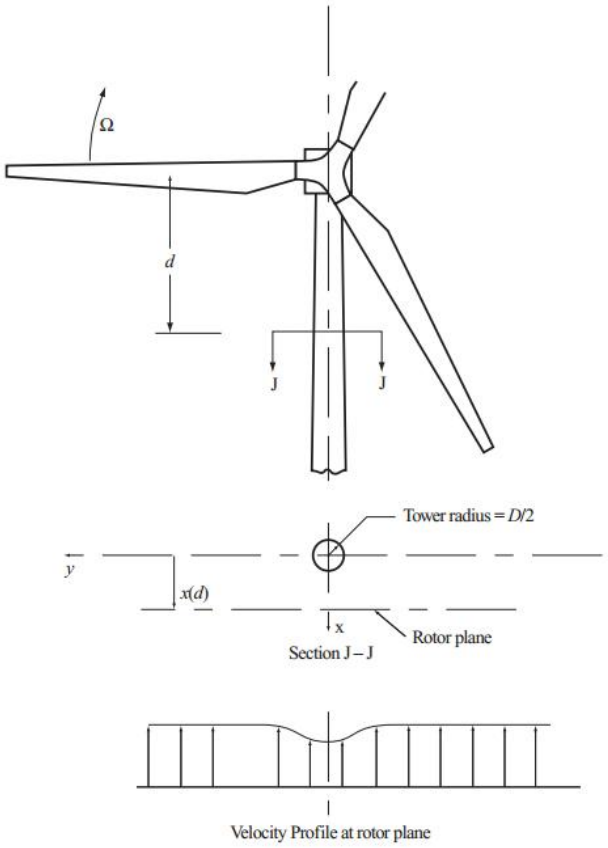

Figure 3.12: Tower shadow parameters

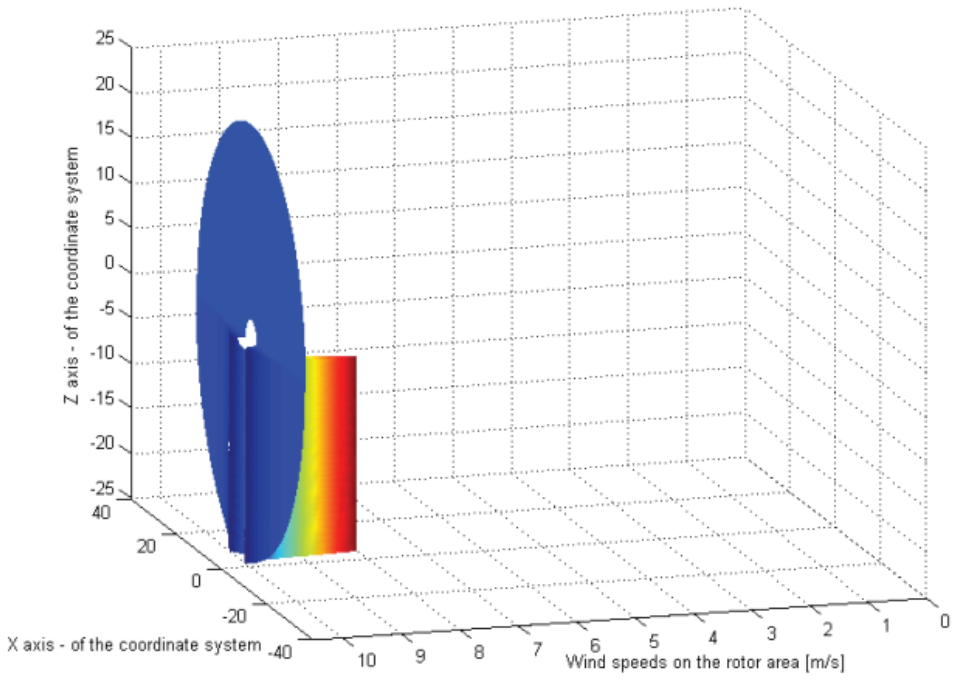

Figure 3.13: Wind speed field interference by the tower shadow

4 The algorithm

4.1 General

Hopefully, up to this point, the reader has become quite familiar with the fundamental concepts behind the aerodynamics of a wind turbine. On the other hand, it is obvious that the phenomenon of a rotating blade, with a varying thickness-to-chord ratio, exposed to a continuously changing wind stream is one of great complexity and it is beyond the scope of this thesis to describe it to its full depth. However, the conscious reader is encouraged to seek the additional information in the references at the end of the current dissertation.

Nevertheless, what remains within the scope of this thesis is, firstly, the production of an algorithm that will be able to simulate the aerodynamics of the previous chapter, as accurately as possible and, secondly, the evaluation of the results of its execution. For this purpose, the Matlab environment was considered to be a hospitable one and, thus, the whole of the code was written in the Matlab language.

4.2 Flow of the algorithm

The flow of the algorithm can be basically described by the following chart:

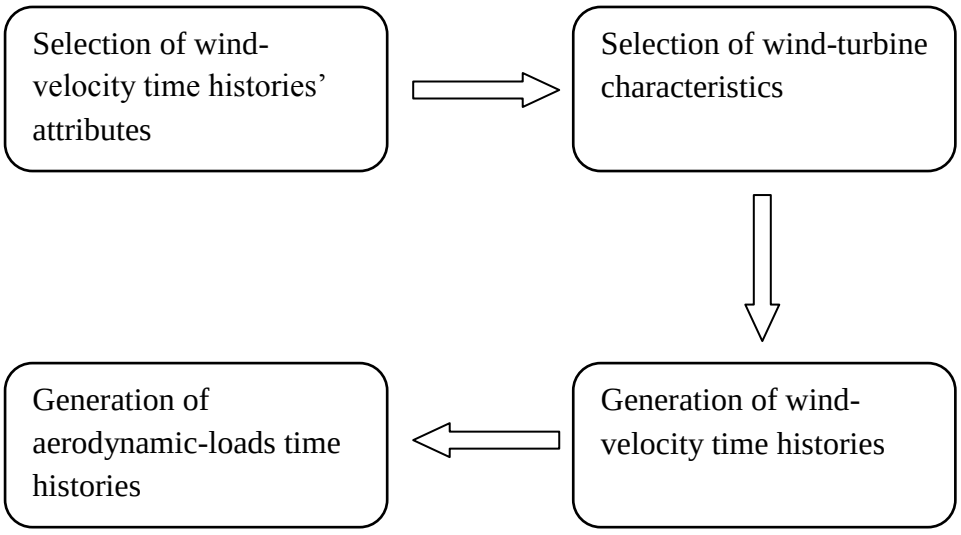

Figure 4.1: Algorithm's basic concept

At the first step of the algorithm, the user has to provide the properties of the desired wind field, which are the following:

1. Maximum frequency of time histories
2. Discretization in the frequency domain
3. Maximum time period for each time history
4. Discretization in the time domain
5. Number of points along each blade, at which the wind velocity will be calculated
6. Azimuth angle discretization

The second step requires from the user to provide the characteristics of the wind turbine in question. These are the:

1. Wind turbine rotational speed[3]
2. Blade radius
3. Number of blades
4. Hub height
5. Tower diameter[4]
6. Blade - tower clearance
7. Air density
8. Blade chord variation along the blade
9. Pitch angle variation along the blade[5]
10. Lift coefficient for each possible angle of attack[6]
11. Drag coefficient for each possible angle of attack

The third step of the algorithm consists of all these commands necessary for the generation of the wind-velocity time histories. The program is based on the theory presented and analyzed in Chapter 2 and utilizes the information given by the user in step 1.

The final part takes as input the resulting wind-velocity time history, produced in the previous step, along with the wind turbine characteristics from step 2, and calculates the loads exerted on the blades and, therefore, on the turbine's tower, by simulating the concepts described in Chapter 3.

4.3 Accuracy of the algorithm

At this point, a necessity arises for an assurance, regarding the accuracy of the created algorithm. A relatively appropriate way to evaluate the results of the program is to compare them with those of the references. The following comparative diagrams, referring to the various parameters that characterize the function of a wind

[3] This implies that the rotational speed of the wind turbine remains constant, regardless of the wind velocity. However, in order to produce the highest possible power, modern wind turbines change their rotational speed depending on the wind velocity, as to maintain a desirable tip-speed ratio.

[4] In fact, the diameter of the tower varies with height. In order to take the tower shadow effect into account, however, only the diameter at the top matters. Therefore the required information refers to that value.

[5] Ideally, a wind turbine has to continuously alter the pitch angle along the blades, depending on the attack angle, which, in turn, depends on the wind velocity.

[6] In fact, it is impossible to provide lift and drag coefficient values for every possible angle of attack. Thus, the alogorithm uses the technique of linear interpolation to determine the coefficients for angles not included in the tables.

turbine, present an agreement between the results of this algorithm and the ones found in the literature.

The first diagram represents the variation of the attack angle across the blade, while the second and third diagrams refer to the variation of the axial and tangential induction factors with radius, respectively. Each one of the parameters above is calculated for a range of Tip Speed Ratios, as the legend of each chart shows. The wind turbine, under examination, is a 3-blade one, with a rotor diameter of 17m and the characteristics that appear on the following table:

Radius r (mm)	$\mu = r/R$	Chord c (mm)	Pitch β (degree)	Thickness/chord ratio of blade (%)
1700	0.20	1085	15.0	24.6
2125	0.25	1045	12.1	22.5
2150	0.30	1005	9.5	20.7
2975	0.35	965	7.6	19.5
3400	0.40	925	6.1	18.7
3825	0.45	885	4.9	18.1
4250	0.50	845	3.9	17.6
4675	0.55	805	3.1	17.1
5100	0.60	765	2.4	16.6
5525	0.65	725	1.9	16.1
5950	0.70	685	1.5	15.6
6375	0.75	645	1.2	15.1
6800	0.80	605	0.9	14.6
6375	0.85	565	0.6	14.1
7225	0.90	525	0.4	13.6
8075	0.95	485	0.2	13.1
8500	1.00	445	0.0	12.6

Table 4.1: Blade design of a 17m-diameter rotor

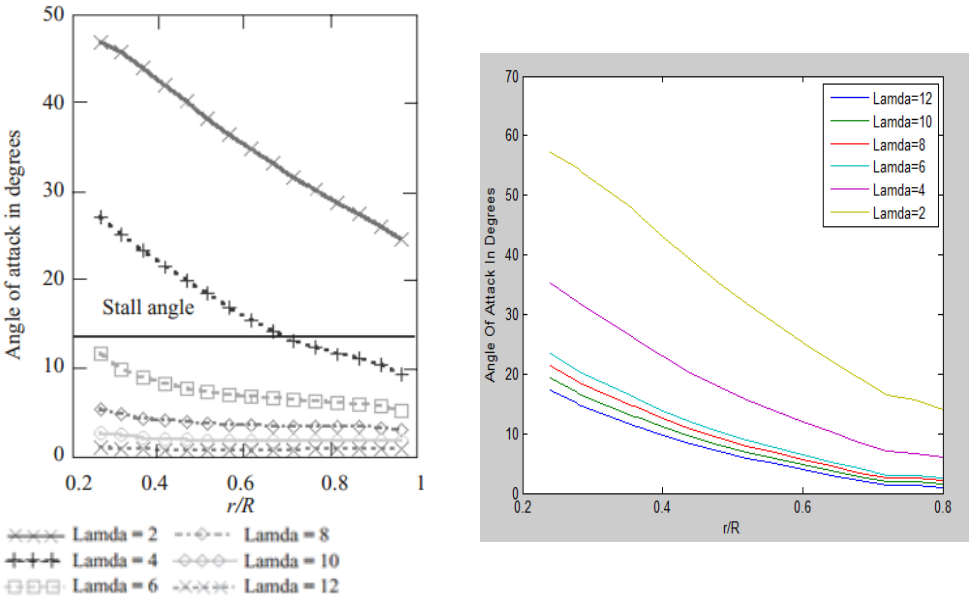

(a)

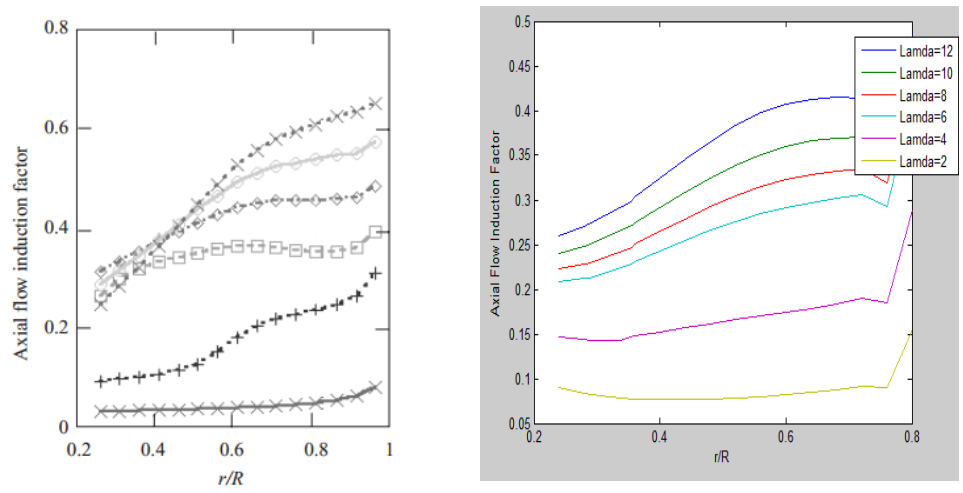

(b)

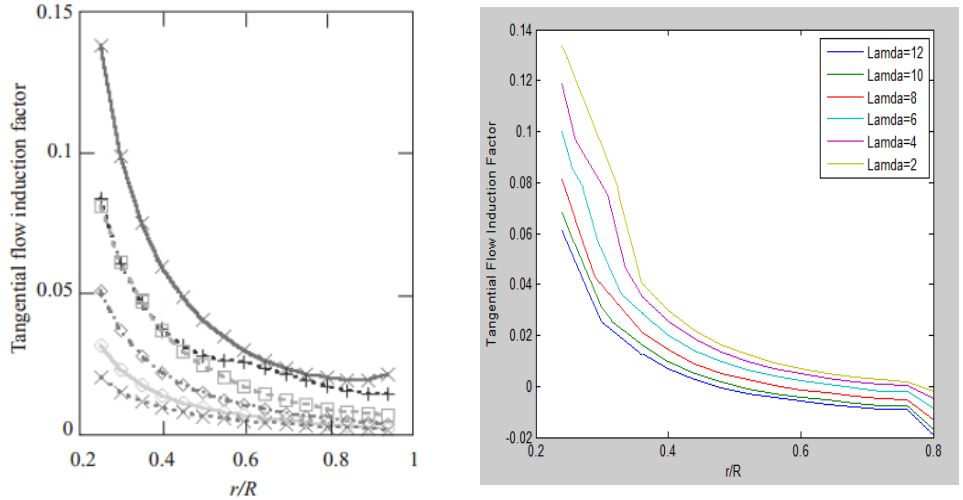

(c)

Figure 4.2: Comparison between the results of reference [1] and this thesis's algorithm, regarding the distribution of the inflow angle (a), the axial induction factor (b) and the tangential induction factor (c) along the blade

The similarity between each pair of diagrams is considered satisfactory enough, regarding both the form and the numerical values of the graphs.

Concerning the natural meaning of these curves, the high angles of attack at the root of the blade are due to practical constraints, which impose the high pitch angles presented on the table of blade characteristics. The angle of attack, then, decreases with the also decreasing pitch angle, while approaching the blade's outer part. The high attack angles at the root create stall conditions which, in turn, deteriorate the aerodynamic efficiency of the blade. This explains the relatively low induction factors at the inner part of the blade and the higher ones while leaving the stalled root and reaching the blade's tip. Nevertheless, we should always keep in mind that an efficient blade is one that is functioning near the Betz limit, which refers to an induction factor of approximately 0.33. Any value beyond that, irrespective of whether it is higher or lower, leads to a decreased power extraction. That is, the higher induction factors, accompanied by increased tip-speed ratios, are not related to evenly high efficiencies. Therefore, a wind turbine must change its rotational speed according to the wind velocity, in order to maintain a tip-speed ratio that leads to an axial induction factor of about 0.33. In this example, this happens at a tip-speed ratio of 6 (according to the reference's diagram or 10 according to this thesis's algorithm).

5 Results

5.1 The two methods of induction factors' calculation

Prior to the comparison of the different airfoils and the examination of the effects the variations of the parameters have on the loads, the two different methods, mentioned in chapter 3, should be tested as to find out whether remarkable differences exist between them or not. As already stated, the two methods are referring to the calculation of the axial and tangential induction factors after the determination of the inflow angle, the chord solidity, the tip-loss factor and the normal and tangential coefficients. The four final calculations derived, which are presented in the last section of the previous chapter are based on the same theories (also described in chapter 3), but take different assumptions into account. The tests which were carried out showed that the deviations between the methods are practically negligible, with the procedure of M. Hansen being slightly more conservative, leading to higher axial induction factors and, thus, to higher out-of-plane forces. Due to this conclusion, from now on, the M. Hansen method will be used.

In order to provide a clearer perspective of the comparison, the following 3D figure demonstrates the variations of the out-of-plane load calculated with the two methods, with respect to both the radius and the azimuth value.

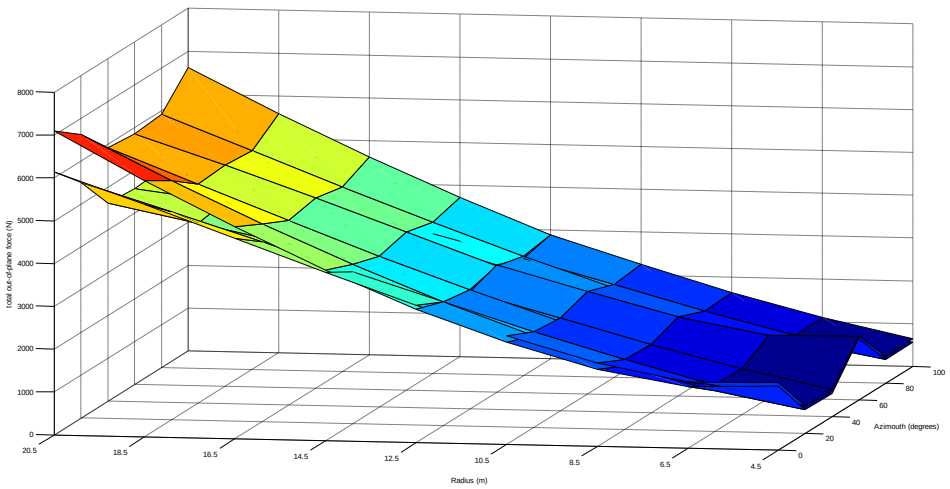

Figure 5.1: Comparison between methods 1 [1], 2 [10] regarding the out of plane force distribution, with respect to both the azimuth and radius of the blades. For the extraction of the force, the contribution of all the three blades was taken into account. The upper surface corresponds to method 2, while the lower one is the result of method 1

The airfoil used for the extraction of this diagram is of a Nordtank NTK 500/41 wind turbine. The parameters were selected according to reference [10] and are the following:

Rotational speed: 27.1 rpm;
Air density: 1.225 kg/m^3;
Rotor radius: 20.5m;
Number of blades: 3;
Hub height: 35.0 m.

The characteristics of the airfoil are the following:

Blade description

r [m]	twist [degrees]	chord [m]
4.5	20.0	1.63
5.5	16.3	1.597
6.5	13.0	1.540
7.5	10.05	1.481
8.5	7.45	1.420
9.5	5.85	1.356
10.5	4.85	1.294
11.5	4.00	1.229
12.5	3.15	1.163
13.5	2.60	1.095
14.5	2.02	1.026
15.5	1.36	0.955
16.5	0.77	0.881
17.5	0.33	0.806
18.5	0.14	0.705
19.5	0.05	0.545
20.3	0.02	0.265

Table 5.1: Blade characteristics of a Nordtank NTK 500/41 wind turbine

5.2 Out-of-plane and in-plane force calculation for constant wind velocity

Having certified the accuracy of the algorithm's results, we can now focus on the main subject of this research, which is the extraction of typical load values, experienced by the tower's top, where the rotor hub is located. The forces which are of significant importance, regarding the tower loading, are the out-of-plane (of rotation) forces, which are always present while the wind turbine is operating. It would also be interesting to compare the results obtained, by changing various parameters which affect these loads. As to study the correlation of these factors with

the out-of-plane forces, several types of wind turbines will be tested and, additionally, for each wind turbine, the tip-loss factor will be differentiated, by either changing the mean wind speed or the blades' rotational speed. Besides, as already been stated, it is the ratio of these two factors that yields the tip-speed ratio and determines the distribution of the forces along a blade and not their values individually.

To begin with, the airfoils which will be examined are 6 in total and their types are: 'Airfoil DU40_A17', 'Airfoil DU35_A17', 'Airfoil DU30_A17', 'Airfoil DU25_A17', 'Airfoil DU21_A17' and 'Airfoil NACA64_A17'. All the airfoils have 3 blades of radius 61.5m, each and the height of their towers is 120m. The lift and drag coefficients along with the attack angle to which they refer are available through relative tables. However, the attack angle is continuously changing values, following the variations of the axial and tangential induction factors and therefore the tables with the airfoil characteristics cannot contain all the possible values the angle may take. In order to determine the lift and drag coefficients referring to the unconcluded values, the most appropriate solution is considered to be the linear interpolation between the two nearest values. Additionally, due to the insufficiency of data, some rational assumptions have to be made. Thus, the tower diameter at the top is considered to be 2m and the clearance between the blades and the tower is chosen to be equal to 2m, as well. With an air density of 1.225 kg/m^3, the results of the program's execution are the following:

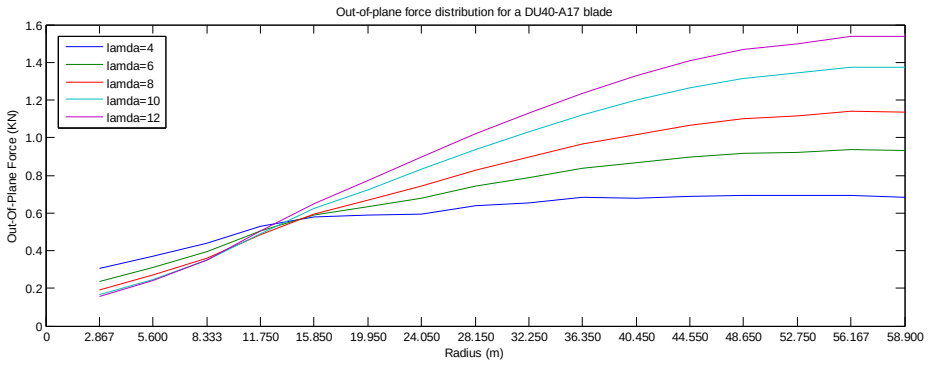

(a)

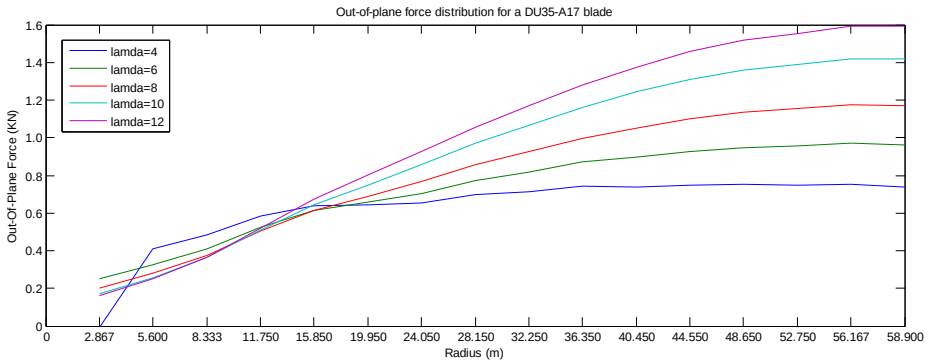

(b)

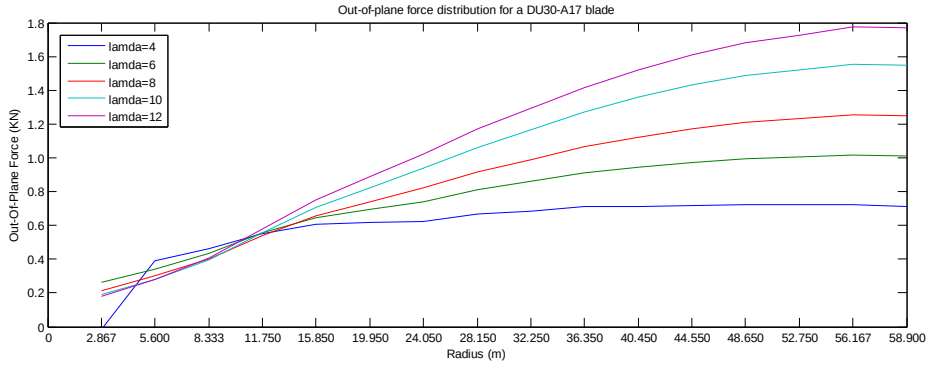

(c)

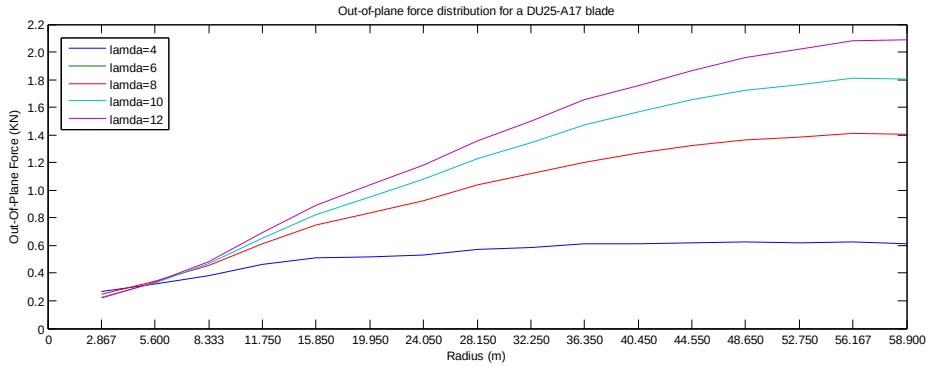

(d)

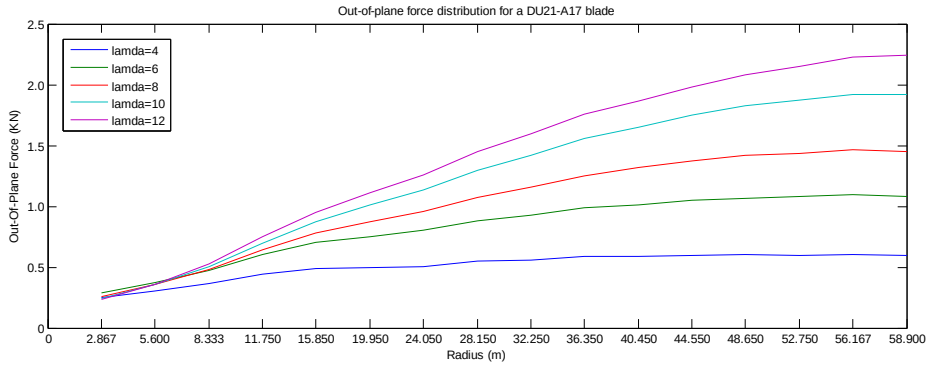

(e)

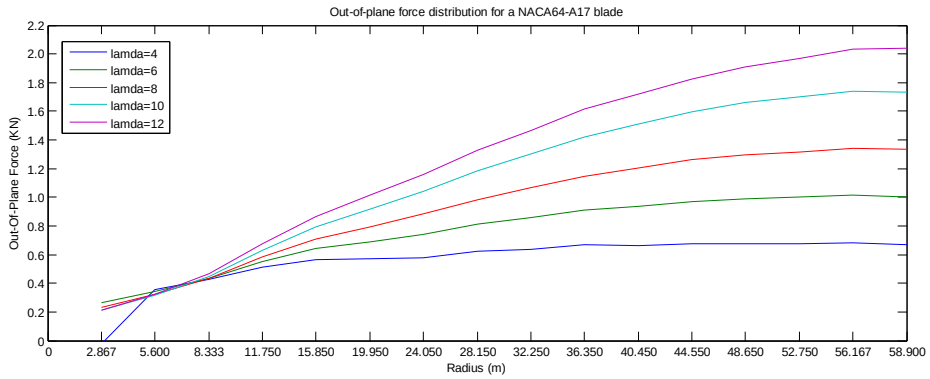

(f)

Figure 5.2: Program results regarding the out-of-plane force distribution along the blade, for different tip-speed ratios. The airfoil types examined are the 'DU40_A17' (a), 'DU35_A17' (b), 'DU30_A17' (c), 'DU25_A17' (d), 'DU21_A17' (e) and 'NACA64_A17' (f)

These diagrams depict the distribution of the out-of-plane force along a blade, for different tip-speed ratios. The wind turbine is operating at a rotation speed of 8.6, 12.5, 16.6, 21.5 and 25.0 rounds per minute, for factor lamda equal to 4, 6, 8, 10, 12, respectively and the mean wind speed is 10 m/s. The out-of-plane force is increasing approximately linearly with radius, in spite of the reducing blade chord, until the effects of tip loss are felt beyond about 75 percent of tip radius. It has to be noted that the same results would be derived from any other combination of wind speed and speed of rotation yielding the same tip-speed ratio.

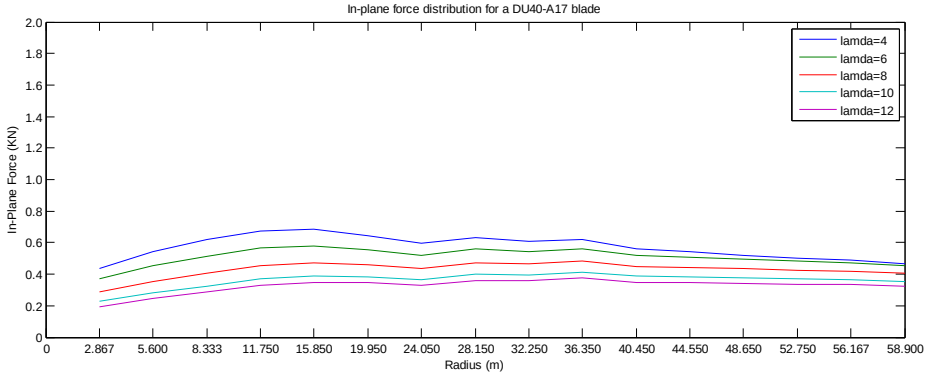

(a)

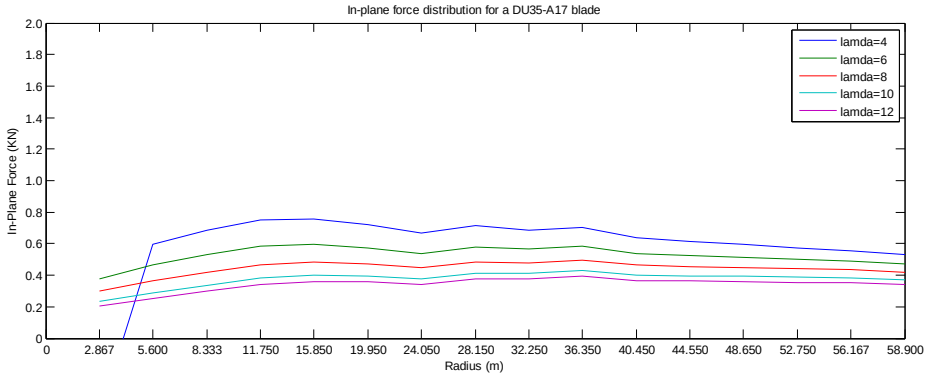

(b)

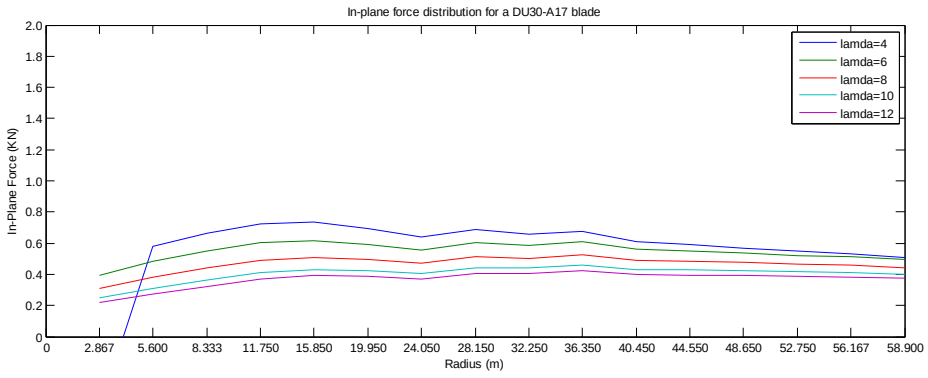

(c)

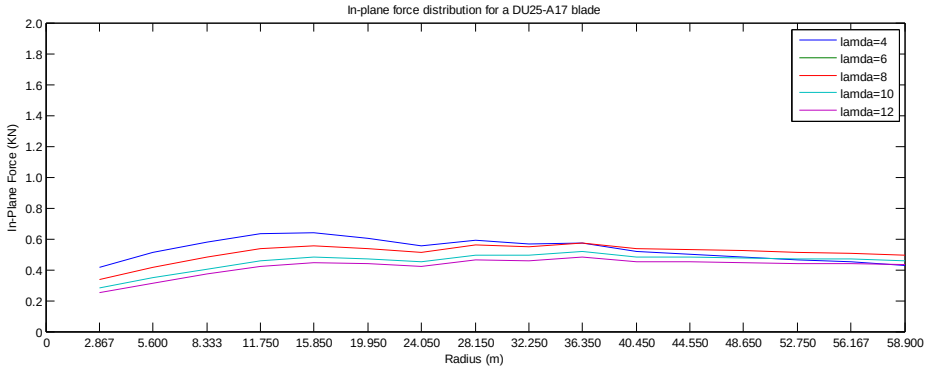

(d)

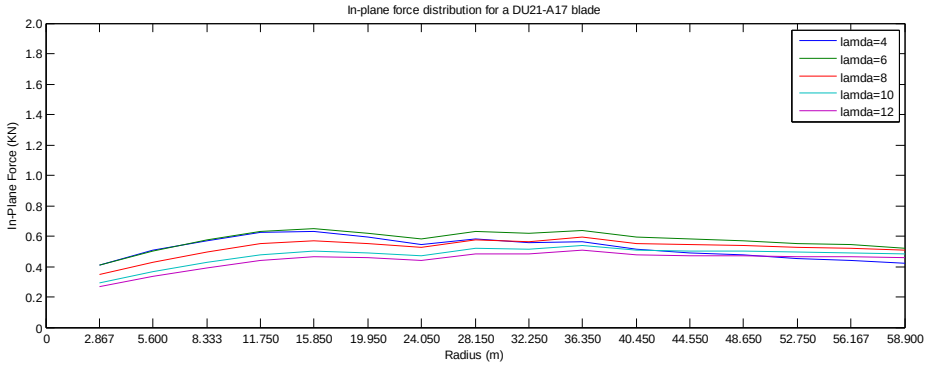

(e)

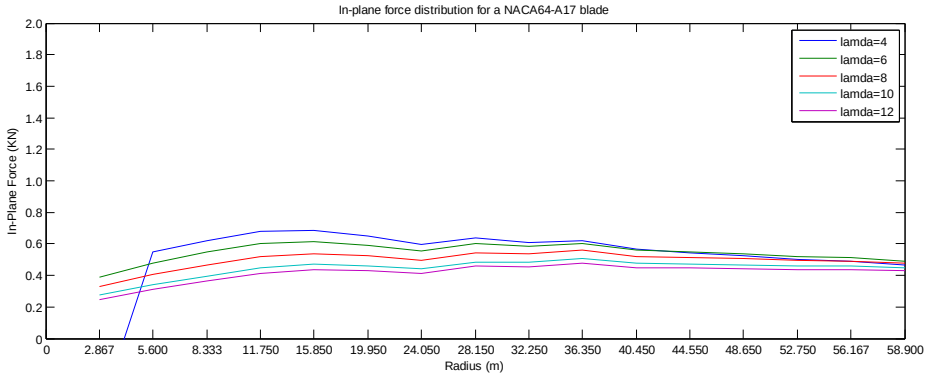

(f)

Figure 5.3: Program results regarding the in-plane force distribution along the blade, for different tip-speed ratios. The airfoil types examined are the 'DU40_A17' (a), 'DU35_A17' (b), 'DU30_A17' (c), 'DU25_A17' (d), 'DU21_A17' (e) and 'NACA64_A17' (f)

It is clear that the DU21-A17 airfoil is the one yielding the highest values of out-of-plane loads, while producing approximately the same in-plane loads as every other blade type. Thus, the most unfavorable conditions are connected with this airfoil. Meanwhile, it is also obvious that, regarding the examined airfoil types, a rotational speed yielding a tip-speed ratio of about a value of 4 is the one that simultaneously exposes the blade to the highest in-plane and the lowest out-of-plane forces. This means that any combination of rotational speed and wind velocity that creates a tip-speed ratio around the value of 4 is the most effective, as far as the wind turbine loads are concerned.

5.3 Generation of wind velocity time histories

As stated in Chapter 2, it is the wind, above all, that predetermines, both qualitatively and quantitatively, the loads to which a wind turbine is exposed. Therefore, the initial step, in order to specify the forces exerted on the blades and, consequently, on the tower of a wind turbine, is the determination of the variations of wind velocity with time. The first part of the algorithm produced for this thesis is, as described in Chapter 4, dedicated to this task.

Figure 5.6, below, demonstrates the variation of the wind velocity with time for each point from which a blade passes, during a complete rotation. Due to the big number of points at which the wind speed has been calculated, a selection of points to be represented was considered necessary. Thus, the point presented below for each azimuth position is the one at the very end of the blade, while the azimuth at each position differs from its previous one by 20 degrees. Apparently, though, the program takes into account all those points that cover the entirety of the rotor disk, according to the grid density defined by the user. In this particular case, the program was customized as to calculate the wind speed variations at the points presented in Figure 5.5. The number of points to be considered along each blade is 17 and the azimuth angle step is 20 degrees, as in the example of Figure 5.6. This gives a total number of $17 * \frac{360}{20} + 1 = 307$ points at which the wind-velocity time histories are generated. In this calculation, the last point added represents the center of the actuator disk.

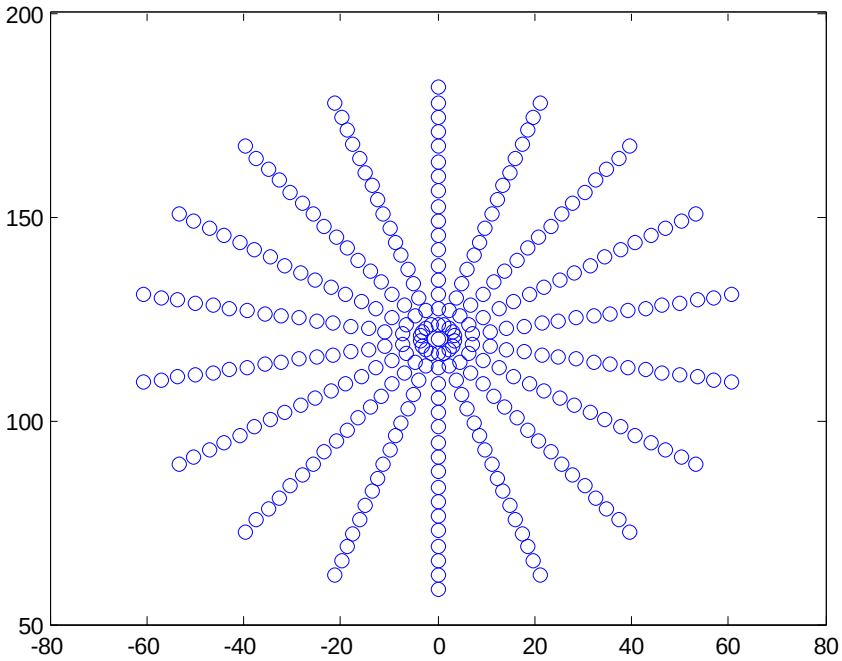

Figure 5.4: Grid of points at which the wind-velocity time histories are generated

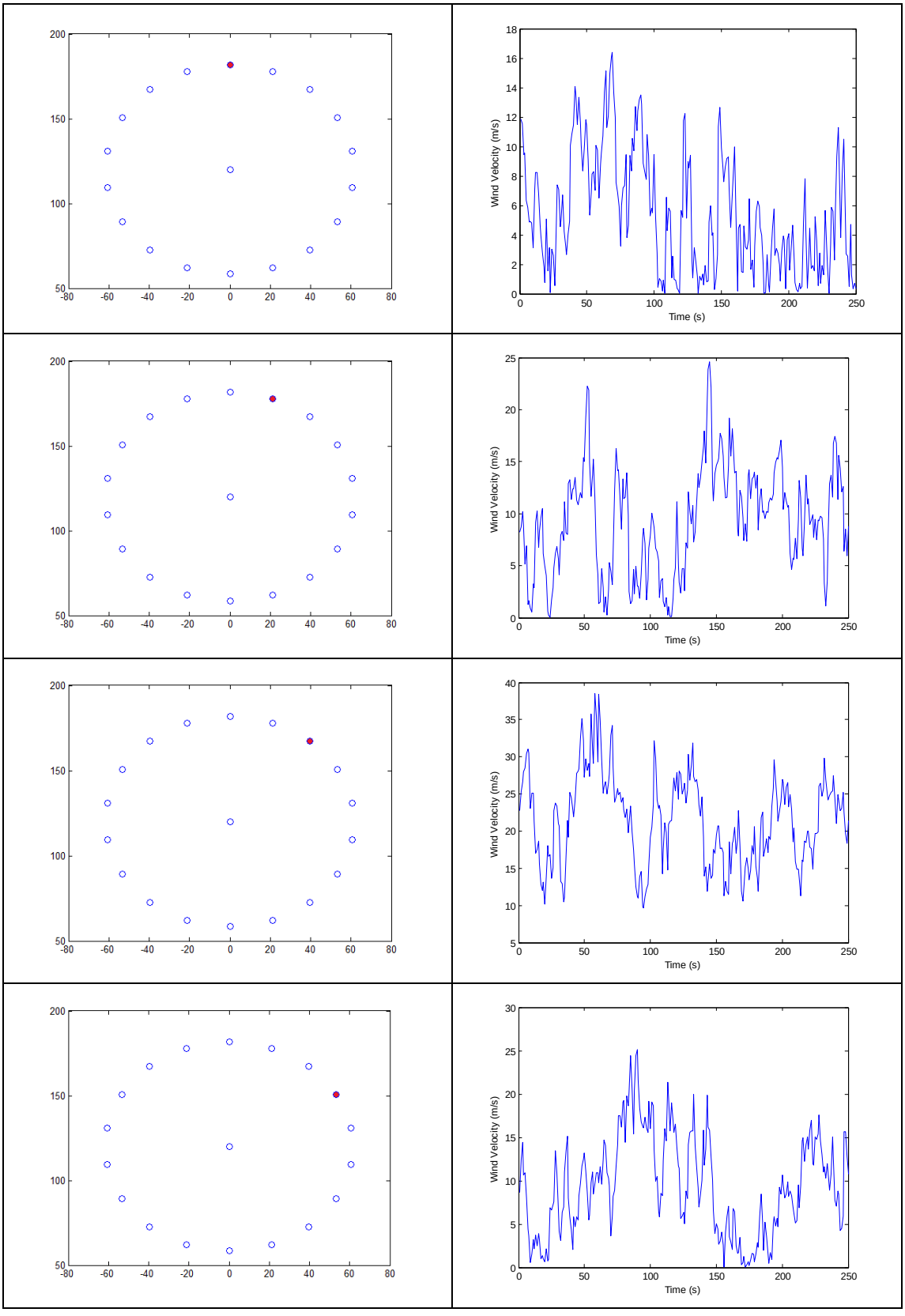
Wind Velocity (m/s)
Time (s)

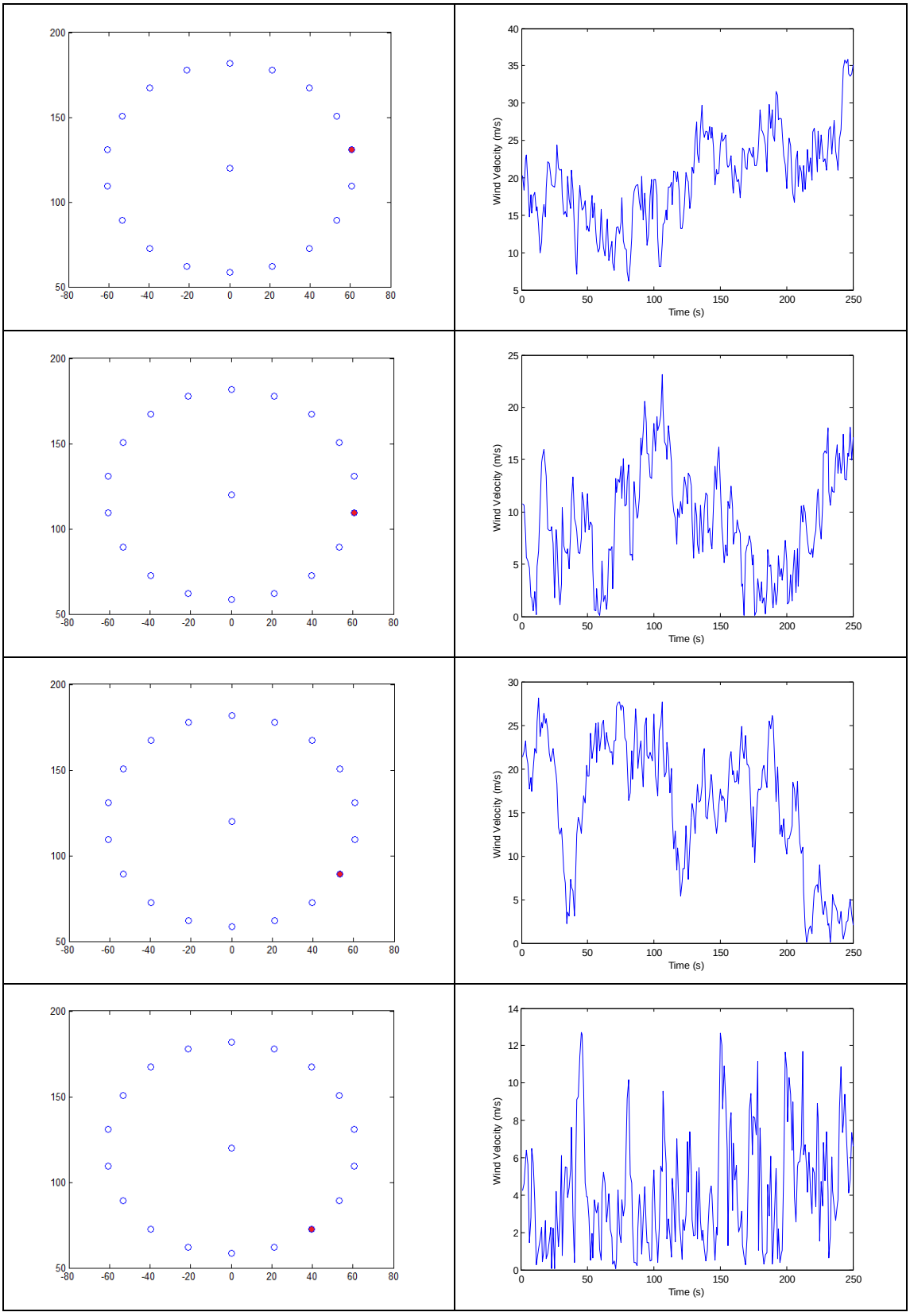
Wind Velocity (m/s)
Time (s)

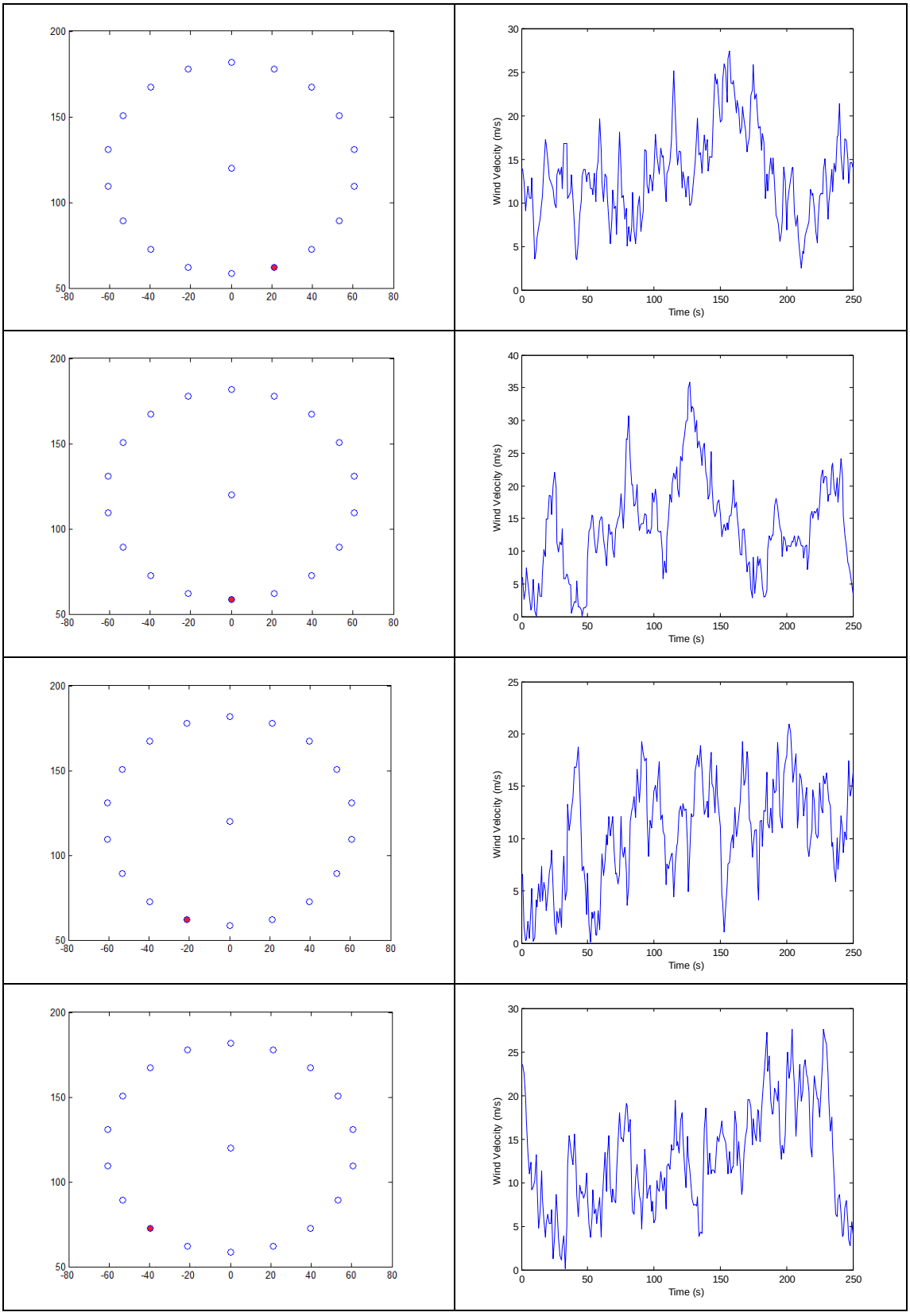
Wind Velocity (m/s)
Time (s)

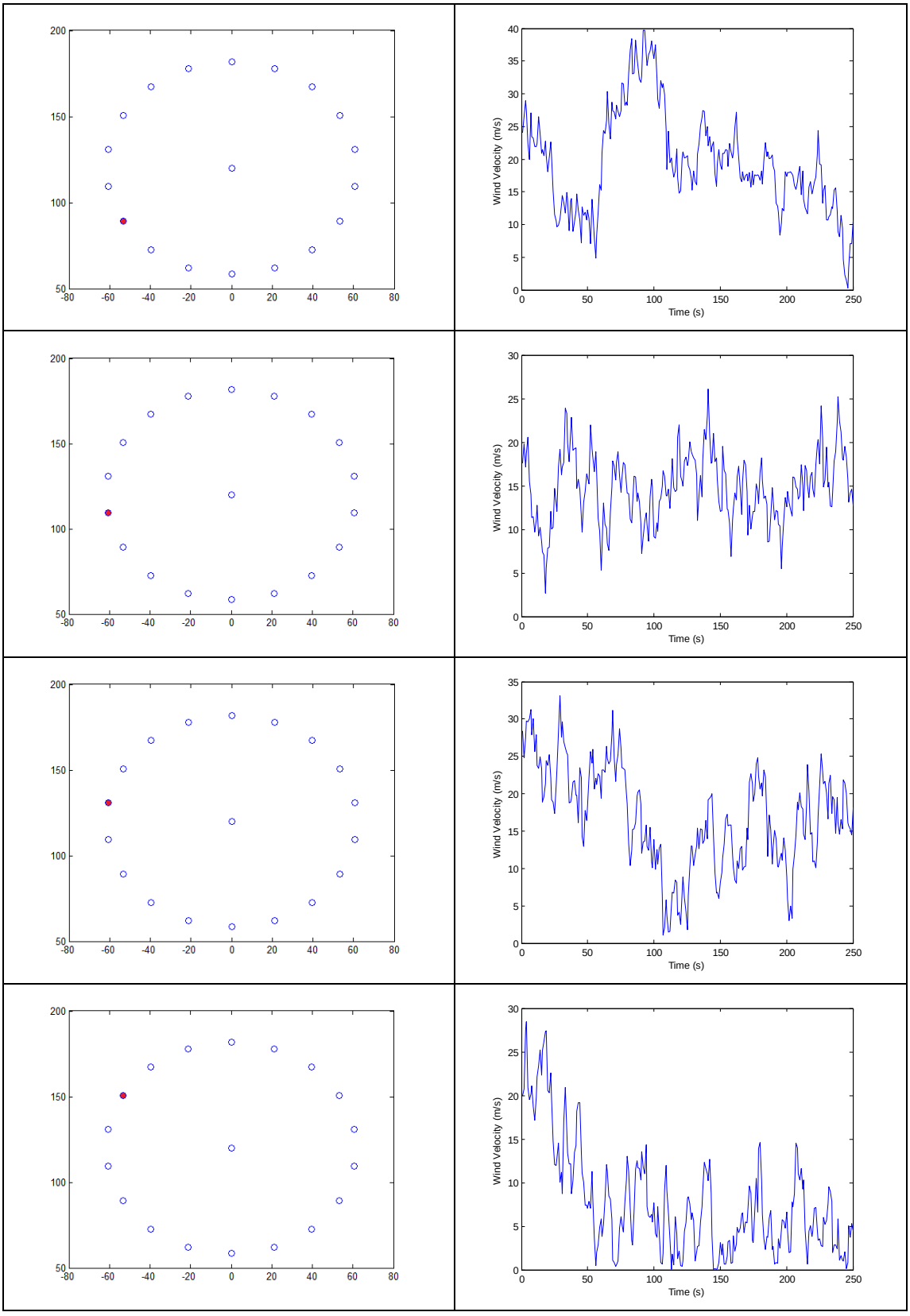
Wind Velocity (m/s)
Time (s)

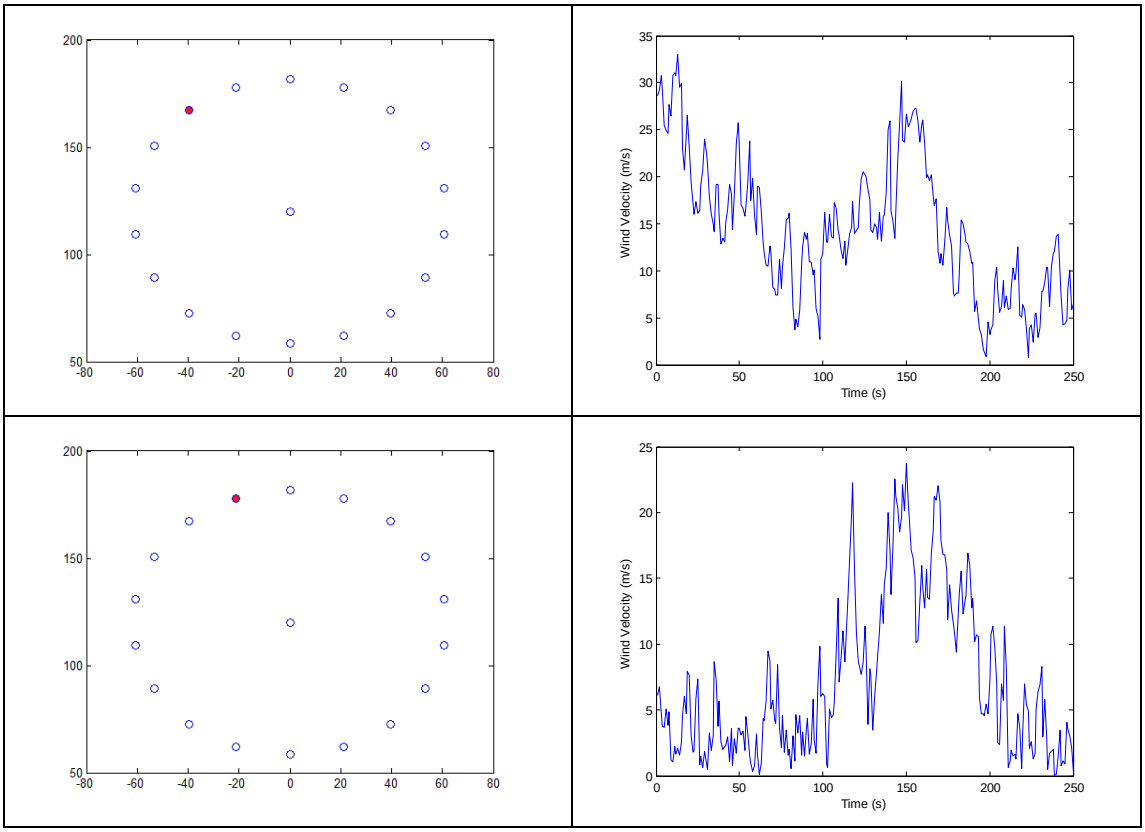

Figure 5.5: Wind-velocity time history at the outer part of the blade, for each azimuth position, during the blade's rotation.

As can be seen in the diagrams above, the duration of the time histories is 250 seconds. The time step for the generation their generation is 1 second. Regarding the frequency domain, the program uses a discretization of 250, the same as in the time domain.

5.4 Generation of aerodynamic-loads time histories

Apparently, the out-of-plane-load time histories directly depend on the pertinent wind-velocity time histories they are based on. This becomes visually clear through Figure 5.6, which demonstrates how the former time histories can differ between each other, according to the form of the latter. In the examples presented below, four random wind-velocity time histories produce different load histories for three certain rotational speed values, randomly selected.

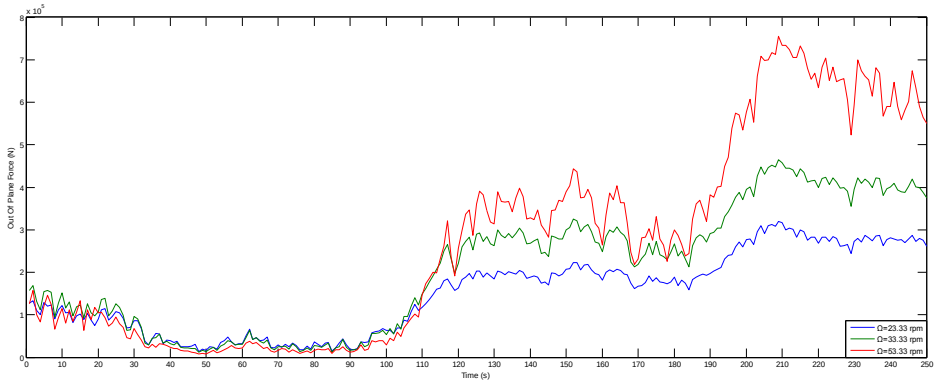
x 10^5
Out Of Plane Force (N)
Time (s)
Ω=23.33 rpm
Ω=33.33 rpm
Ω=53.33 rpm

(a)

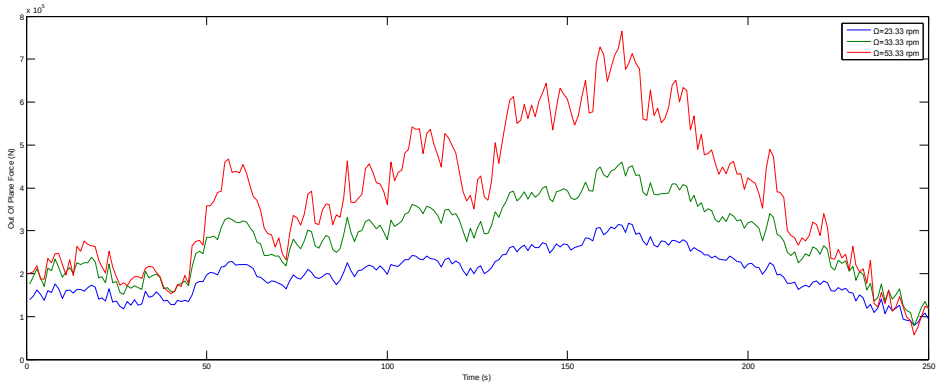
x 10^5
Out Of Plane Force (N)
Time (s)
Ω=23.33 rpm
Ω=33.33 rpm
Ω=53.33 rpm

(b)

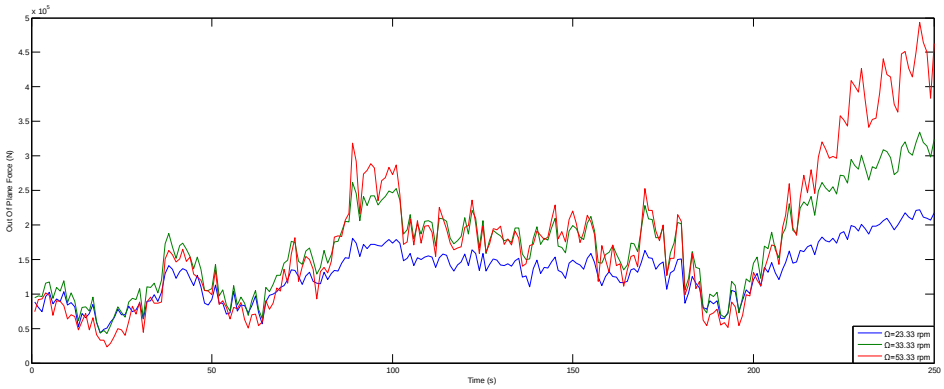
x 10^5
Out Of Plane Force (N)
Time (s)
Ω=23.33 rpm
Ω=33.33 rpm
Ω=53.33 rpm

(c)

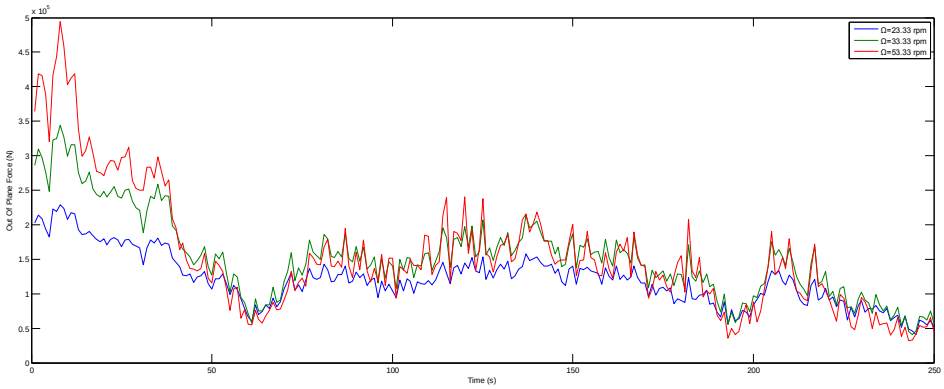
x 10^5
Out Of Plane Force (N)
Time (s)
Ω=23.33 rpm
Ω=33.33 rpm
Ω=53.33 rpm

(d)

Figure 5.6: Out-of-plane-loads time histories for different blade rotational speeds. Each set of time histories, (a), (b), (c), (d), is based on different wind-velocity time histories.

In order to check whether the load-values are realistic in these results, a simple calculation can be proved to be very useful. For a constant wind velocity *V*, the axial force exerted on a solid disk of a certain radius *r* can be calculated by the well-known expression:

$$F = \frac{1}{2}\rho\pi r^2 V^2 \tag{5.1}$$

where ρ is the air density. In the case of the examples of Figure 5.6, it is:

$$F = \frac{1}{2} * 1.225 * \pi * 61.5^2 * 10^2 \approx 728\ KN$$

The wind velocity value of 10 *m/s* in the calculation is the basic wind speed used for the generation of the wind-velocity time histories. Although the assumption of a solid disk and constant wind speed is far from the real case, the order of magnitude of the load obtained is comparable to the load values extracted from the program, a fact which strengthens the allegation that the program results are accurate enough.

Concerning the differences presented in each diagram of Figure 5.6, depending on the rotational speed of the rotor, it is clear that as the latter increases, so does the axial force on the blades. The explanation of this phenomenon is based on the origin of the resultant wind velocity. As can be derived from Figure 3.10, the higher the rotational speed of the rotor gets, the higher the resultant wind velocity becomes, as well.

6 Dynamic Analysis

6.1 General

In this chapter the resulting load time histories of the previous one are applied on a tower model, produced in the SAP2000 environment, in order to extract some basic conclusions, regarding the effects of the out-of-plane loads on the wind turbine's tower. That is, as soon as a proper model is created as described in section 6.2, the wind load time history is implemented and the pertinent displacements and stresses are presented, through a non-linear, dynamic analysis. The results are then examined and the dimensioning of the tower is accomplished accordingly.

6.2 Tower model

In order to achieve both the desired strength and the maximum economy with respect to material utilization, the tower of a wind turbine varies with height, in terms of section dimensions. Assuming that the tower can be simulated by a cantilever tubular beam, though such an assumption is significantly simplistic, the maximum bending moments are exerted on the ground level where the foundation is located. Therefore, at its base, the tower must be constituted of a relatively big diameter and an adequate thickness, as to be able to withstand the high load values. Contrary, at the top, the diameter can be smaller and so does the thickness of the cylindrical section.

On this basis, the tower designed for this thesis has the characteristics presented on Table 6.1. The tower is constituted of beam elements, while the material used is steel S235 with the properties shown in Table 6.2. The outside diameter and the thickness in each section has been chosen so that the diameter/thickness ratio is maintained below 90, which, for a steel type S235, is the limit between the 3^{rd} and 4^{th} section class. This was in order to avoid 4^{th} class sections, due to their limited buckling resistance. In fact, the tubular tower presents smoother variations of its sections with height. However, as to maintain the complexity of the model at low levels, the sections follow the value variations of the previously mentioned table. To conclude with, the tower model is demonstrated in Figure 6.2

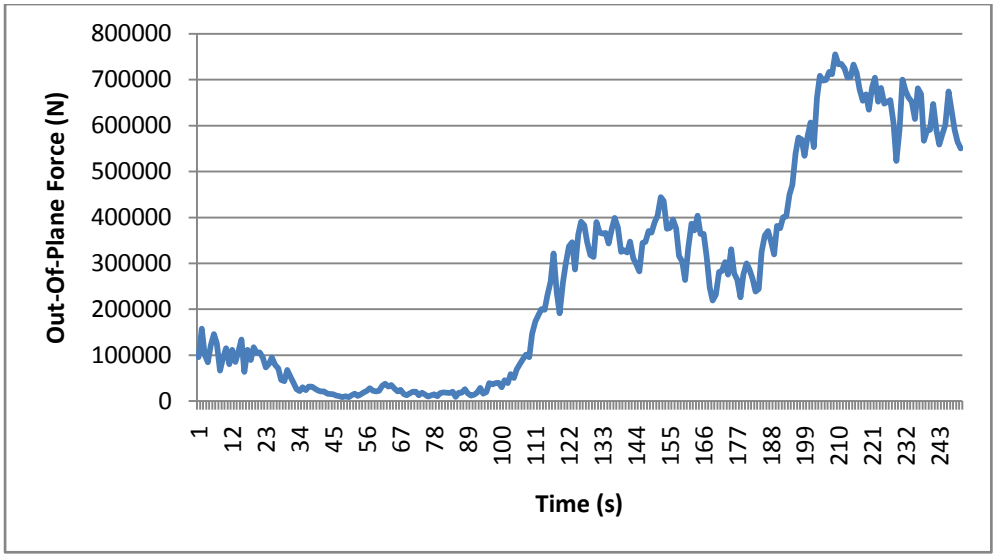

Figure 6.1: Out-of-plane-force time history for tower loading

Height (m)	Outside Diameter (m)	Thickness (m)	Diameter/ Thickness	Section Class
0	5.0	0.060	83.3	3
5	4.9	0.059	83.1	3
10	4.8	0.058	82.8	3
15	4.7	0.057	82.5	3
20	4.6	0.056	82.1	3
25	4.5	0.055	81.8	3
30	4.4	0.054	81.5	3
35	4.3	0.053	81.1	3
40	4.2	0.052	80.8	3
45	4.1	0.051	80.4	3
50	4.0	0.050	80.0	3
55	3.9	0.049	79.6	3
60	3.8	0.048	79.2	3
65	3.7	0.047	78.7	3
70	3.6	0.046	78.3	3
75	3.5	0.045	77.8	3
80	3.4	0.044	77.3	3
85	3.3	0.043	76.7	3
90	3.2	0.042	76.2	3
95	3.1	0.041	75.6	3
100	3.0	0.040	75.0	3
105	2.9	0.039	74.4	3
110	2.8	0.038	73.7	3
115	2.7	0.037	73.0	3
120	2.6	0.036	72.2	3

Table 6.1: Tower sections' characteristics

S235			
Modulus of Elasticity, E	2.100E+08	Minimum Yield Stress, Fy	2.35E+05
Poisson's Ratio, U	0.3	Minimum Tensile Stress, Fu	3.60E+05
Coefficient of Thermal Expansion, A	1.175E-05	Effective Yield Stress, Fye	379211.7
Shear Modulus, G	80769231	Effective Tensile Stress, Fue	492975.2

Table 6.2: Material properties

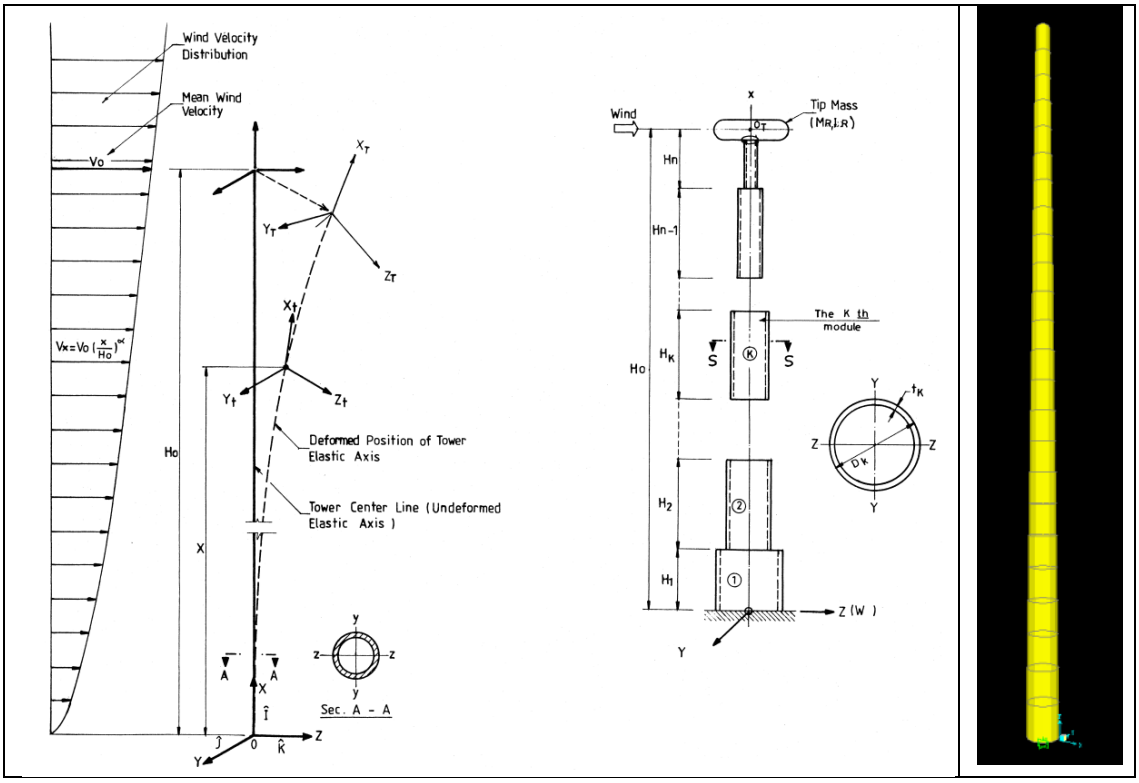

Figure 6.2: Sketches of the tower model (left) and pertinent simulation created in SAP2000 (right)

6.3 Tower loading

6.3.1 Displacements

The tower is loaded with the load time history shown in Figure 6.2 at the top section. Table 6.3 presents the displacements as a result of the loading, while Figure 6.3 demonstrates the axial-displacement time history, caused by the out-of-plane loads.

TABLE: Joint Displacements							
StepType	StepNum	U1	U2	U3	R1	R2	R3
Text	Unitless	m	m	m	Radians	Radians	Radians
Time	0	0	0	0	0	0	0
Time	1	1.766E-09	1.465E-10	3.929E-18	-2.422E-11	1.47E-10	0
Time	2	0.11164	0.000086	7.7E-12	-0.000014	0.002638	0
Time	3	0.268112	0.000093	-5.166E-13	-0.000015	0.003793	0
Time	4	0.391725	-0.00000682	-4.534E-12	0.000001128	0.005626	0
Time	5	0.354992	0.000031	6.322E-12	-0.000005173	0.005346	0
Time	6	0.188815	0.000123	5.967E-12	-0.00002	0.002892	0
Time	7	0.080558	0.000045	3.694E-12	-0.000007504	0.001811	0
Time	8	0.035707	-0.000021	-4.331E-12	0.00000355	0.000877	0
Time	9	0.075813	0.000081	-1.968E-12	-0.000013	0.001176	0
Time	10	0.193216	0.000079	1.05E-11	-0.000013	0.00342	0
Time	11	0.261963	-0.000019	1.057E-13	0.000003216	0.003368	0
Time	12	0.301995	0.000053	2.289E-12	-0.000008772	0.004924	0
Time	13	0.209572	0.000092	-1.637E-13	-0.000015	0.002962	0
Time	14	0.107283	0.000012	-3.733E-12	-0.000002056	0.001924	0
Time	15	0.058593	0.000026	9.406E-12	-0.000004342	0.001424	0
Time	16	0.088203	0.000084	4.862E-12	-0.000014	0.00132	0
Time	17	0.195052	0.000049	-1.516E-12	-0.000008175	0.003324	0
Time	18	0.248465	-0.000015	-2.836E-12	0.000002472	0.003573	0
Time	19	0.268847	0.000084	-2.487E-13	-0.000014	0.003967	0
Time	20	0.226299	0.000083	1.312E-11	-0.000014	0.003713	0
Time	21	0.137382	-0.000005876	5.523E-13	9.717E-07	0.001983	0
Time	22	0.106373	0.000036	-4.842E-12	-0.000005971	0.002223	0
Time	23	0.078148	0.000089	1.685E-12	-0.000015	0.001073	0
Time	24	0.118549	0.000008509	1.486E-13	-0.000001407	0.002011	0
Time	25	0.16667	0.000001605	9.512E-12	-2.655E-07	0.002687	0
Time	26	0.19448	0.000087	3.027E-12	-0.000014	0.002866	0
Time	27	0.200286	0.000042	-8.335E-12	-0.000006995	0.003063	0
Time	28	0.125443	-0.000037	-5.757E-14	0.000006132	0.001804	0
Time	29	0.0336	0.000042	4.093E-12	-0.000006905	0.00049	0
Time	30	-0.012202	0.000074	1.113E-11	-0.000012	0.000519	0
Time	31	-0.005153	-0.000024	-4.286E-12	0.000003994	-0.000204	0

Time	32	0.107919	0.00000193	-1.097E-11	-3.191E-07	0.001921	0
Time	33	0.158549	0.000069	7.113E-12	-0.000011	0.001962	0
Time	34	0.151805	-0.000007675	5.584E-12	0.000001269	0.002179	0
Time	35	0.065208	-0.000034	2.422E-12	0.000005608	0.001139	0
Time	36	-0.052667	0.000056	-3.005E-12	-0.000009196	-0.000757	0
Time	37	-0.074621	0.000035	-9.386E-12	-0.000005789	-0.000786	0
Time	38	-0.025226	-0.000043	7.385E-12	0.000007156	-0.000142	0
Time	39	0.081961	0.000025	7.257E-12	-0.000004055	0.001024	0
Time	40	0.18122	0.00006	1.148E-12	-0.000009951	0.002887	0
Time	41	0.145434	-0.000032	-7.851E-12	0.000005339	0.001572	0
Time	42	0.069272	-0.000017	-7.541E-12	0.000002754	0.001254	0
Time	43	-0.059851	0.000064	1.376E-11	-0.000011	-0.000774	0
Time	44	-0.117113	-3.345E-07	5.729E-12	5.531E-08	-0.001492	0
Time	45	-0.061069	-0.000046	-8.96E-12	0.000007573	-0.000618	0
Time	46	0.03397	0.000043	-3.346E-12	-0.000007087	0.000331	0
Time	47	0.141266	0.000035	-1.503E-12	-0.000005801	0.001919	0
Time	48	0.151974	-0.000052	1.055E-11	0.00000855	0.002266	0
Time	49	0.052465	0.00000625	2.659E-12	-0.000001033	0.000423	0
Time	50	-0.044386	0.000058	-8.589E-12	-0.000009609	-0.000213	0
Time	51	-0.13266	-0.000028	-3.497E-12	0.000004613	-0.002022	0
Time	52	-0.080775	-0.000028	1.247E-12	0.000004572	-0.000816	0
Time	53	0.033207	0.000059	1.225E-11	-0.000009715	0.000569	0
Time	54	0.132263	0.000009708	-9.045E-14	-0.000001605	0.001649	0
Time	55	0.174335	-0.000048	-1.48E-11	0.000007881	0.002454	0
Time	56	0.093417	0.000039	3.8E-12	-0.000006479	0.001327	0
Time	57	-0.016302	0.000051	7.048E-12	-0.000008472	-0.000164	0
Time	58	-0.076862	-0.000042	4.736E-12	0.000006923	-0.000633	0
Time	59	-0.078233	3.544E-07	-3.64E-12	-5.86E-08	-0.00133	0
Time	60	0.036433	0.000067	-8.987E-12	-0.000011	0.000868	0
Time	61	0.126279	-0.000009602	5.464E-12	0.000001588	0.001696	0
Time	62	0.178584	-0.000026	5.858E-12	0.000004284	0.00255	0
Time	63	0.148617	0.000063	3.09E-12	-0.00001	0.002204	0
Time	64	0.036173	0.000029	-3.071E-12	-0.000004821	0.000457	0
Time	65	-0.041885	-0.000045	-1.085E-11	0.000007426	-0.000381	0
Time	66	-0.067551	0.000029	9.832E-12	-0.000004773	-0.000622	0
Time	67	-0.021595	0.000056	8.001E-12	-0.000009336	-0.000417	0
Time	68	0.087283	-0.000039	-5.103E-12	0.000006486	0.001479	0
Time	69	0.124427	-0.000013	-4.486E-12	0.000002207	0.001396	0
Time	70	0.118146	0.000064	-2.575E-12	-0.000011	0.00185	0
Time	71	0.031662	-0.000005123	8.568E-12	8.472E-07	0.000536	0
Time	72	-0.055891	-0.00004	3.121E-12	0.000006582	-0.000796	0
Time	73	-0.065142	0.000048	-5.51E-12	-0.000007972	-0.000706	0
Time	74	-0.027329	0.000032	-3.515E-13	-0.000005254	-0.000306	0
Time	75	0.061191	-0.00005	-4.105E-12	0.000008308	0.000819	0

Time	76	0.12543	0.000013	8.23E-12	-0.000002194	0.001932	0
Time	77	0.093721	0.000056	4.84E-12	-0.000009311	0.00094	0
Time	78	0.039646	-0.000032	-9.633E-12	0.000005314	0.000848	0
Time	79	-0.055206	-0.000024	-8.333E-13	0.000003937	-0.000807	0
Time	80	-0.077632	0.000063	2.931E-12	-0.00001	-0.000878	0
Time	81	-0.026229	0.000004778	5.188E-12	-7.901E-07	-0.000202	0
Time	82	0.053423	-0.000045	4.439E-13	0.000007413	0.000598	0
Time	83	0.137293	0.000042	-7.348E-12	-0.000006989	0.002002	0
Time	84	0.129859	0.000042	3.542E-12	-0.00000689	0.001906	0
Time	85	0.050042	-0.00005	-2.861E-13	0.000008189	0.000495	0
Time	86	-0.032545	0.000006034	3.182E-12	-9.978E-07	-0.000107	0
Time	87	-0.100533	0.000063	4.095E-12	-0.00001	-0.001547	0
Time	88	-0.040668	-0.000019	-8.909E-12	0.000003085	-0.00016	0
Time	89	0.051439	-0.00003	8.278E-13	0.000004901	0.000706	0
Time	90	0.134345	0.000057	5.351E-12	-0.000009387	0.001722	0
Time	91	0.148482	0.000013	1.302E-12	-0.000002158	0.002136	0
Time	92	0.053188	-0.000048	2.521E-13	0.000007878	0.000662	0
Time	93	-0.036038	0.000038	-6.63E-12	-0.000006307	-0.000257	0
Time	94	-0.081787	0.000048	3.854E-12	-0.000007975	-0.000898	0
Time	95	-0.050292	-0.000041	2.795E-12	0.000006741	-0.000855	0
Time	96	0.067918	0.00000491	1.477E-13	-0.000000812	0.001336	0
Time	97	0.150195	0.000073	4.043E-12	-0.000012	0.001971	0
Time	98	0.195569	-0.000003409	-7.668E-12	5.637E-07	0.002908	0
Time	99	0.13436	-0.000027	6.329E-13	0.000004467	0.001911	0
Time	100	0.019935	0.00006	8.955E-12	-0.000009967	0.000253	0
Time	101	-0.046617	0.000037	-2.497E-13	-0.000006153	-0.000208	0
Time	102	-0.054605	-0.000039	-1.403E-12	0.000006514	-0.000623	0
Time	103	0.051075	0.000042	-5.401E-12	-0.000006897	0.000943	0
Time	104	0.177089	0.00007	5.155E-12	-0.000012	0.002637	0
Time	105	0.237711	-0.000013	7.785E-12	0.00000215	0.00324	0
Time	106	0.230858	0.000014	-2.72E-12	-0.000002241	0.00368	0
Time	107	0.133538	0.000098	1.552E-12	-0.000016	0.002057	0
Time	108	0.069417	0.000034	-3.494E-12	-0.000005704	0.001389	0
Time	109	0.071147	-0.000007825	3.192E-12	0.000001294	0.001385	0
Time	110	0.151123	0.000105	1.363E-11	-0.000017	0.00263	0
Time	111	0.307063	0.000105	-1.886E-12	-0.000017	0.004946	0
Time	112	0.440807	0.000028	-2.936E-12	-0.000004591	0.006668	0
Time	113	0.489846	0.000094	2.061E-12	-0.000016	0.007229	0
Time	114	0.437683	0.000141	1.076E-11	-0.000023	0.006848	0
Time	115	0.312472	0.000067	1.127E-11	-0.000011	0.005109	0
Time	116	0.260663	0.000084	-5.26E-12	-0.000014	0.004724	0
Time	117	0.345616	0.000198	2.807E-12	-0.000033	0.006027	0
Time	118	0.52693	0.000108	7.143E-12	-0.000018	0.007857	0
Time	119	0.653474	0.00003	6.519E-12	-0.00000488	0.009742	0

Time	120	0.557838	0.000144	1.23E-11	-0.000024	0.008479	0
Time	121	0.386383	0.000172	-3.879E-12	-0.000028	0.006408	0
Time	122	0.306373	0.000099	-6.105E-13	-0.000016	0.005749	0
Time	123	0.391608	0.000146	1.341E-11	-0.000024	0.006458	0
Time	124	0.631591	0.000185	1.186E-11	-0.000031	0.009967	0
Time	125	0.789766	0.000135	7.885E-12	-0.000022	0.012081	0
Time	126	0.8148	0.000133	-5.326E-12	-0.000022	0.012271	0
Time	127	0.747496	0.000222	6.013E-12	-0.000037	0.011935	0
Time	128	0.568758	0.000167	1.802E-11	-0.000028	0.008832	0
Time	129	0.446192	0.000084	5.628E-12	-0.000014	0.007532	0
Time	130	0.384901	0.000161	4.393E-12	-0.000027	0.006627	0
Time	131	0.452584	0.000219	-2.836E-13	-0.000036	0.007439	0
Time	132	0.670828	0.000117	5.283E-12	-0.000019	0.010821	0
Time	133	0.836072	0.000145	1.867E-11	-0.000024	0.012606	0
Time	134	0.87054	0.000221	7.407E-12	-0.000036	0.01317	0
Time	135	0.724415	0.000138	-1.22E-13	-0.000023	0.011283	0
Time	136	0.481564	0.000119	-3.492E-13	-0.00002	0.007801	0
Time	137	0.379173	0.000222	1.264E-11	-0.000037	0.007068	0
Time	138	0.460298	0.000193	1.964E-11	-0.000032	0.007827	0
Time	139	0.673078	0.000088	-2.197E-12	-0.000015	0.010226	0
Time	140	0.833498	0.000155	-9.142E-13	-0.000026	0.012715	0
Time	141	0.772495	0.000197	8.13E-12	-0.000033	0.011416	0
Time	142	0.596685	0.000116	1.005E-11	-0.000019	0.009719	0
Time	143	0.376535	0.00011	1.305E-11	-0.000018	0.006364	0
Time	144	0.285511	0.000189	-1.399E-12	-0.000031	0.004992	0
Time	145	0.366322	0.000122	-1.439E-12	-0.00002	0.006335	0
Time	146	0.536383	0.000099	9.812E-12	-0.000016	0.008497	0
Time	147	0.74794	0.000191	1.241E-11	-0.000032	0.011585	0
Time	148	0.847635	0.000198	1.183E-11	-0.000033	0.012965	0
Time	149	0.777631	0.000109	-4.952E-12	-0.000018	0.011658	0
Time	150	0.63546	0.000173	3.005E-12	-0.000029	0.010462	0
Time	151	0.485466	0.000236	1.886E-11	-0.000039	0.008162	0
Time	152	0.514631	0.000167	9.215E-12	-0.000028	0.008857	0
Time	153	0.700157	0.000157	6.245E-12	-0.000026	0.011329	0
Time	154	0.891547	0.000221	7.184E-13	-0.000037	0.01321	0
Time	155	0.953881	0.000173	5.909E-12	-0.000029	0.014683	0
Time	156	0.768669	0.000119	1.613E-11	-0.00002	0.011775	0
Time	157	0.530372	0.000196	7.049E-12	-0.000032	0.008729	0
Time	158	0.356907	0.000182	3.58E-12	-0.00003	0.006273	0
Time	159	0.318248	0.000083	-9.392E-13	-0.000014	0.005389	0
Time	160	0.441343	0.000108	5.332E-12	-0.000018	0.007271	0
Time	161	0.588891	0.000207	1.877E-11	-0.000034	0.009352	0
Time	162	0.72152	0.000149	2.566E-12	-0.000025	0.011007	0
Time	163	0.810772	0.000123	-3.528E-14	-0.00002	0.012695	0

Time	164	0.761409	0.000228	8.392E-12	-0.000038	0.011709	0
Time	165	0.664919	0.000178	9.281E-12	-0.00003	0.010568	0
Time	166	0.545555	0.000105	1.238E-11	-0.000017	0.008986	0
Time	167	0.452183	0.000159	1.642E-12	-0.000026	0.007061	0
Time	168	0.45069	0.000157	9.867E-13	-0.000026	0.007418	0
Time	169	0.409595	0.000052	4.904E-12	-0.000008519	0.006342	0
Time	170	0.374291	0.000083	5.101E-12	-0.000014	0.005893	0
Time	171	0.375897	0.000183	1.297E-11	-0.00003	0.006545	0
Time	172	0.407268	0.000114	-4.984E-13	-0.000019	0.006203	0
Time	173	0.546219	0.000084	-1.068E-12	-0.000014	0.009041	0
Time	174	0.609694	0.000165	1.118E-11	-0.000027	0.009156	0
Time	175	0.624198	0.000173	8.121E-12	-0.000029	0.009713	0
Time	176	0.562998	0.000068	6.18E-12	-0.000011	0.008798	0
Time	177	0.437623	0.000125	9.682E-13	-0.000021	0.006831	0
Time	178	0.336679	0.000153	1.753E-12	-0.000025	0.005652	0
Time	179	0.288201	0.000085	9.594E-12	-0.000014	0.005175	0
Time	180	0.358319	0.000104	4.538E-12	-0.000017	0.005757	0
Time	181	0.554553	0.000184	9.033E-12	-0.00003	0.008986	0
Time	182	0.670148	0.000116	1.536E-12	-0.000019	0.009818	0
Time	183	0.658365	0.000052	-1.681E-12	-0.000008624	0.009944	0
Time	184	0.466432	0.000143	1.19E-11	-0.000024	0.007331	0
Time	185	0.257503	0.000178	8.014E-12	-0.00003	0.004661	0
Time	186	0.270668	0.000108	4.634E-12	-0.000018	0.005416	0
Time	187	0.504652	0.000163	4.322E-12	-0.000027	0.00838	0
Time	188	0.830696	0.000211	3.817E-12	-0.000035	0.012434	0
Time	189	0.997028	0.000113	1.174E-11	-0.000019	0.014853	0
Time	190	0.848584	0.000132	6.989E-12	-0.000022	0.012623	0
Time	191	0.566236	0.000221	7.743E-12	-0.000037	0.009462	0
Time	192	0.335039	0.000186	4.779E-12	-0.000031	0.006302	0
Time	193	0.347325	0.000123	1.278E-12	-0.00002	0.006238	0
Time	194	0.640006	0.000226	1.698E-11	-0.000037	0.010709	0
Time	195	0.993402	0.000253	1.272E-11	-0.000042	0.015135	0
Time	196	1.251701	0.00019	3.757E-12	-0.000031	0.019073	0
Time	197	1.256548	0.000243	7.816E-12	-0.00004	0.019369	0
Time	198	1.044014	0.000313	9.837E-12	-0.000052	0.016031	0
Time	199	0.802579	0.000218	1.792E-11	-0.000036	0.013419	0
Time	200	0.637574	0.000211	1.088E-11	-0.000035	0.010868	0
Time	201	0.745384	0.000319	6.37E-12	-0.000053	0.012749	0
Time	202	1.033451	0.000267	8.518E-12	-0.000044	0.01622	0
Time	203	1.307452	0.000234	1.041E-11	-0.000039	0.020171	0
Time	204	1.447813	0.000333	2.295E-11	-0.000055	0.022369	0
Time	205	1.40313	0.000364	1.507E-11	-0.00006	0.021943	0
Time	206	1.205107	0.000265	6.468E-13	-0.000044	0.018875	0
Time	207	1.028465	0.000295	1.311E-11	-0.000049	0.017082	0

Time	208	0.970083	0.00038	1.929E-11	-0.000063	0.015863	0
Time	209	1.127688	0.000326	2.135E-11	-0.000054	0.018591	0
Time	210	1.372171	0.000273	8.323E-12	-0.000045	0.021396	0
Time	211	1.550974	0.000371	3.868E-12	-0.000061	0.023859	0
Time	212	1.516254	0.000353	1.867E-11	-0.000058	0.023284	0
Time	213	1.284082	0.000254	1.792E-11	-0.000042	0.020257	0
Time	214	1.005781	0.00032	1.651E-11	-0.000053	0.016513	0
Time	215	0.886459	0.000384	1.061E-11	-0.000064	0.015208	0
Time	216	1.011943	0.000281	1.006E-12	-0.000046	0.016381	0
Time	217	1.301399	0.000269	1.964E-11	-0.000044	0.02053	0
Time	218	1.481287	0.00035	2.215E-11	-0.000058	0.022427	0
Time	219	1.431964	0.000299	1.103E-11	-0.000049	0.022144	0
Time	220	1.151223	0.000226	2.354E-12	-0.000037	0.017948	0
Time	221	0.863542	0.000337	7.202E-12	-0.000056	0.014627	0
Time	222	0.781001	0.000354	2.568E-11	-0.000059	0.013482	0
Time	223	0.990098	0.000236	1.679E-11	-0.000039	0.016222	0
Time	224	1.314119	0.000296	4.599E-12	-0.000049	0.020398	0
Time	225	1.513493	0.00035	8.921E-12	-0.000058	0.022924	0
Time	226	1.44657	0.000264	8.665E-12	-0.000044	0.022094	0
Time	227	1.13665	0.000248	2.303E-11	-0.000041	0.018112	0
Time	228	0.803895	0.000324	1.633E-11	-0.000054	0.013283	0
Time	229	0.63927	0.000247	-1.445E-12	-0.000041	0.011033	0
Time	230	0.693194	0.000202	6.045E-12	-0.000033	0.011642	0
Time	231	1.01176	0.000335	1.781E-11	-0.000055	0.016797	0
Time	232	1.408456	0.000353	2.359E-11	-0.000058	0.021573	0
Time	233	1.642117	0.000242	9.384E-12	-0.00004	0.024837	0
Time	234	1.504144	0.00027	-1.829E-12	-0.000045	0.022644	0
Time	235	1.088777	0.000339	1.66E-11	-0.000056	0.017346	0
Time	236	0.682365	0.000286	1.842E-11	-0.000047	0.012168	0
Time	237	0.594815	0.000245	1.578E-11	-0.000041	0.010912	0
Time	238	0.883754	0.000304	7.428E-12	-0.00005	0.014203	0
Time	239	1.278863	0.000286	1.018E-12	-0.000047	0.019766	0
Time	240	1.460589	0.0002	1.536E-11	-0.000033	0.021692	0
Time	241	1.372395	0.000302	2.027E-11	-0.00005	0.021562	0
Time	242	1.017606	0.00032	1.196E-11	-0.000053	0.015664	0
Time	243	0.709008	0.000202	3.293E-12	-0.000033	0.012224	0
Time	244	0.572084	0.00023	2.121E-12	-0.000038	0.010132	0
Time	245	0.744784	0.000333	2.371E-11	-0.000055	0.012602	0
Time	246	1.159685	0.000293	1.757E-11	-0.000048	0.018615	0
Time	247	1.505426	0.000225	4.223E-12	-0.000037	0.022478	0
Time	248	1.582848	0.000306	7.716E-12	-0.000051	0.023672	0
Time	249	1.245812	0.000286	9.317E-12	-0.000047	0.019298	0
Time	250	0.69926	0.000184	1.731E-11	-0.00003	0.011356	0

Table 6.3: Displacements due to tower loading with zero damping

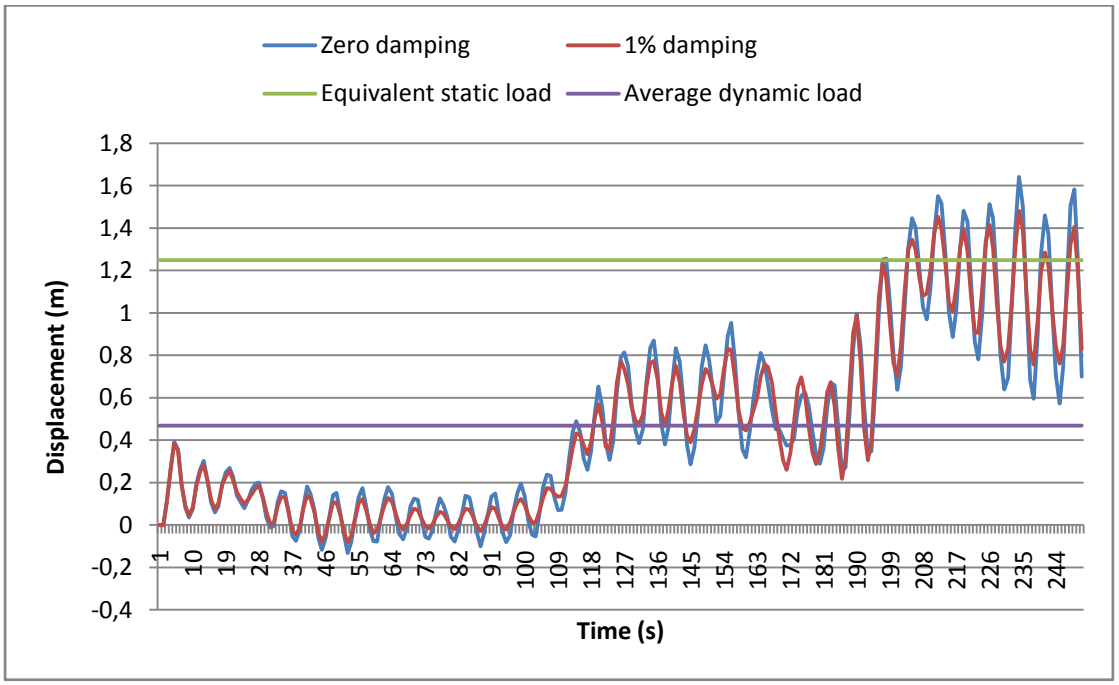

Figure 6.3: Displacement time history in the direction of the force exerted on the tower

As can be derived from Figure 6.3, the maximum displacement for zero damping is 1.64 m, which as a proportion of the total tower height is 1.37%, while for 1% damping the pertinent displacement is 1.48 m, or 1.23%. The equivalent static load, calculated in section 5.4 (728 KN), gives a constant displacement of 1.24 m and the average dynamic load which is 272.47 KN yields a displacement of 0.48 m. The displacements in the other directions are negligible, as shown in Table 6.3.

In order to check whether the previous results are realistic or not, a rough calculation is made , using the well known expression which gives the displacement of a cantilever's edge, for certain values of load, length, modulus of elasticity and moment of inertia:

$$\delta = \frac{PL^3}{3EI} = \begin{cases} \dfrac{728 * 120^3}{3 * 210 * 10^6 * 1.5396} = 1.25\ m, & \text{for the equivalent static load} \\ \dfrac{272.47 * 120^3}{3 * 210 * 10^6 * 1.5396} = 0.49\ m, & \text{for the average dynamic load} \end{cases} \quad (6.1)$$

Obviously, the results of the two methods are in complete agreement.

6.3.2 Stresses

Table presents the resulting reactions due to the out-of-plane loads exerted on the wind turbine's tower. In figures 6.4, 6.5, the reactions at the foundation of the tower are displayed for zero damping, damping of 1%, for the equivalent static load of section 5.4 and the average dynamic load, as in section 6.3.1.

StepNum	F1	F2	F3	M1	M2	M3
Unitless	KN	KN	KN	KN-m	KN-m	KN-m
0	0	0	0	0	0	0
1	0.00003251	0.00007139	1.812E-10	-0.000537	0.0001838	0
2	6.63	42.07	0.0002434	-316.4404	-1207.2319	0
3	-39.342	45.226	0.0001404	-340.1786	-20159.9898	0
4	-459.947	-3.324	0.00006587	24.9991	-35711.7978	0
5	-183.572	15.245	0.0001648	-114.668	-23483.3967	0
6	-326.677	59.775	0.00009638	-449.614	-19701.1399	0
7	277.535	22.113	0.0001798	-166.3319	4335.2019	0
8	-91.865	-10.461	0.0001034	78.6824	-3127.7847	0
9	130.895	39.364	0.00005445	-296.0854	-2653.9635	0
10	-240.46	38.675	0.0001968	-290.9051	-12827.942	0
11	-240.621	-9.478	-0.00001862	71.2918	-24367.3654	0
12	-164.034	25.851	0.000181	-194.4467	-20549.632	0
13	-58.643	44.773	0.0001636	-336.7776	-15847.4519	0
14	-168.45	6.06	0.00002477	-45.586	-8578.6497	0
15	116.391	12.795	0.0001788	-96.2412	3498.6743	0
16	-181.305	40.822	0.00005908	-307.0529	-11430.5212	0
17	252.204	24.091	0.0001375	-181.2098	-4985.0416	0
18	-543.571	-7.286	0.0001523	54.803	-27012.8006	0
19	-13.274	40.881	0.00002351	-307.5019	-17103.9785	0
20	-281.442	40.672	0.0001995	-305.9295	-17875.6205	0
21	19.979	-2.864	0.00007757	21.5404	-9530.1142	0
22	46.891	17.596	0.0001047	-132.3543	-2818.6755	0
23	-90.465	43.512	0.0001595	-327.2874	-6656.2444	0
24	-151.146	4.147	-0.00002135	-31.1914	-9372.5086	0
25	51.196	0.782	0.0001399	-5.8849	-7589.0634	0
26	-272.976	42.238	0.0001354	-317.707	-20000.4874	0
27	114.792	20.614	0.00003145	-155.0526	-9335.8078	0
28	-484.678	-18.072	0.0001035	135.9327	-16626.2184	0
29	199.816	20.35	-0.00004573	-153.0693	1249.4637	0
30	129.16	36.163	0.0001532	-272.0134	6091.4116	0
31	4.005	-11.77	0.00006821	88.5303	-472.135	0
32	-70.09	0.941	-0.00002794	-7.0742	-5920.7729	0
33	-218.011	33.471	0.000115	-251.7603	-15717.0652	0
34	-178.701	-3.74	-0.00004198	28.1322	-14846.452	0
35	204.223	-16.528	0.0000353	124.3166	1410.6175	0
36	-223.081	27.101	0.000103	-203.8504	-1758.7873	0
37	362.39	17.061	-0.00005941	-128.3294	14395.5244	0
38	-206.346	-21.09	0.00009747	158.6338	-774.9315	0
39	120.434	11.949	-0.00001437	-89.8799	-5091.2247	0
40	-93.117	29.324	0.00005251	-220.5723	-12651.4734	0
41	-354.08	-15.735	0.0000588	118.3563	-18128.648	0

42	-37.672	-8.117	-0.00007634	61.0573	-3738.6637	0
43	199.892	31	0.0001073	-233.1775	8019.6151	0
44	46.999	-0.163	0.000004115	1.2263	8086.2678	0
45	294.359	-22.319	-0.00004811	167.8785	12654.4777	0
46	-398.343	20.885	0.0001098	-157.0909	-10813.799	0
47	133.517	17.096	-0.00007181	-128.5894	-7612.5897	0
48	-242.914	-25.198	0.00005719	189.531	-14413.3635	0
49	-45.447	3.046	0.000003838	-22.9088	-6530.6703	0
50	117.979	28.318	-0.00002377	-212.9995	7756.7786	0
51	-0.088	-13.594	0.00008019	102.2527	9138.6329	0
52	159.38	-13.473	-0.00005974	101.3401	9171.4267	0
53	196.136	28.631	0.00006233	-215.358	1911.0718	0
54	-424.525	4.731	0.00004163	-35.5856	-18691.5447	0
55	8.614	-23.225	-0.00008741	174.6957	-9957.8497	0
56	-311.179	19.093	0.0001422	-143.6141	-12783.4975	0
57	298.739	24.966	-0.00001671	-187.79	5888.374	0
58	77.659	-20.403	0.00001351	153.4681	9582.9122	0
59	-62.802	0.173	0.00004801	-1.2993	3596.4491	0
60	86.305	32.527	-0.00002472	-244.6627	641.8601	0
61	-95.226	-4.679	0.0001183	35.1959	-10646.1565	0
62	-228.448	-12.626	-0.0000113	94.9694	-17373.1313	0
63	62.283	30.802	0.00001508	-231.6845	-7459.3779	0
64	-355.834	14.207	0.0001114	-106.8609	-9539.3873	0
65	319.809	-21.883	-0.00007132	164.6019	10409.9561	0
66	37.484	14.065	0.0001217	-105.7925	6254.2752	0
67	103.206	27.514	0.00000653	-206.9551	2128.6707	0
68	-115.105	-19.115	-0.0000538	143.7785	-5586.5121	0
69	-277.311	-6.505	0.00008572	48.9295	-14941.3575	0
70	37.175	31.4	-0.00001315	-236.1838	-8037.0561	0
71	94.357	-2.497	0.00006497	18.7794	523.842	0
72	-187.415	-19.397	-0.000009318	145.9042	224.8812	0
73	301.725	23.493	-0.00004759	-176.7096	12131.3262	0
74	-156.048	15.483	0.0001432	-116.46	-1353.4348	0
75	148.687	-24.484	-0.00006711	184.1668	-2040.3765	0
76	-161.292	6.466	0.00003602	-48.639	-10440.3696	0
77	-221.325	27.44	0.00003106	-206.4014	-12420	0
78	35.056	-15.661	-0.00006566	117.8025	-119.893	0
79	59.002	-11.603	0.0001097	87.2749	4757.1785	0
80	153.481	30.547	-0.000003174	-229.767	7649.277	0
81	145.084	2.329	-0.000008321	-17.5152	6721.422	0
82	-384.302	-21.846	0.00003728	164.3224	-11266.7707	0
83	164.652	20.598	-0.00003721	-154.9334	-6230.3132	0
84	-203.381	20.305	0.000148	-152.7289	-13165.557	0
85	-39.187	-24.132	-0.00006442	181.518	-5053.553	0

86	42.738	2.941	-0.00002837	-22.1185	5884.8629	0
87	12.735	30.555	0.0001047	-229.8313	6074.607	0
88	238.936	-9.091	-0.00003563	68.3804	8646.8962	0
89	-32.243	-14.444	0.00007939	108.6433	-3712.4541	0
90	-292.4	27.664	-7.283E-07	-208.0798	-16128.1482	0
91	12.514	6.358	-0.00005564	-47.8262	-8486.308	0
92	-296.83	-23.217	0.0001009	174.637	-9974.1765	0
93	367.441	18.586	-0.00001556	-139.8003	9802.6968	0
94	27.911	23.502	0.00008282	-176.7765	7403.1832	0
95	-70.328	-19.865	-0.00002494	149.4177	2246.6133	0
96	64.841	2.393	-0.00002874	-17.9991	-1210.5658	0
97	-158.549	35.592	0.0001756	-267.7194	-14958.4842	0
98	-96.456	-1.661	-0.0000144	12.4967	-14925.096	0
99	-147.438	-13.163	0.00002704	99.0093	-10377.0012	0
100	-207.476	29.374	0.00006394	-220.9435	-5806.2322	0
101	411.508	18.134	-0.00001602	-136.4012	13079.1363	0
102	-102.594	-19.196	0.0001426	144.3847	2077.6332	0
103	135.689	20.324	0.00001206	-152.8743	326.4646	0
104	-223.256	34.177	0.00005206	-257.0715	-15170.7835	0
105	-326.382	-6.336	0.00009791	47.6574	-22526.447	0
106	20.19	6.604	0.00002132	-49.672	-13859.1954	0
107	-97.196	47.604	0.0002211	-358.0719	-10512.7751	0
108	-57.599	16.811	0.0000629	-126.4462	-3383.4985	0
109	46.579	-3.813	0.00003478	28.6835	-843.2825	0
110	-137.777	51	0.0002578	-383.6121	-11309.6921	0
111	93.804	51.078	0.0001403	-384.1977	-16950.0062	0
112	-504.253	13.529	0.0002576	-101.7612	-36386.5183	0
113	-421.78	45.726	0.00019	-343.9389	-39121.2224	0
114	-197.653	68.945	0.0001877	-518.5897	-30617.3125	0
115	-168.581	32.821	0.0003383	-246.8726	-21088.4236	0
116	36.933	41.082	0.0002194	-309.0137	-12208.8274	0
117	-104.472	96.347	0.000413	-724.7008	-18926.0609	0
118	-568.321	52.443	0.000265	-394.4656	-44568.0828	0
119	-295.256	14.382	0.0001213	-108.1824	-46994.4453	0
120	-494.264	70.018	0.0004081	-526.6612	-45242.0744	0
121	-63.644	83.88	0.0002855	-630.9318	-23039.1718	0
122	-86.586	48.045	0.0003593	-361.3827	-13505.3059	0
123	-277.511	71.152	0.0004147	-535.1892	-27694.0213	0
124	-132.71	90.387	0.0002749	-679.8785	-41251.8396	0
125	-595.784	65.758	0.0004862	-494.6172	-59806.1741	0
126	-746.905	64.676	0.0003731	-486.4824	-65689.7517	0
127	-283.448	108.136	0.0004213	-813.3757	-47965.0479	0
128	-502.929	81.159	0.0004587	-610.4668	-45465.5773	0
129	43.115	40.719	0.0002564	-306.2833	-23521.0897	0

130	-189.183	78.7	0.0004321	-591.9679	-22984.6846	0
131	-293.287	106.636	0.0004215	-802.0987	-31529.835	0
132	-264.152	57.026	0.0003546	-428.9436	-42785.8327	0
133	-669.195	70.634	0.0004826	-531.299	-66092.5882	0
134	-504.423	107.505	0.0003577	-808.6336	-65629.4205	0
135	-520.391	67.316	0.0004225	-506.3416	-52007.9324	0
136	-398.093	57.81	0.0003962	-434.8371	-35139.2057	0
137	201.46	107.954	0.0004169	-812.0143	-13938.7796	0
138	-182.773	94.005	0.0005197	-707.0876	-28595.9681	0
139	-498.091	42.799	0.0002629	-321.9243	-51534.223	0
140	-602.622	75.715	0.0003952	-569.5156	-61633.2524	0
141	-701.219	95.912	0.0004137	-721.4304	-64451.0365	0
142	-87.7	56.358	0.0003117	-423.9145	-35916.3426	0
143	-252.158	53.622	0.0004172	-403.3351	-24731.0727	0
144	-55.761	92.149	0.0002843	-693.1281	-16003.7769	0
145	-92.786	59.541	0.0003255	-447.8574	-19683.2972	0
146	-377.794	48.43	0.0004212	-364.2803	-39453.1851	0
147	-318.901	93.075	0.0003289	-700.0971	-52864.2906	0
148	-640.566	96.659	0.0004879	-727.0475	-63726.9548	0
149	-738.144	52.915	0.0003432	-398.0163	-63285.7981	0
150	-140.525	84.191	0.0004317	-633.2683	-37687.5783	0
151	-223.904	115.148	0.0005525	-866.1254	-32171.196	0
152	-30.072	81.202	0.0003912	-610.784	-27682.5833	0
153	-507.75	76.712	0.0005214	-577.0116	-48195.285	0
154	-739.727	107.901	0.0004258	-811.6144	-72307.0682	0
155	-466.118	84.529	0.0004085	-635.8122	-67642.895	0
156	-623.298	58.186	0.0004999	-437.6638	-59621.2326	0
157	-204.887	95.584	0.0003318	-718.9622	-33954.3391	0
158	-91.676	88.672	0.0004027	-666.9758	-18436.6359	0
159	-231.912	40.414	0.0003455	-303.9889	-22200.8483	0
160	41.766	52.55	0.0002529	-395.2702	-24325.7336	0
161	-425.237	100.786	0.0004696	-758.0952	-43037.5413	0
162	-543.192	72.609	0.0003271	-546.1535	-55065.6279	0
163	-536.881	59.852	0.000427	-450.1979	-57369.3491	0
164	-475.594	111.201	0.0005253	-836.4356	-57445.9879	0
165	-267.167	86.96	0.0003584	-654.0986	-45401.9783	0
166	-305.517	51.219	0.0004318	-385.2619	-34281.8858	0
167	-443.377	77.616	0.0002957	-583.8094	-36605.1076	0
168	5.753	76.677	0.0003115	-576.7504	-24628.8141	0
169	-363.938	25.104	0.0003051	-188.8288	-32788.0007	0
170	-117.24	40.263	0.0001641	-302.8514	-24973.6764	0
171	-176.388	89.265	0.0003765	-671.4308	-21130.8127	0
172	-364.13	55.624	0.0002762	-418.3967	-33137.0369	0
173	-112.992	41.089	0.000331	-309.0658	-32106.55	0

174	-443.974	80.52	0.0004017	-605.6546	-47927.7122	0
175	-419.866	84.239	0.0002793	-633.6336	-46333.3441	0
176	-398.343	33.187	0.0003172	-249.6241	-39174.4166	0
177	-363.025	60.845	0.0003064	-457.6628	-34639.3579	0
178	139.683	74.583	0.0002638	-560.9968	-16557.7492	0
179	-187.011	41.294	0.0003655	-310.6078	-16936.1787	0
180	-209.637	50.872	0.0002131	-382.6516	-24673.3805	0
181	-299.06	89.649	0.0003778	-674.3255	-36675.5237	0
182	-498.372	56.364	0.0003331	-423.9612	-54363.5882	0
183	-447.674	25.416	0.0002164	-191.1761	-50410.3695	0
184	-276.629	69.741	0.0003347	-524.5762	-31824.1419	0
185	-161.581	86.977	0.0002893	-654.2253	-16321.2502	0
186	207.944	52.505	0.0004089	-394.9328	-5228.2075	0
187	-282.131	79.407	0.0004826	-597.2825	-34529.963	0
188	-464.934	102.59	0.0003432	-771.6653	-62469.938	0
189	-969.119	55.078	0.0003914	-414.2858	-80273.1769	0
190	-634.467	64.208	0.000343	-482.9635	-66684.3697	0
191	-179.411	107.672	0.0004784	-809.8908	-35514.639	0
192	131.367	90.789	0.000514	-682.8972	-12178.4607	0
193	-214.725	59.734	0.0003457	-449.3061	-21324.1875	0
194	-177.745	110.061	0.0005415	-827.8548	-36414.9701	0
195	-783.027	123.201	0.0005262	-926.6949	-78668.7666	0
196	-679.674	92.677	0.0005884	-697.0979	-90744.9091	0
197	-1000.628	118.619	0.0007123	-892.2311	-95644.4115	0
198	-643.614	152.453	0.0005536	-1146.7245	-77156.1782	0
199	-413.211	106.19	0.000632	-798.7406	-50606.6801	0
200	-93.42	102.762	0.0006323	-772.9602	-36451.4397	0
201	-227.335	155.599	0.0006929	-1170.3914	-45149.8923	0
202	-600.314	129.988	0.0006779	-977.748	-71663.5393	0
203	-1036.488	113.822	0.0006241	-856.1477	-99996.3194	0
204	-820.378	162.21	0.0008362	-1220.1169	-104075.162	0
205	-868.994	177.561	0.0008416	-1335.5804	-102331.726	0
206	-654.621	129.143	0.000713	-971.3873	-84744.9968	0
207	-662.433	143.671	0.0008546	-1080.6671	-67937.4916	0
208	-276.065	185.292	0.0007361	-1393.7309	-61135.9049	0
209	-545.61	158.675	0.0008841	-1193.5259	-74229.5502	0
210	-779.13	132.879	0.00084	-999.4893	-97192.9873	0
211	-1142.759	180.865	0.0007731	-1360.4352	-117708.851	0
212	-1002.561	172.077	0.0008729	-1294.3316	-111262.059	0
213	-830.781	123.893	0.0007219	-931.9019	-93157.3598	0
214	-246.418	156.147	0.0008008	-1174.5136	-61659.1471	0
215	-430.051	187.249	0.0009073	-1408.4554	-55031.81	0
216	-421.214	137.017	0.0006885	-1030.6184	-65475.3472	0
217	-958.543	130.868	0.0008135	-984.3633	-95058.0819	0

218	-821.262	170.653	0.0007252	-1283.6192	-109929.054	0
219	-1007.922	145.542	0.0007457	-1094.7422	-107386.166	0
220	-761.085	109.913	0.0007398	-826.7462	-82154.9976	0
221	-375.34	164.366	0.0006967	-1236.3332	-54160.5532	0
222	-66.155	172.462	0.0008551	-1297.2291	-42143.6691	0
223	-555.434	115.222	0.0007152	-866.6784	-67227.9885	0
224	-666.903	144.26	0.0007075	-1085.096	-91947.6372	0
225	-1403.028	170.328	0.0008316	-1281.1764	-121566.823	0
226	-741.318	128.784	0.00063	-968.6919	-103420.164	0
227	-801.921	120.979	0.0007753	-909.9864	-82927.9807	0
228	-168.075	157.845	0.0007041	-1187.2852	-48270.0772	0
229	-286.523	120.439	0.0005308	-905.923	-38587.79	0
230	-294.852	98.212	0.0007099	-738.7349	-41820.5551	0
231	-413.491	163.407	0.0007463	-1229.1187	-65460.7379	0
232	-764.35	171.821	0.0007876	-1292.4086	-102214.015	0
233	-1450.885	118.142	0.0007536	-888.6408	-130006.886	0
234	-961.103	131.8	0.0006354	-991.3797	-112492.302	0
235	-801.183	165.406	0.0008127	-1244.1571	-80007.9106	0
236	210.097	139.386	0.0007029	-1048.4369	-29862.8999	0
237	-264.902	119.481	0.00073	-898.7139	-33349.6746	0
238	-375.497	147.94	0.0006817	-1112.7797	-56967.713	0
239	-909.417	139.513	0.0006062	-1049.3894	-96214.7374	0
240	-1093.262	97.531	0.000717	-733.613	-114523.552	0
241	-805.71	147.352	0.000704	-1108.3567	-97909.119	0
242	-613.853	155.989	0.0006348	-1173.318	-74678.8708	0
243	-469.852	98.678	0.0006739	-742.2346	-44355.0328	0
244	185.517	111.979	0.0005676	-842.2866	-25118.2391	0
245	-451.103	162.32	0.0007866	-1220.9434	-50831.6699	0
246	-326.621	142.827	0.0007091	-1074.3228	-72053.7524	0
247	-1528.348	109.485	0.0006408	-823.5265	-125579.399	0
248	-1038.864	149.008	0.0007466	-1120.8135	-119078.163	0
249	-789.61	139.433	0.0006098	-1048.7902	-92922.6702	0
250	-289.409	89.479	0.0006247	-673.0435	-45676.2068	0

Table 6.4: Reactions at the foundation of the structure due to tower loading with zero damping

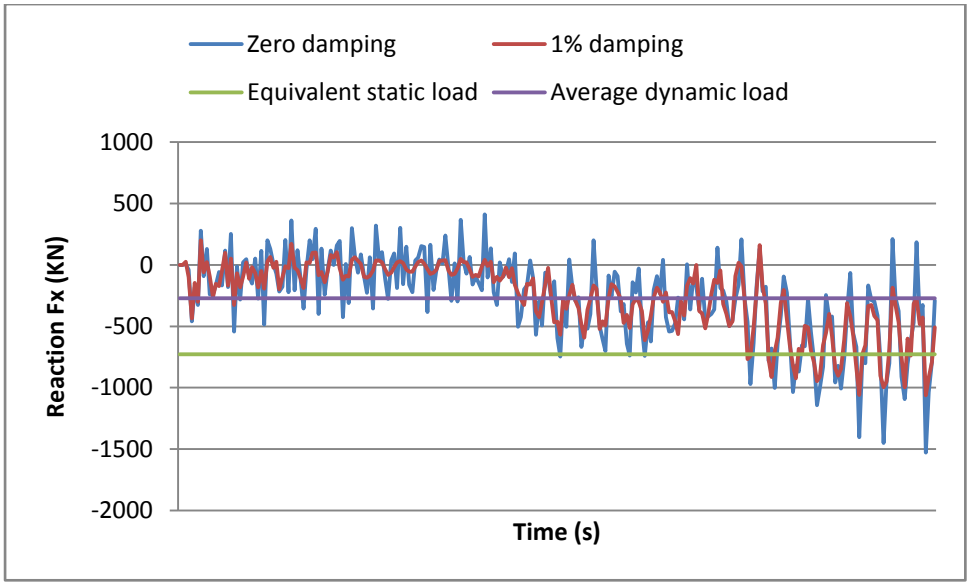

Figure 6.4: Reaction Fx due to out-of-plane loading

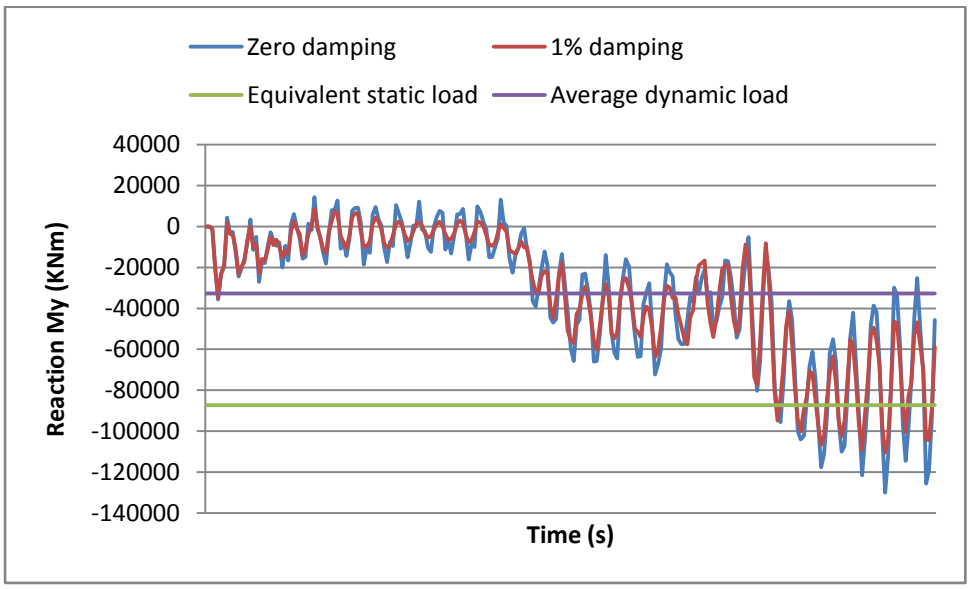

Figure 6.5: Reaction My due to out-of-plane loading

The maximum reaction Fx is equal to 1528.35 KN, while the maximum moment My is equal to 130007 KNm (both for zero damping).

At this point it would be crucial to check whether these reactions are within the strength limits of the tower's section at the base, or a change in section properties is necessary. The moment of resistance of the section is given by Eq. 6.2:

$$w = \frac{I}{r} = \frac{2.8409}{2.5} = 1.136\, m^3 \tag{6.2}$$

where I is the moment of inertia of the section and r is the radius of it.
The yield stress of the steel must be higher than the quantity:

$$f_y > \frac{M_y}{w} \xrightarrow{yields} 235000 > \frac{130007}{1.136} = 114443\ KN/m^2 \quad (6.3)$$

which is true, hence, the selection of material and section dimensions is adequate for the current maximum loads.

7 Final remarks and suggestions for further research

The scope of this thesis was, first of all, to provide a programming tool, with the utilization of which the researcher can, as realistically as possible, repoduce the conditions to which a wind turbine is exposed, as far as the wind factor is concerned. With use of the two parts of the pertinent algorithm, based on the theory described in Chapters 2, 3, a wind field is firstly generated and, subsequently, this field becomes the source of loading for the blades of the wind turbine, as soon as a series of aerodynamic parameters have been appropriately incorporated into the calculations. Furthermore, the results of several executions of the program are presented, depticting the behavior of the wind turbine in different conditions. These results were in agreement with those obtained from the bibliography and also with the ones yielded from the rough calculations referring to a simpler model of the rotor. This was also the case with the exertion of the load time histories, derived from the previous steps, on the tower model created in the SAP2000 environment. Indeed, the dynamic analysis of this simulation resulted in displacement and stress values not far from the ones obtained from simple calculations, based on the equivalent static load conditions.

Regardless of the decent performance of the program, however, significant aspects of the phenomenon of wind flow passing through the rotor of a wind turbine have been neglected, in order to simplify the simulation. One of the most important is the fact that the rotor axis of a wind turbine rotor is usually not aligned with the wind because the wind is continuously changing direction; the rotor is not capable of following this variability and so spends most of its time in a yawed condition. The yawed rotor is less efficient than the non-yawed rotor and so it is vital to assess the efficiency for purposes of energy production estimation. In the yawed condition, even in a steady wind, the angle of attack on each blade is continuously changing as it rotates and so the loads on the rotor blades are fluctuating, causing fatigue damage. The changes in angle of attack mean that the blade forces cause not only a thrust in the axial direction but also moments about the yaw (z) axis and the tilt axis.

Regarding the structural engineering part of the subject, further research has to be carried out concerning the fatigue factor. From earlier chapters it is clear that the loads on a wind turbine vary constantly with time, giving rise to a possible breakdown due to accumulated fatigue damage. This fact, therefore, should be taken into consideration in any future venture, in which wind turbine towers are involved.

8 References

1. Burton T., Sharpe D., Jenkins N., Bossanyi E. (2001). "Wind energy handbook" John Wiley & Sons, Ltd Baffins Lane, Chichester West Sussex, PO19 1UD, England.
2. Carassale L., Solari, G. (2006). "Monte Carlo simulation of wind velocity fields on complex structures" Journal of Wind Engineering and Industrial Aerodynamics 94 (2006) 323–339.
3. CISM (2009). International APT Course Environmental Wind Engineering and Wind Energy Structures "Steel substructures of onshore and offshore wind energy systems" 14. - 18. September 2009, Udine, Italy.
4. Connell J. R., (1982). "The spectrum of wind speed fluctuations encountered by a rotating blade of a wind energy conversion system" Solar Energy, Vol. 29, No. 5, pp. 363-375, 1982 0038~92X/821110363-13503.00/0 Printed in Great Britain.
5. Deodatis G. (1996). "Simulation of ergodic multivariate stochastic processes" Journal of Engineering Mechanics, Vol.122, No. 8, August, 1996, ASCE, Paper No. 8943.
6. Di Paola M. (1998). "Digital simulation of wind field velocity" Journal of Wind Engineering and Industrial Aerodynamics 74-76 (1998) 91-109.
7. Gasch R., Twele J. (2012). "Wind Power Plants, Fundamentals, Design, Construction and Operation, 2nd Edition" Springer-Verlag, Berlin, Heidelberg, Germany
8. Gwon T. (2011). "Structural Analyses of Wind Turbine Tower for 3 kW Horizontal-Axis Wind Turbine" PhD Thesis, Faculty of California Polytechnic State University, San Luis Obispo.
9. Halfpenny A. (1998) "Dynamic analysis of both on and offshore wind turbines in the frequency domain" Doctor of Philosophy Dissertation, Faculty of Engineering, University College London, London, England.
10. Hansen M. (2008). "Aerodynamics of Wind Turbines, 2nd Edition" Earthscan, London, U.K.
11. Hansen M., Hansen A., Larsen J., Oye S., Sorensen P., Fuglsang P. (2005). "Control design for a pitch-regulated, variable speed wind turbine" Risø National Laboratory, Roskilde, Denmark, January 2005.
12. Hansen M., Sorensen J., Voutsinas S., Sorensen N., Madsen H. (2006). "State of the art in wind turbine aerodynamics and aeroelasticity" Progress in Aerospace Sciences 42 (2006) 285–330.
13. Hau E. (2006). "Wind Turbines, Fundamentals, Technologies, Application, Economics, 2nd Edition" Springer-Verlag, Berlin, Heidelberg, Germany.
14. Lavassas I., Nikolaidis G., Zervas P., Efthimiou E., Doudoumis I., Baniotopoulos C. (2003). "Analysis and design of the prototype of a steel 1-MW wind turbine tower" Engineering Structures 25 (2003) 1097–1106.

15. Li J., Chen J., Chen X. (2010). “Aerodynamic response analysis of wind turbines” Journal of Mechanical Science and Technology 25 (1) (2010) 89~95.
16. Madsen H., Thomsen K. (2011). “Advances in Wind Energy Conversion Technology” Springer-Verlag, Berlin, Heidelberg, Germany.
17. Negm H., Maalawi Y. (1999). “Structural design optimization of wind turbine towers” Computers and Structures 74 (2000) 649-666.
18. Nicholson J. (2011). “Design of wind turbine tower and foundation systems: optimization approach” Master's Thesis, University of Iowa.
19. Petrini F., Gkoumas K., Zhou W., Li H. (2012). “Multi-level structural modeling of an offshore wind turbine” Structural Engineering and Mechanics
20. Petrini F., Li H., Bontempi F. (2010). “Basis of design and numerical modeling of offshore wind turbines” Structural Engineering and Mechanics, Vol. 36, No. 5 (2010) 599-624.
21. Rosas P. (2003). “Dynamic influences of wind power on the power system” PhD Thesis, submitted to Ørsted Institute, Section of Electric Power Engineering, Technical University of Denmark.
22. Saranyasoontorn K., Manuel L. (2005). “Low-Dimensional Representations of Inflow Turbulence and Wind Turbine Response Using Proper Orthogonal Decomposition” Transactions of the ASME, Vol. 127.
23. Saranyasoontorn K., Manuel L. (2006). “Design Loads for Wind Turbines Using the Environmental Contour Method” Journal of Solar Energy Engineering, Vol. 128.
24. Simiu E., Scanlan R. (1986). “Wind Effects on Structures, 2nd Edition” John Wiley & Sons, Inc., U.S.A.
25. Stathopoulos T., Baniotopoulos C. (2007) “Wind Effects on Buildings and Design of Wind-Sensitive Structures” SpringerWien, New York, U.S.A.
26. Stathopoulos T. “Introduction to Environmental Aerodynamics” In: Baniotopoulos C., Borri C., Stathopoulos T. “Environmental Wind Engineering and Design of Wind Energy Structures”
27. Stathopoulos T. “Applications of Environmental Aerodynamics” In: Baniotopoulos C., Borri C., Stathopoulos T. “Environmental Wind Engineering and Design of Wind Energy Structures”
28. Blocken B. “Computational Wind Engineering: Theory and Applications” In: Baniotopoulos C., Borri C., Stathopoulos T. “Environmental Wind Engineering and Design of Wind Energy Structures”
29. Zasso A., Schito P. “Aero-Servo-Elastic Design of Wind Turbines: Numerical and Wind Tunnel Modeling Contribution” In: Baniotopoulos C., Borri C., Stathopoulos T. “Environmental Wind Engineering and Design of Wind Energy Structures”
30. Schaumann P., Boker C., Bechtel A., Lochte-Holtgreven S. “Support Structures of Wind Energy Converters” In: Baniotopoulos C., Borri C., Stathopoulos T. “Environmental Wind Engineering and Design of Wind Energy Structures”

31. Baniotopoulos C. Lavassas I., Nikolaidis G., Zervas P. “Topics on the design of tubular steel wind turbine towers” In: Baniotopoulos C., Borri C., Stathopoulos T. “Environmental Wind Engineering and Design of Wind Energy Structures”
32. Borri C., Biagini P., Marino E. “Large wind turbines in earthquake areas: structural analyses, design/construction & in-situ testing” In: Baniotopoulos C., Borri C., Stathopoulos T. “Environmental Wind Engineering and Design of Wind Energy Structures”